REPORT DOCUMENTATION PAGE

Form Approved OMB NO. 0704-0188

1. REPORT DATE (DD-MM-YYYY)	2. REPORT TYPE	3. DATES COVERED (From - To)
20-04-2016	Final Report	23-Jan-2012 - 22-Jan-2016

4. TITLE AND SUBTITLE
Final Report: Interoperable Communications for Hierarchical Heterogeneous Wireless Networks

5a. CONTRACT NUMBER
W911NF-12-1-0054

5b. GRANT NUMBER

5c. PROGRAM ELEMENT NUMBER
206022

6. AUTHORS
Lijun Qian, Husheng Li

5d. PROJECT NUMBER

5e. TASK NUMBER

5f. WORK UNIT NUMBER

7. PERFORMING ORGANIZATION NAMES AND ADDRESSES
Prairie View A&M University
P.O. Box 667

Prairie View, TX 77446 -0667

8. PERFORMING ORGANIZATION REPORT NUMBER

9. SPONSORING/MONITORING AGENCY NAME(S) AND ADDRESS (ES)
U.S. Army Research Office
P.O. Box 12211
Research Triangle Park, NC 27709-2211

10. SPONSOR/MONITOR'S ACRONYM(S)
ARO

11. SPONSOR/MONITOR'S REPORT NUMBER(S)
60443-NS-REP.28

12. DISTRIBUTION AVAILIBILITY STATEMENT
Approved for Public Release; Distribution Unlimited

13. SUPPLEMENTARY NOTES
The views, opinions and/or findings contained in this report are those of the author(s) and should not contrued as an official Department of the Army position, policy or decision, unless so designated by other documentation.

14. ABSTRACT
The goal of the project is to advance the performance of interoperable communications for hierarchical heterogeneous wireless networks enabled by cognitive radio technology. The PIs have been working closely with students to carry out all the proposed research tasks, and published 6 journal papers and 15 conference papers during the funding period. A cognitive radio test bed using USRP2/GNUradio and LabVIEW is built to test the analytical results through experiments. New course materials based on the research results were developed and offered. Two graduate students obtained their PhD degrees and two graduate students obtained their MS degrees

15. SUBJECT TERMS
Cognitive radio; Wireless Networks

16. SECURITY CLASSIFICATION OF:			17. LIMITATION OF ABSTRACT	15. NUMBER OF PAGES	19a. NAME OF RESPONSIBLE PERSON
a. REPORT	b. ABSTRACT	c. THIS PAGE			Lijun Qian
UU	UU	UU	UU		19b. TELEPHONE NUMBER 936-261-9908

Report Title

Final Report: Interoperable Communications for Hierarchical Heterogeneous Wireless Networks

ABSTRACT

The goal of the project is to advance the performance of interoperable communications for hierarchical heterogeneous wireless networks enabled by cognitive radio technology. The PIs have been working closely with students to carry out all the proposed research tasks, and published 6 journal papers and 15 conference papers during the funding period. A cognitive radio test bed using USRP2/GNUradio and LabVIEW is built to test the analytical results through experiments. New course materials based on the research results were developed and offered. Two graduate students obtained their PhD degrees and two graduate students obtained their MS degrees during the course of this project. Undergraduate students participated through senior design projects. The PIs and students participated many conferences, workshops, and training for professional development. PIs and students from the two participating institutions have visited each other's campus to strengthen collaborations.

Enter List of papers submitted or published that acknowledge ARO support from the start of the project to the date of this printing. List the papers, including journal references, in the following categories:

(a) Papers published in peer-reviewed journals (N/A for none)

Received		Paper
08/01/2014	20.00	Lanchao Liu, Zhu Han, Zhiqiang Wu, Lijun Qian. Spectrum Sensing and Primary User Localization in Cognitive Radio Networks via Sparsity, EAI Endorsed Transactions on Wireless Spectrum, (04 2014): 1. doi: 10.4108/ws.1.1.e2
08/23/2013	8.00	Lijun Qian, Xiangfang Li, Shuangqing Wei. Anomaly Spectrum Usage Detection in Multihop Cognitive Radio Networks: A Cross-Layer Approach, Journal of Communications, (04 2013): 259. doi: 10.12720/jcm.8.4.259-266
08/23/2013	9.00	Paul Potier, CaLynna Sorrells, Yonghui Wang, Lijun Qian, Husheng Li. Spectrum inpainting: a new framework for spectrum status determination in large cognitive radio networks, Wireless Networks, (07 2013): 0. doi: 10.1007/s11276-013-0614-9
08/23/2013	11.00	Lijun Qian, Paul Potier. Management of cognitive radio ad hoc networks using a congestion-based metric, INTERNATIONAL JOURNAL OF NETWORK MANAGEMENT, (08 2013): 0. doi: 10.1002/nem.1835
08/23/2013	12.00	CaLynna Sorrells, Lijun Qian. Quickest Detection of Denial-of-Service Attacksin Cognitive Wireless Networks, International Journal of Network Security, (08 2013): 0. doi:
08/29/2015	23.00	Lijun Qian, Oluwaseyi Omotere, Riku Jäntti. Performance Analysis on the Coexistence of Multiple Cognitive Radio Networks, EAI Endorsed Transactionson Cognitive Communications, (05 2015): 1. doi: 10.4108/cogcom.1.2.e1
TOTAL:		**6**

Number of Papers published in peer-reviewed journals:

(b) Papers published in non-peer-reviewed journals (N/A for none)

Received Paper

TOTAL:

Number of Papers published in non peer-reviewed journals:

(c) Presentations

Number of Presentations: 0.00

Non Peer-Reviewed Conference Proceeding publications (other than abstracts):

Received Paper

TOTAL:

Number of Non Peer-Reviewed Conference Proceeding publications (other than abstracts):

Peer-Reviewed Conference Proceeding publications (other than abstracts):

Received	Paper
06/01/2012	1.00 Jari Nieminen , Lijun Qian, Riku Jäntti. Per-Node Throughput Performance of Overlapping Cognitive Radio Networks, 7th International Conference on Cognitive Radio Oriented Wireless Networks. 18-JUN-12, . : ,
06/01/2012	2.00 Husheng Li, Lijun Qian. Joint Congestion Control and Routing Subject to Dynamic Interruptions in Cognitive Radio Networks, 7th International Conference on Cognitive Radio Oriented Wireless Networks. 18-JUN-12, . : ,
08/01/2014	15.00 Oluwaseyi Omotere, Lijun Qian, Riku Jantti. Performance Bounds of Prioritized Access in Coexisting Cognitive Radio Networks, 9th International Conference on Cognitive Radio Oriented Wireless Networks and Communications (CROWNCOM). 02-JUN-14, . : ,
08/01/2014	16.00 O. Omotere, Lijun Qian, Xiaojiang Du. Performance Bound of Ad Hoc Device-to-Device Communications using Cognitive Radio, 2013 IEEE Globecom Workshops. 09-DEC-13, . : ,
08/01/2014	17.00 Yifan Wang, Husheng Li, Lijun Qian. Belief Propagation Based Spectrum Sensing Subject to Dynamic Primary User Activities: Phantom of Quickest Detection, MILCOM 2013 - 2013 IEEE Military Communications Conference. 17-NOV-13, San Diego, CA, USA. : ,
08/01/2014	21.00 Wasiu Opeyemi Oduola, Lijun Qian, Xiangfang Li. Femtocell as a relay with application of physical layer network coding, 2014 IEEE 11th Consumer Communications and Networking Conference (CCNC). 09-JAN-14, Las Vegas, NV, USA. : ,
08/01/2014	22.00 Wasiu Opeyemi Oduola, Lijun Qian, Xiangfang Li, Deepak Kataria. Mitigating Uplink interference in femtocell networks with Physical Layer Network coding, 2013 IEEE International Conference on Advanced Networks and Telecommuncations Systems (ANTS). 14-DEC-13, Kattankulathur, India. : ,
08/18/2012	3.00 Husheng Li, Qi Zeng , Lijun Qian. GPS Spoofing Attack on the Time Synchronization in Wireless Networks and Detection Scheme Design, IEEE Military Communications Conference (Milcom). 30-OCT-12, . : ,
08/18/2012	4.00 Paul Potier, Lijun Qian, Harold Zheng, Sherry Wang. Performance Management in Cognitive Radio Ad Hoc Networks using Congestion based Metric, IEEE Military Communications Conference (Milcom). 30-OCT-12, . : ,
08/25/2013	13.00 Lijun Qian, Xiangfang Li, Shuangqing Wei. Cross-layer detection of stealthy jammers in multihop cognitive radio networks, 2013 International Conference on Computing, Networking and Communications (ICNC). 27-JAN-13, San Diego, CA, USA. : ,
08/25/2013	14.00 Lijun Qian, CaLynna Sorrells, Xiangfang Li, Deepak Kataria. Detection of Spectrum Congestion in CognitiveRadio Ad Hoc Networks, IEEE International Conference on Advanced Networks and Telecommunications Systems. 17-DEC-12, . : ,

08/29/2015	24.00	Wasiu Opeyemi Oduola, Xiangfang Li, Lijun Qian, Zhu Han. Power control for device-to-device communications as an underlay to cellular system, ICC 2014 - 2014 IEEE International Conference on Communications. 09-JUN-14, Sydney, Australia. : ,
08/29/2015	27.00	Ojemba Babatundi, Lijun Qian, Julian Cheng. Downlink scheduling in visible light communications, 2014 Sixth International Conference on Wireless Communications and Signal Processing (WCSP). 22-OCT-14, Hefei, China. : ,
08/29/2015	25.00	Fahira Sangare, Ali Arab, Miao Pan, Lijun Qian, Suresh K. Khator, Zhu Han. RF energy harvesting for WSNs via dynamic control of unmanned vehicle charging, 2015 IEEE Wireless Communications and Networking Conference (WCNC). 08-MAR-15, New Orleans, LA. : ,
10/08/2012	7.00	CaLynna Sorrells, Lijun Qian, Husheng Li. Quickest Detection of Denial-of-Service Attacks in Cognitive Wireless Networks, IEEE Conference on Technologies for Homeland Security (HST '12). 13-NOV-12, . : ,

TOTAL: **15**

Number of Peer-Reviewed Conference Proceeding publications (other than abstracts):

(d) Manuscripts

Received	Paper

TOTAL:

Number of Manuscripts:

Books

Received	Book

TOTAL:

Received	Book Chapter

TOTAL:

Patents Submitted

Patents Awarded

Awards

(1) The PhD student, Paul Potier, who participated this project and supervised by the PI, was awarded "Outstanding PhD Student" in the Roy G. Perry College of Engineering at Prairie View A&M University in 2012.
(2) The PhD student, Joseph Kamto, who participated this project and supervised by the PI, was awarded "Outstanding PhD Student" in the Roy G. Perry College of Engineering at Prairie View A&M University in 2013.
(3) The PhD student, Nan Zou supervised by the PI, won the Best Poster Award in the STEAM Research Symposium on March 21, 2014.

Graduate Students

NAME	PERCENT_SUPPORTED	Discipline
Oluwaseyi Omotere	0.50	
Hossein Jafari	0.50	
Nan Zou	0.50	
Yifan Wang	0.50	
Samuel Bamgbose	0.25	
Joshua Bassey	0.25	
Safat Mahmood	0.25	
Remilekun Sabayo	0.25	
Semiu Olowogemo	0.10	
Wasiu Oduola	0.25	
Upendar Kallu	0.10	
FTE Equivalent:	**3.45**	
Total Number:	**11**	

Names of Post Doctorates

NAME	PERCENT_SUPPORTED
FTE Equivalent:	
Total Number:	

Names of Faculty Supported

NAME	PERCENT_SUPPORTED	National Academy Member
Lijun Qian	0.30	
Husheng Li	0.00	
FTE Equivalent:	**0.30**	
Total Number:	**2**	

Names of Under Graduate students supported

NAME	PERCENT_SUPPORTED	Discipline
Christopher St. Julian	0.00	Electrical Engineering
Brandon Norman	0.00	Electrical Engineering
Eric Steen	0.00	Electrical Engineering
FTE Equivalent:	**0.00**	
Total Number:	**3**	

Student Metrics

This section only applies to graduating undergraduates supported by this agreement in this reporting period

The number of undergraduates funded by this agreement who graduated during this period: 3.00

The number of undergraduates funded by this agreement who graduated during this period with a degree in science, mathematics, engineering, or technology fields:..... 3.00

The number of undergraduates funded by your agreement who graduated during this period and will continue to pursue a graduate or Ph.D. degree in science, mathematics, engineering, or technology fields:..... 0.00

Number of graduating undergraduates who achieved a 3.5 GPA to 4.0 (4.0 max scale):..... 1.00

Number of graduating undergraduates funded by a DoD funded Center of Excellence grant for Education, Research and Engineering:..... 0.00

The number of undergraduates funded by your agreement who graduated during this period and intend to work for the Department of Defense 0.00

The number of undergraduates funded by your agreement who graduated during this period and will receive scholarships or fellowships for further studies in science, mathematics, engineering or technology fields:..... 0.00

Names of Personnel receiving masters degrees

NAME
Oluwaseyi Omotere
Wasiu Oduola
Total Number: 2

Names of personnel receiving PHDs

NAME
Paul Potier
CaLynna Sorrells
Total Number: 2

Names of other research staff

NAME	PERCENT_SUPPORTED
FTE Equivalent:	
Total Number:	

Sub Contractors (DD882)

1 a. University of Tennessee at Knoxville

1 b. Office of Sponsored Programs
1534 White Avenue
Knoxville TN 379961529

Sub Contractor Numbers (c): FC10053
Patent Clause Number (d-1): N/A
Patent Date (d-2): 1/23/12 12:00AM
Work Description (e): The team at UTK performed signal processing in research task 1, and helped building the
Sub Contract Award Date (f-1): 1/23/12 12:00AM
Sub Contract Est Completion Date(f-2): 1/22/16 12:00AM

1 a. University of Tennessee at Knoxville

1 b. 404 Andy Holt Tower
Knoxville TN 379960001

Sub Contractor Numbers (c): FC10053
Patent Clause Number (d-1): N/A
Patent Date (d-2): 1/23/12 12:00AM
Work Description (e): The team at UTK performed signal processing in research task 1, and helped building the
Sub Contract Award Date (f-1): 1/23/12 12:00AM
Sub Contract Est Completion Date(f-2): 1/22/16 12:00AM

Inventions (DD882)

Scientific Progress

Please refer to the attached detailed report in Attachment.

Technology Transfer

Some of the cognitive radio technologies developed in this project may have potential for technology transfer. Although this project is completed, the PI plans to interact with ARL researchers in the future to explore opportunities for joining CRA or CTA for technology transfer.

INTEROPERABLE COMMUNICATIONS FOR HIERARCHICAL HETEROGENEOUS WIRELESS NETWORKS: SCIENTIFIC PROGRESS AND ACCOMPLISHMENTS

BY PI: LIJUN QIAN

Department of Electrical and Computer Engineering

Roy G. Perry College of Engineering

Prairie View A&M University

Prairie View, Texas

April, 2016

ABSTRACT

During the funding period (Jan 2012 - Jan 2016), important theoretical and simulation results are obtained for all three tasks and the test bed proposed for the project.

In task 1, the problem of spectrum status determination is considered for large cognitive radio ad hoc networks. Spectrum sensing and spectrum decision are critical for cognitive radio network throughput and hence obtaining accurate knowledge of the spectrum status is vitally important to better spectrum usage decisions. By representing the spectrum sensing results across the network as an image, spectrum status determination is formulated as an image recovery problem. The method of total variation inpainting is applied to solve the problem with low determination error. Then cross-network collaboration based spectrum sensing in cognitive radio is studied. Because of the security requirements among different networks, the co-existing networks can only communicate through certain gateway nodes. The limited communication capability of gateway nodes incurs significant challenges for the collaboration. The technique of Belief Propagation is proposed and studied for the cross-network collaboration with the assumption of Markov random field for the spectrum occupancies. The effectiveness of the proposed algorithm is demonstrated by extensive simulations.

In task 2, we focus on joint routing and congestion control to enhance the robustness of the cognitive radio networks. Furthermore, a novel Cognitive Radio Network Management Protocol (CNMP) is proposed to address the unique challenges of managing cognitive radio ad hoc networks that have distributed, multi-hop architectures with dynamic spectrum availability. We focus on performance management for these networks, and address the problem of network congestion for secondary users, because of its significant impact on data throughput. For practical implementation, we further propose a cluster based management architecture that utilizes a designated central manager and cluster heads that function as distributed managers. Numerical simulation shows that the proposed algorithms achieve the optimal or near-optimal performance.

As for task 3, we consider two geographically overlapping cognitive radio networks

coexisting together with a primary network. We specifically study the achievable per-node throughput performance of the cognitive radio networks. Firstly, an interference model is specified which models the situation. By using this model we derive the per-node throughput for overlapping cognitive radio networks. Furthermore, the upper bound for the probability of false alarm, which is required to achieve a certain throughput, is deduced. The results illustrate how the different cognitive radio network parameters, such as network density, transmission probability, and sensing performance, impacts the achievable per-node throughput in overlapping cognitive radio networks. This may be served as guidance for the deployment of multiple cognitive radio networks.

In the experimental front, a distributed spectrum monitoring and surveillance test bed is developed for identifying and locating RF signals using the Universal Software Radio Peripheral (USRP). In addition, the RF signatures of various wireless devices (cellular, WiFi, bluetooth, etc.) are captured using USRP2 and GNUradio platform, and the traces are available on a storage server. These traces may be used for evaluations of various schemes proposed for cognitive radio wireless networks, and can be replayed in the test bed.

Details of the research results from this project are also available on a dedicated website:
http://cebcom.pvamu.edu/webpage/updated/HHN.htm

Table of Contents

List of Tables

List of Figures

List of Abbreviations

AWGN	Additive White Gaussian Noise
BER	Bit Error Rate
BP	Belief Propagation
BPSK	Binary Phase Shift Keying
CR	Cognitive Radio
CRAHN	Cognitive Radio Ad Hoc Network
CSMA	Carrier Sense Multiple Access
FCC	Federal Communications Commission
ISM	Industrial, Scientific and Medical
JTRS	Joint Tactical Radio System
LLP	Limited Lookahead Policy
MAC	Medium Access Control
MANET	Mobile Ad Hoc Network
POMDP	Partially Observable Markov Decision Process
PU	Primary User
QoS	Quality of Service
SCA	Software Communication Architecture
SDR	Software Defined Radio
SINR	Signal-to-Interference-Plus-Noise Ratio
SU	Secondary User
USRP2	Universal Software Radio Peripheral 2
WRAN	Wireless Regional Area Network

Chapter 1

Spectrum Inpainting for Spectrum Status Determination in Large Cognitive Radio Networks

In this chapter, the problem of spectrum status determination is considered for large cognitive radio (CR) ad hoc networks. Spectrum sensing and spectrum decision are critical for cognitive radio network throughput and hence obtaining accurate knowledge of the spectrum status is vitally important to better spectrum usage decisions. The major challenge of this type of problem lies in the fact that for a network covering a large geographical area, only very limited measurements of spectrum occupancy during spectrum sensing may be obtained by the CR users for a certain location in any given time slot. This is due to both the hardware limitations as well as the tradeoff between spectrum sensing time and data throughput of the CR users. By representing the spectrum sensing results across the network as an image, spectrum status determination is formulated as an image recovery problem. The method of total variation inpainting is applied to solve the problem with low determination error. The proposed method takes advantage of the correlations in multiple dimensions and the numerical results demonstrate the effectiveness of the proposed scheme.

1.1 Introduction

The introduction of cognitive radio (CR) shifts the paradigm of spectrum management from command and control to dynamic spectrum access for the CR users, or secondary users (SUs), and thus improves the spectrum utilization. In this work, we use the terms CR users and SUs interchangeably. In order to fulfill this transition, spectrum awareness is a must and spectrum sensing plays a pivotal role in achieving such awareness. Many studies have been done on spectrum sensing, mostly focus on sensing

a small geographic area, either by a single CR user or collaboratively by a group of CR users [19] [53], but have not approached spectrum awareness as an image processing problem.

In this work, it is considered that a cognitive wireless network is deployed in a large geographical area, where different spectrum may be available at various locations in the network due to diverse primary user (PU) activities. In such a network, the spectrum sensing results from the CR users may provide spectrum availability information for a small portion of the locations. Furthermore, there are hardware limitations of the many existing cognitive radios: at a specific location, each radio can only sense a small portion of the frequency bands out of a very wide candidate pool of spectrum during a short time interval. For example, the frequency response of the Universal Software Radio Peripheral 2 (USRP2) receiver shows the effective 3dB bandwidth is approximately 13.7 MHz [125]. Sweeping a very wide spectrum would require longer time, thus reducing the amount of time per slot for data transmission, and consequently the throughput of the cognitive radio network [22]. These limitations create challenges for achieving network-wide spectrum awareness in a large network.

In this work, it is assumed that the spectrum usage by the PUs is correlated in space, time, and frequency. An example is given in Fig. 1.3 and Fig. 1.4 to illustrate the spatial and time correlation. While it is well-known and quite intuitive that the spectrum usage is spatially correlated, the time correlation also exists and it is discussed later in the simulation section. For a very wide band, e.g., 800MHz - 2.7GHz, the measurement results have indicated that the actual spectral utilization is not uniform [23]. Some portions of spectrum with high usage demands were found to be very congested over a long period of time, while other portions of spectrum were found to be only lightly used or completely unused during the entire measurement time span. However, in this work, we consider the case where each primary user typically occupies a frequency band that spans several consecutive channels used by secondary users. As a result, spectral correlation exists for the same PU as well.

An illustrative example is given in Fig. 1.1, where a cognitive wireless network is deployed in a 2.5km$\times$2.5km area. There are 5 primary users and 75 CR users in the

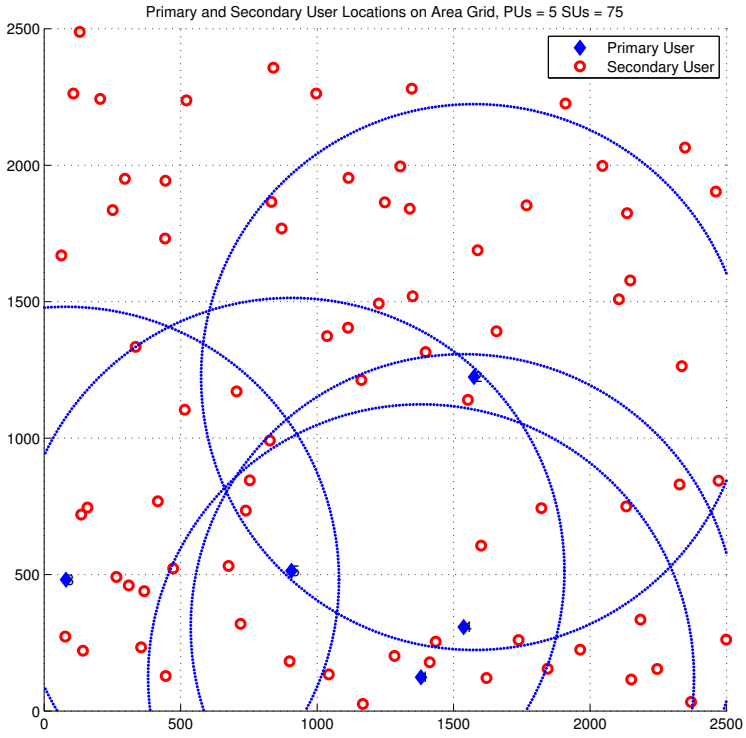

Figure 1.1 An example of randomly deployment of 5 primary users and 75 CR users.

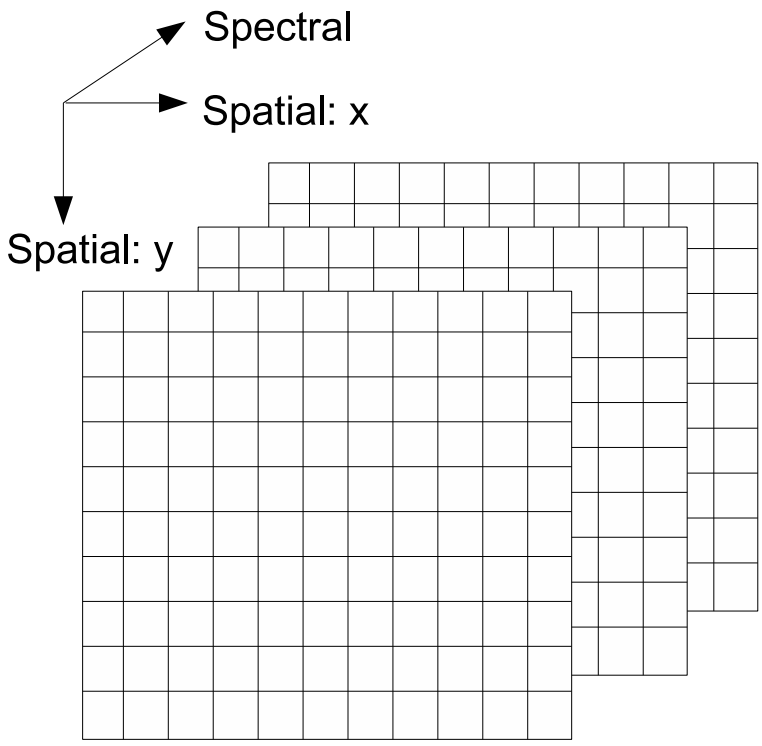

Figure 1.2 Spectrum occupancy across the network can be viewed as a 3-D image.

area, and there are 10 licensed channels. Each primary user constantly transmits on a random number of channels and occupies a circular range with radius of 1km, within which the channels used by the primary user are not available to the CR users. Here we note that the actual amount of signal sensed by the SUs is the algebraic sum of the active PU's signal strength in a particular location. However, we use a simplified PU circular interference model to adequately provide a basis for SU detection of a PU. This is reasonable, since we also assume that for a given channel, only a single PU can be active on a channel at one time. The focus of our work is on the data fusion of a number of SU devices to create a spectrum image, and we use the circular model to generally capture spectrum occupation by the PUs. The 2.5km×2.5km square area is divided into 10×10 sub areas, with each sub area a 250m×250m square. Assuming that each cognitive user can only detect one channel within one (its own) sub area at any given time slot, then the percentage of observed spectrum usage in the entire network at any given time slot is $75/(10 \times 10 \times 10) = 7.5\%$ or less. The reason that the observation may be less is that some of the CR users may detect the same channels in the same neighborhood, as later observed in the simulation section. Even if each cognitive user can detect more channels, say 5 channels at any given time slot, which requires more sensing time within the slot, reducing the data throughput [22], the percentage of observed spectrum usage in the entire network is still only 37.5% or less.

The purpose of this study is to determine the spectrum status in the entire wide-area network from the limited observations obtained from spectrum sensing by CR users. If the spectrum availability of one channel in the entire network is viewed as a black-and-white image, with the black pixel representing the channel not available in that sub area, then the spectrum availability of all the channels in the entire network can be viewed as a set of images. This corresponds to the hard decision case where each SU makes its own decision based on its own measurement and makes judgement, then it sends its black/white judgement to the fusion center. A colored image may be used if the detailed measurements of the spectrum are considered and/or soft decision rather than hard decision is applied. Since soft decision may incur too much overhead, we only consider hard decision here, although the framework also applies to the soft

decision case. Mathematically, each image can be represented as a 2-D matrix, and the set of images can be represented as a 3-D matrix, as shown in Fig. 1.2, with the third dimension (the number of the images) equal to the number of the channels. With this mathematical representation, the problem of determining the spectrum status in the entire network becomes a matrix completion problem.

Recent advances in matrix completion show that it is possible to reconstruct the entire matrix from partial observations [24]. In fact, if the matrix has low rank and satisfies the incoherence property, the matrix can be reconstructed exactly with high probability from just a few entries [25]. Low rank is indicated in [25] as the rank, r, of an $n_1 \times n_2$ matrix, M, where $n = \max(n_1, n_2)$ as $r \leq n^{\frac{1}{2}}$.

The incoherence of a data matrix characterizes how difficult it is to complete the matrix from random samples, which may be different even for matrices of the same rank. The incoherence property is based on the matrices U, V, and Σ, comprising the singular value decomposition (SVD) of the matrix, M, complying with the coherence conditions specified in [24].

Instead of using the standard algorithms for matrix completion, such as SVD [25] or nuclear norm optimization [26], the previous study [27] applied the technique of belief propagation and the spatial correlation was exploited. The basic idea is to let the beliefs on the spectrum occupancy be propagated from the locations that have been sensed to the unsensed locations and iterate until converged. It is observed that the belief propagation approach in [27] achieves a much lower reconstruction error probability over the standard SVD algorithm. This is because the SVD method is designed for general matrix completion problems and the belief propagation approach is suitable for only matrices in which neighboring elements are highly correlated.

In this work, two new contributions are made to the spectrum status determination problem:

1. The applicability of image reconstruction methods to the problem at hand is explored. Specifically, the method of Total Variation (TV) Inpainting [28] is employed, since the spectrum occupancy across the network at any time instant may

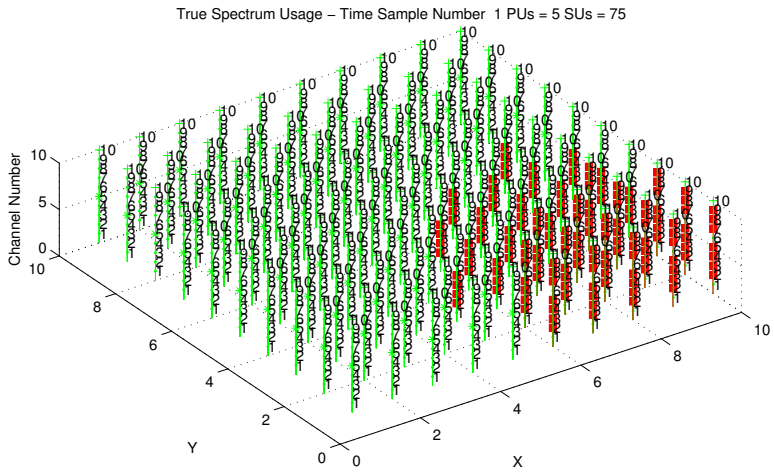

Figure 1.3 Actual Spectrum Occupancy at Sample Time 1 with 5 PUs and 75 SUs (Some of the PUs are not active at the sample time).

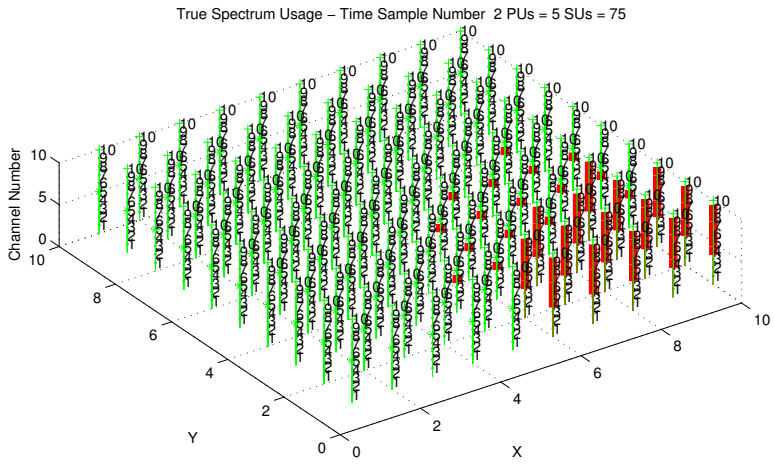

Figure 1.4 Actual Spectrum Occupancy at Sample Time 2 with 5 PUs and 75 SUs (Some of the PUs are not active at the sample time).

be viewed as an image. It is observed that for the cases of highly correlated spectrum usage, the method of total variation inpainting results in marginally better performance compared to belief propagation. When the degree of correlation drops, the performance of total variation inpainting degrades gracefully.

2. Secondly, the spectrum occupancy across the network as a function of time is considered, i.e., both the temporal and spatial characteristics of spectrum occupancy are examined. Since each snapshot of the spectrum occupancy across the network can be viewed as a 3-D image, where X and Y represent spatial location, and Z represents frequency channels, the multiple snapshots along time can be viewed as a 4-D data set.

   An example of this can be seen from the 3-D images shown in Fig. 1.3 and Fig. 1.4. These figures show the channels occupied by the PUs as distributed in Fig.1.1, and represent the PU activity for timeslot 1 and timeslot 2. The 3-D graphs show that channels are on the vertical axis in each geographic sub area, or pixel, of the location grid. In this case, the channels on each axis range from 1 to 10, and a red dot at a channel value on the axis represents that channel as occupied by a PU. If a channel is not occupied by a PU, the channel location on the graph is green. This convention has been used for all the 3-D figures in this work.

   In Fig. 1.3, which represents timeslot 1, it can be noted that there are more occupied channels than in Fig. 1.4, which represents timeslot 2, since a Poisson traffic model is assumed for the primary users. Hence, the 4-D matrix is a collection of the X and Y spatial data, the channel occupied or idle state, and the timeslot. It is observed that the spectrum occupancy is highly correlated in the spatial, spectral as well as the temporal domains, which provides the basis for the success of the proposed method.

The rest of this chapter is organized as follows. A brief review of total variation inpainting and the proposed algorithmic model for the spectrum status determination from partial observations is given in Section 1.2. Section 1.3 provides the simulation

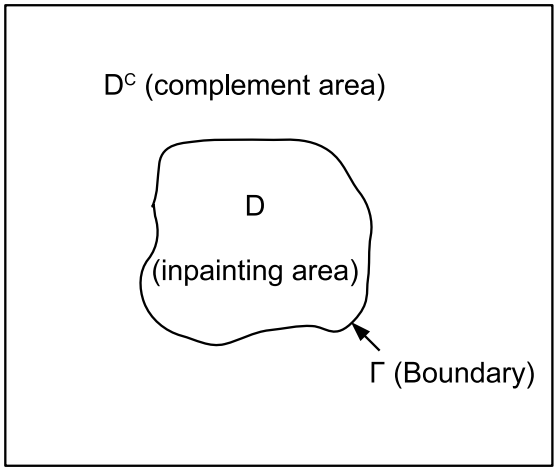

Figure 1.5 The TV inpainting model finds the best guess for $u|_D$ based on the TV norm on the extended area $D^C \cup D$ and the noise constraint on D^C.

studies and numerical results. Related work is discussed in Section 1.4, and Section 1.5 contains the concluding remarks.

1.2 Total Variation Inpainting for Spectrum Occupancy Determination

In this section, total variation inpainting technique from image processing is introduced firstly, then an effective algorithm that stems from the principle of total variation inpainting is proposed for the reconstruction of spectrum occupancy in a large CR network.

1.2.1 Background on Total Variation Inpainting

Total Variation (TV) Inpainting model has been studied extensively in image processing, e.g., see [28] and the references therein. Initially, inpainting is referred to the technique carried out by skilled image restoration artists to reconstruct lost or deteriorated parts of a valuable painting. In the digital world, image inpainting is referred to as the image processing technique in which sophisticated algorithms are applied to reconstruct or replace lost or corrupted parts of image data. As shown in Fig. 1.5, area D is the lost or corrupted part of the image and area D^C is the known or uncorrupted

part of the image. The purpose of image inpainting is to find the best estimate for pixels in the unknown area D based on the known information on its complement area D^C. Specifically, with the assumption that the initial condition of the image, $u^0|D^C$, is contaminated by homogeneous white noise in area D, to find a function u which fits the extended inpainting domain $D^C \cup D$, the TV inpainting model is to solve the unconstrained inpainting problem such that it minimizes the regularity functional

$$J_\lambda[u] = \int_{D^C \cup D} |\bigtriangledown u| dxdy + \frac{\lambda}{2} \int_{D^C} |u - u^0|^2 dxdy, \tag{1.1}$$

where u^0 is the initial condition and λ is the Lagrange multiplier. According to the variation principle [28], the Euler-Lagrange equation for J_λ is

$$- \bigtriangledown \cdot (\frac{\bigtriangledown u}{|\bigtriangledown u|} + \lambda_e (u - u^0) = 0, \tag{1.2}$$

where the extended Lagrange multiplier λ_e is given by

$$\lambda_e = \begin{cases} \lambda, & \text{for area } D^C, \\ 0, & \text{for area } D. \end{cases} \tag{1.3}$$

For practical applications and from the numerical point of view, $|\bigtriangledown u|$ is replaced by $|\bigtriangledown u|_\varepsilon = \sqrt{|\bigtriangledown u|^2 + \varepsilon^2}$ for small value ε to avoid divided by zero. Then the model becomes

$$J_\lambda[u]_\varepsilon = \int_{D^C \cup D} |\bigtriangledown u|_\varepsilon dxdy + \frac{\lambda}{2} \int_{D^C} |u - u^0|^2 dxdy, \tag{1.4}$$

This TV inpainting model is motivated by the inpainting principles of locality, which means the inpainting models only rely on local features instead of global features. In terms of numerical mathematics, as explained by Shannon's Sampling Theorem [29]: *if one expects an accurate reconstruction of a band-limited signal, then the sampling distance has to be small enough according to the band-width*, locality in TV inpainting is necessary for a faithful reconstruction of the missing image information. From the point of view of vision analysis, locality is closely connected to two problems in vision analysis: *local inference* and *the factor of scale* [28], which makes it a natural choice for simplified simulation of human vision systems and implementation of image inpainting applications. This locality property ensures that the TV inpainting model is capable of restoring broken smooth edges, and is robust to noise.

1.2.2 Algorithmic Method

In the context of spectrum occupancy in cognitive radio networks, matrix A is defined as the spectrum status matrix whose entries A_{ij} denote the channel availability at location (i, j) in pixels. Then D corresponds to the unknown entries in A, which represents the area to be inpainted, while D^C, the complement of the unknown area, is comprised of the known entries in A.

In the proposed algorithm, TV inpainting is applied on the reconstruction of the 3-D matrix as depicted in Fig. 1.2. Specifically, to utilize the correlation on both spatial and spectral domains, a 3-D TV inpainting process is implemented. The algorithm is presented as pseudocode in Algorithm 1 and graphically as a flow chart in the Appendix. Definitions of the terms used in the algorithm are included in Table 1.1.

The algorithm begins by setting the value of the Lagrange multiplier, λ, to a large value, such that it will have a small effect on changing the values of the known matrix elements. This is because λ tunes the denoising strength and balances between deblurring accuracy and noise reduction, where smaller lambda implies stronger noise reduction but at the cost of deblurring accuracy [30].

The first round of TV inpainting is applied spatially on each channel (part (a) in Algorithm 1). That is, there is a X,Y plane at each frequency in the network, and each plane contains an image. The TV inpainting algorithm is applied to the image on the plane to fill in the unknown area, D, based on the assumed correlation with the information from the known area, D^C. A 3-D matrix, u_1, stores the spatially inpainted image created at each frequency.

Then the second round of inpainting is on the spectral domain along the Y direction (part (b) in Algorithm 1). This holds the X spatial coordinate constant and creates a Y,Z plane of Y spatial values and Z channel values, for which the image on that Y,Z plane is inpainted. This is done for each X value and stored in the 3-D matrix u_2. Similarly, the TV inpainting algorithm is applied on the spectral domain along the X direction (part (c) in Algorithm 1), for inpainting of the image on the X,Z plane, for all values of Y and is stored in the 3-D matrix, u_3.

Algorithm 1 Total Variation Inpainting Implementation

Generate channel occupancy matrix: channelOcc
Generate channel occupancy matrix by spectrum sensing:
channelOccCR $\lambda \Leftarrow 10^4$
$uThreshold \Leftarrow 0.1$
$D \Leftarrow$ (channelOccCR == unknown)
$D^C \Leftarrow$ (channelOccCR == known)
(**a**).
Inpaint y-channel plane for each x value
channel = 1:numChannels u1(:,:,channel) $\Leftarrow$ tvinpaint(channelOccCR,λ,D > $uThreshold$)
(**b**).
Inpaint y-channel plane for each x location
row = 1:numXLocation col = 1:numYLocation ftemp(col, :) $\Leftarrow$ f(row, col, :)
Dtemp(col, :) $\Leftarrow$ D(row, col, :)
u2temp $\Leftarrow$ tvinpaint(ftemp,λ,Dtemp) > $u\_threshold$
col = 1:numYLocations u2(row, col, :) $\Leftarrow$ u2temp(col, :)
clear ftemp; Dtemp; u2temp
(**c**).
Inpaint x-channel plane for each y location
col = 1:numYLocations row = 1:numXLocation ftemp(col, :) $\Leftarrow$ f(row, col, :)
Dtemp(col, :) $\Leftarrow$ D(row, col, :)
u3temp $\Leftarrow$ tvinpaint(ftemp,λ,Dtemp) > uThreshold
row = 1:numXLocation u3(row, col, :) $\Leftarrow$ u3temp(row, :)
clear ftemp; Dtemp; u3temp
(**d**).
Determine the average of the inpainting calculations
$A \Leftarrow (((u1 + u2 + u3)/3) > 0.5)$
$A(D^C) \Leftarrow$ channelOccCR(D^C)
Calculate the reconstruction error rate by comparing A and channelOcc

Table 1.1 Algorithmic Terms Definition

Algorithm Term	Definition
channelOcc	Matrix (x location, y location, channel number) denoting which channels are actually occupied by Primary Users at a given x-y location.
channelOccCR	Matrix (x location, y location, channel number) denoting which channels sampled by Secondary Users are estimated to be occupied by Primary Users at a given x-y location.
λ	Lagrange multiplier that tunes the denoising strength to balance between deblurring accuracy and noise reduction.
uThreshold	Threshold value used to determine whether channel is estimated to be busy or idle.
numChannels	Total number of channels considered in the system.
D	Matrix specifying the unsensed locations of the inpainting domain, as shown in Fig. 1.5.
D^C	Matrix specifying the sensed locations of the complement area of the inpainting domain, as shown in Fig. 1.5.
numXLocations	Total number of X axis locations on XY locations area grid
numYLocations	Total number of Y axis locations on XY locations area grid
f	Matrix (x location, y location, channel number) representing the input image.
ftemp	2 dimensional matrix where each location represents an x or y grid location and a channel.
Dtemp	2 dimensional matrix where each location represents an x or y grid location and a channel.
uiTemp	Matrix to capture intermediate result for inpainting in each 2 dimensional plane, where i = 1, 2, or 3.
ui	3 dimensional matrix (x location, y location, channel number) that captures inpainting result, where i = 1, 2, or 3.
tvinpaint	Function that provides inpainting using information regarding occupied, unoccupied, and unsensed channels, and the Lagrange multiplier

The average for each point in these 3-D images, from matrices u_1, u_2, and u_3, is then calculated and compared to a threshold, u_{th}. The result is a logical value for each matrix coordinate indicating whether the channel is estimated to be busy or idle. This scheme takes advantage of the correlation in the spatial and spectral domains and provides optimal performance.

The above procedure simultaneously denoises and inpaints the channel occupancy matrix A using total variation regularization. "tvinpaint" in Algorithm 1 minimizes the regularity function defined by equation (1.4), and it is solved with the split Bregman method [31]. As stated previously, the parameter λ controls the strength of the noise reduction outside the inpainting region, where smaller λ implies stronger denoising.

In order to take advantage of the correlation in time, a low-pass filter is used on the sensing data, i.e., a decision on an entry in A will be affected by the history:

$$A_{ij}(k) = \alpha A_{ij}^{TV}(k) + (1-\alpha)A_{ij}(k-1) \tag{1.5}$$

where k is the time point, $0 < \alpha \leq 1$ is a design parameter, A_{ij}^{TV} is the value of the entry from the 3-D TV inpainting process.

The major computation of the proposed algorithm is in TV inpainting, and the core algorithm in TV inpainting is Split Bregman. The major computation of Split Bregman is a while loop. Within the while loop, there are 2 fft2 and 2 ifft2 plus 1 shrink2 operations. Suppose that the dimensions of the image are $M \times N$, then fft2 has a complexity order in $O[M * N * log(M * N)]$. The complexity of shrink2 is $O(M * N)$. The total number of while loops is controlled by a preset tolerance value, say ε. The smaller the value of ε, the larger the number of program loops required. Thus, the complexity order of the proposed algorithm is $O[M * N * log(M * N)/\varepsilon]$.

1.3 Numerical Results

In this section, we have performed extensive simulations to illustrate the advantages of using TV inpainting, and provided comparison with other popular algorithms.

1.3.1 Simulation Setup

The purpose of the simulation is to characterize the performance of the inpainting approach relative to a known spectrum status matrix. We use MATLAB for the simulation and specifically leverage code from Pascal Getruer for total variation inpainting called tvreg [32]. The simulation results are obtained by considering a 2.5 km×2.5 km square area, with 5 primary users and a variable number of CR users randomly located, as shown for the case of 75 CR users in Fig. 1.1. It is assumed that there are 10 licensed channels. Each primary user constantly transmits on randomly distributed contiguous channels, from 1 to 5 channels simultaneously per timeslot. The PUs have a circular interference range with radius of 1000 m., within which the channels utilized by the primary user are not available to the CR users. Here we note that the actual amount of signal sensed by the SUs is the algebraic sum of the active PU's signal strength in a particular location. However, we use a simplified PU circular interference model to adequately provide a basis for SU detection of a PU. This is reasonable since we also assume that for a given channel only a single PU can be active on a channel at one time. Since the focus of our work is on the data fusion of a number of SU devices to create a spectrum image, we use the circular model to generally capture spectrum occupation by the PUs. In this work, it is also assumed that each cognitive user can only detect one channel within its own sub field (a 250m×250m square), so the number of known elements in the matrix will be approximately equal to the number of CR users, since overlapping does exist. For example, in this network configuration, if there are 200 CR users each sensing 1 channel, ideally the sampling rate would be 20%, if each channel sensed was unique to a single SU (200 known elements / 1000 total). However, due to overlapping in the simulation, the real sampling rate is only about 17%. Generally speaking, overlapping increases with the density of the CR users in the network.

The effects of this inpainting methodology can be seen from examination of Figs. 1.1, 1.3, 1.4, 1.6, and 1.8. Beginning with the spatial distribution of PU and SU nodes shown in Fig. 1.1, with 5 PUs and 75 SUs randomly distributed over the geographic grid. The activity of the PUs is seen for timeslot 1 and timeslot 2 in Figs. 1.3 and 1.4,

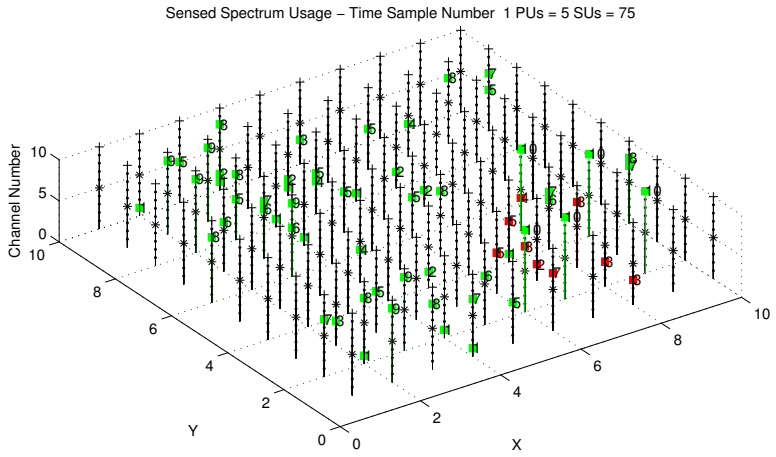

Figure 1.6 Incomplete Spectrum Occupancy Per Spectrum Sensing of 75 SU nodes at Sample Time 1.

respectively, as previously noted. The SUs that are present can sense the state of a single channel, which provides the partially known spectrum status in Fig. 1.6 for timeslot 1 and Fig. 1.8 for timeslot 2. Note from the figures that the actual channel usage differs from timeslot 1 to timeslot 2 due to the changes in the PU activity, and that the SUs may randomly differ in the channels sensed in each timeslot.

1.3.2 Simulation Discussion

The inpainting algorithm is applied to the incomplete spectrum status as determined by the SU sensing, and produces an estimate of the channel usage. Fig. 1.7 shows its estimate with a known location rate of 6.8%, instead of 7.5% for the reasons discussed above, and an error rate of 31% compared to the true spectrum. Similarly, for the second case of 75 SUs, in timeslot 2, Fig. 1.9 shows an error rate of 22.5% for roughly the same percentage of known location values. This difference in the 2 error rates also shows the variability of the algorithm performance as the correlation of the known to unknown points differs.

Another case is considered where the number of SUs is increased to 200 nodes, with 5 PUs, as shown in Fig. 1.10. The true spectrum status is shown in Fig. 1.11, for timeslot 1. A visual comparison of the 200 SU sensed channels in Fig. 1.12 and the 75 sensed channels in Fig. 1.8, show a marked density increase in known channels. When

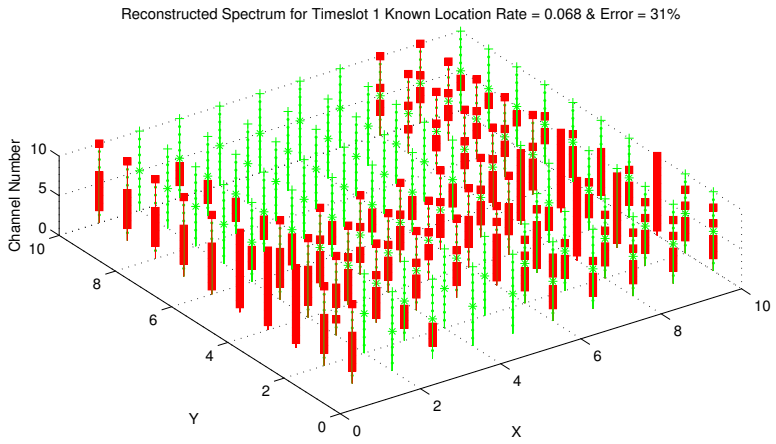

Figure 1.7 Reconstructed Spectrum Occupancy Per TV Inpainting Algorithm using 75 SU nodes at Sample Time 1.

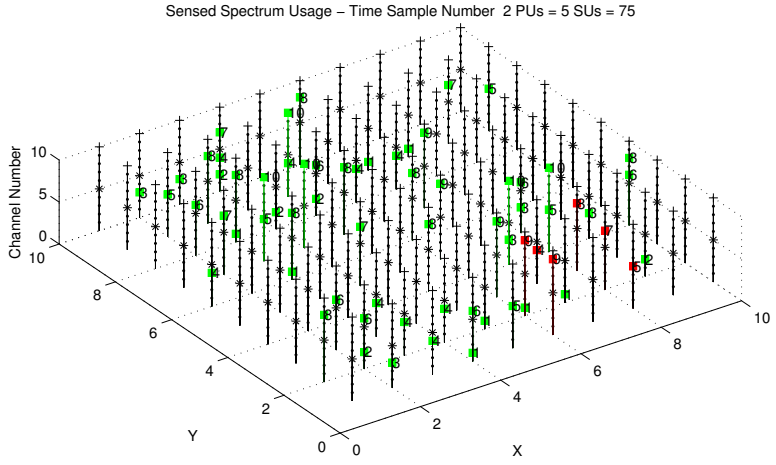

Figure 1.8 Incomplete Spectrum Occupancy Per Spectrum Sensing of 75 SU nodes at Sample Time 2.

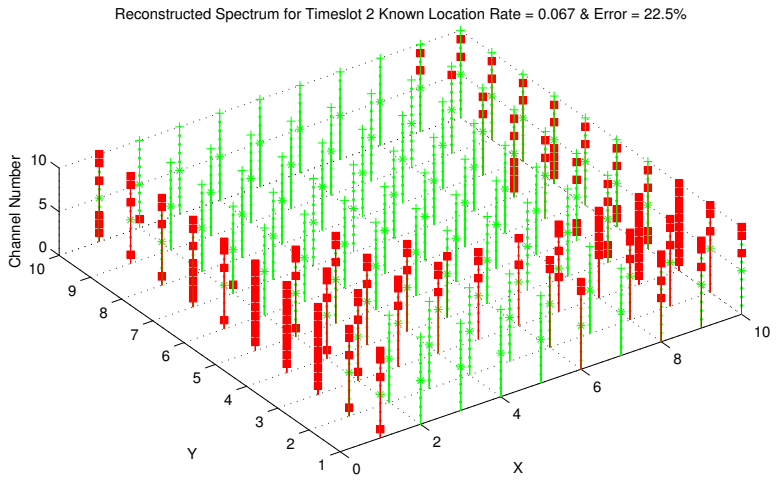

Figure 1.9 Reconstructed Spectrum Occupancy Per TV Inpainting Algorithm using 75 SU nodes at Sample Time 2.

the inpainting algorithm is applied to the 200 SU node case, Fig. 1.13 shows a much lower error rate of 7.4% for a known location rate of 16.5%, due to increased knowledge of the spectrum status that is used by the algorithm. The similarity of the channel occupancy between Fig. 1.11 and Fig. 1.13 is also visually apparent.

1.3.3 Comparison of TV Inpainting with Belief Propagation

In this implementation of the proposed TV inpainting based algorithm, the tvreg [32] program package was used. The performance of the TV inpainting algorithm was compared to that of the belief propagation (BP) method in [27].

As applied to cognitive radio, belief propagation provides channel state prediction over spatial locations and frequency channels. Its purpose is to predict the spectrum occupancies by using the states of channels that have been sensed and leverage the correlations of channel occupancies [27]. BP uses a process in which neighboring variables communicate with each other, passing messages such the sender expresses a 'belief' that the neighboring node belongs in certain states with various likelihoods [33]. The BP algorithm will iteratively update messages until convergence, then estimate the marginal probabilities or most likely states, which are called beliefs. If the network nodes can be represented in a graph, BP provides the exact solution when there are no loops in the

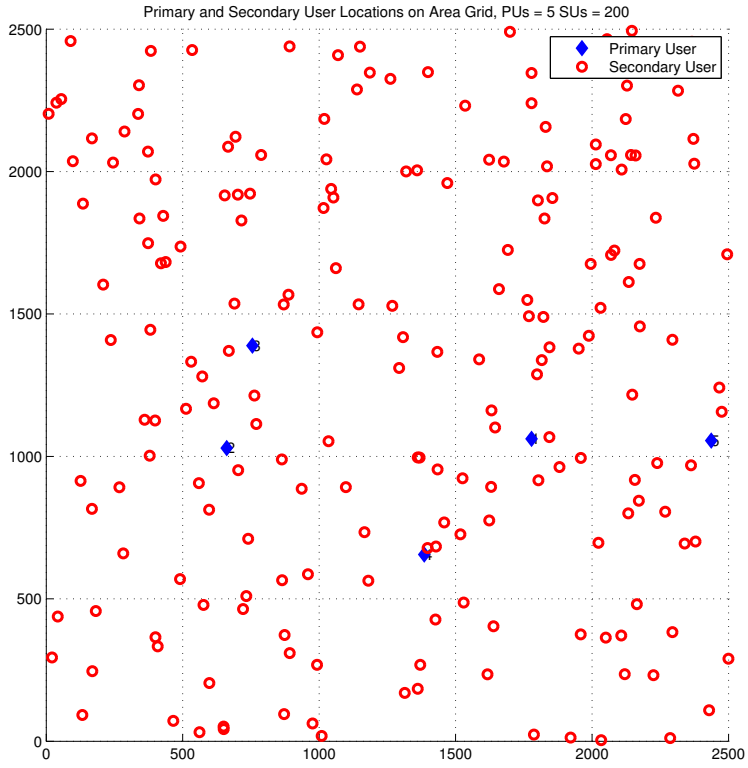

Figure 1.10 An example of randomly deployment of 5 primary users and 200 CR users.

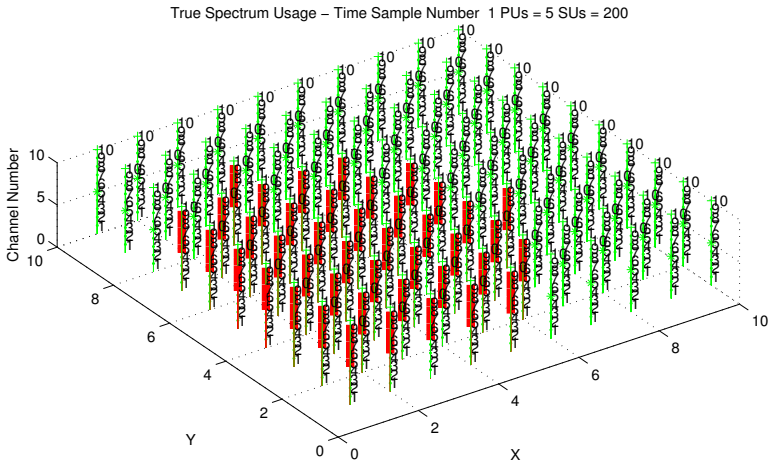

Figure 1.11 Actual Spectrum Occupancy at Sample Time 1 with 5 PUs and 200 SUs.

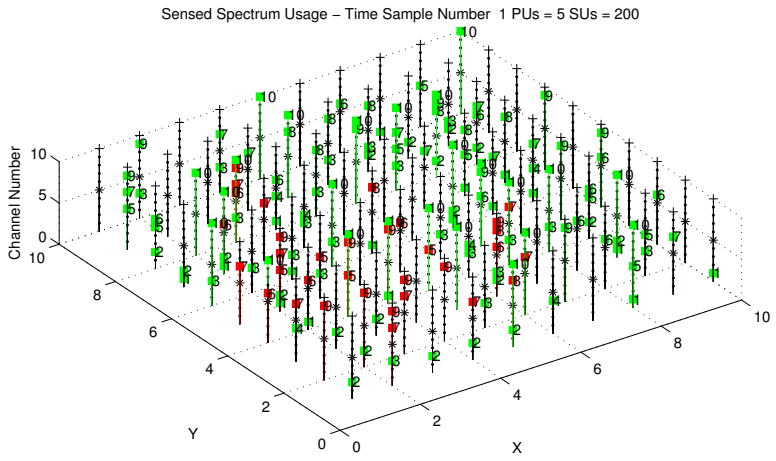

Figure 1.12 Incomplete Spectrum Occupancy Per Spectrum Sensing of 200 SU nodes at Sample Time 1.

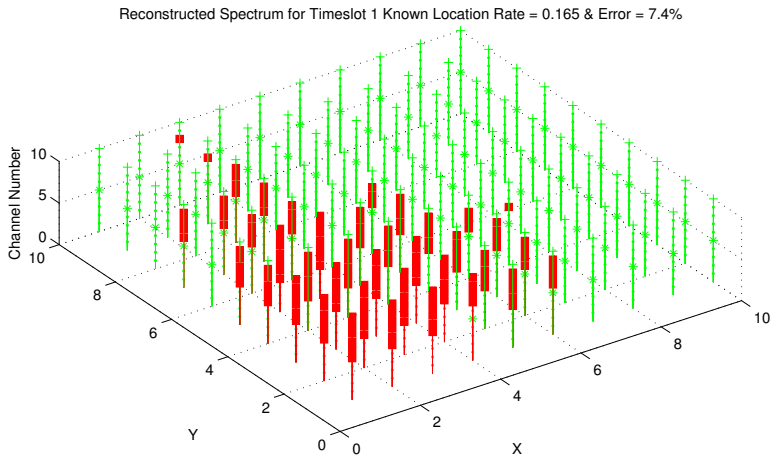

Figure 1.13 Reconstructed Spectrum Occupancy Per TV Inpainting Algorithm using 200 SU nodes at Sample Time 1.

graph. It is equivalent to dynamic programming or the Viterbi algorithm in these cases, otherwise, when graph loops are encountered, BP provides approximate solution [33].

The messages in a BP system with a set of $\mathcal{N}$ nodes are passed from node $i \in \mathcal{N}$ to node $j \in \mathcal{N}$ as $m_{ij}(x_j)$. A high value of $m_{ij}(x_j)$ means that node i "believes" the marginal value $P(x_j)$ to be high. The belief transmitted through these messages is often refined over multiple iterations.

Additionally, BP approach can be centralized or non-centralized. For the centralized approach, SU sensing information is passed to a concentrating node(s) or control center, and used as input for a spectrum occupancy decision. Whereas for the decentralized approach, the SUs share sensing information with their neighbors, then come to a decision independently regarding spectrum occupancy of primary users [27].

The strengths of BP include it's applicability to high dimensionality matrices and ability to work in decentralized problems. It is also able to use a priori information about the similarity of adjacent channels or geographic locations to aid in converging to more accurate marginal probability or maximum probability solutions. However, performance analysis can be difficult since message propagation may have looped paths. And although approximate solutions are possible, analyzing convergence of BP iterations on loopy networks is an open problem. It is further observed in [27], that the performance of BP is degraded if the probability of node correlation in space is too large, which implies that the correlation is overestimated. Other methods may be more accurate, faster or less memory-intensive in some domains [34], but BP tends to increase its accuracy through a number of iterations, until the error rate becomes irreducible, which is shown in [27] to occur at about eight iterations. However, by contrast, our total variation inpainting algorithm requires only a total of three estimates of the 3D matrix to produce its spectrum result.

The performance comparison is given in Fig. 1.14. It is observed that the TV inpainting algorithm outperforms the belief propagation method. For the same sampling rate, the reconstruction error rate of the TV inpainting algorithm is smaller than that of the belief propagation method. This result could be expected since TV inpainting algorithm is designed for image determination, which well fits the needs of spectrum

status determination. It is noteworthy to point out that TV inpainting based algorithm is suitable for general datasets, while as stated in [27], "belief propagation approach is designed only for matrices in which neighboring elements are highly correlated".

1.3.4 Comparison of TV Inpainting with Matrix Completion

Matrix completion aims to correctly populate the unknown values of a matrix based on the knowledge of the known values, given certain assumptions, as discussed in [25]. In this application, if a matrix of geographical coordinates and communication channels is considered, the known values would be the estimated values of the presence of a primary user(s) on the channel. The unknown values would be the channels that were not sensed by the secondary users for any geographic location under consideration. In the matrix completion approach discussed by Candes and Recht [24], a generic low rank matrix, M, defined as a random orthogonal model is used as the matrix to be completed. Employing Singular Value Decomposition (SVD), the matrix M is composed of component matrices U, Σ and V, such that $M = U\Sigma V$. It is assumed that U and V are unstructured and meet the *incoherence condition*, as discussed in [25]. Additional assumptions are that the matrix is of low dimensionality and that the rank is much less than the number of rows or columns of the matrix. The heuristic optimization is to find a matrix of the decision variable, X, that minimizes its nuclear norm, which is the sum of singular values of X. This minimization is subject to the condition that the entries of X be equal to those entries of the matrix M to be completed for which the values are known. This can be shown as,

$$\begin{aligned} &\text{minimize} \quad \| X \|_* \\ &\text{subject to } X_{ij} = M_{ij} \qquad (i,j) \in \Omega \end{aligned} \tag{1.6}$$

where Ω is the set of locations corresponding to the sensed channels in the M array.

OptSpace is an alternative matrix completion algorithm that has been implemented by Keshavan, Montanari, and Oh, [25] which is based on trimming the incomplete matrix to remove some rows and columns whose values are less significant in determining the unknown entries. The trimmed matrix is then adjusted to minimize the error

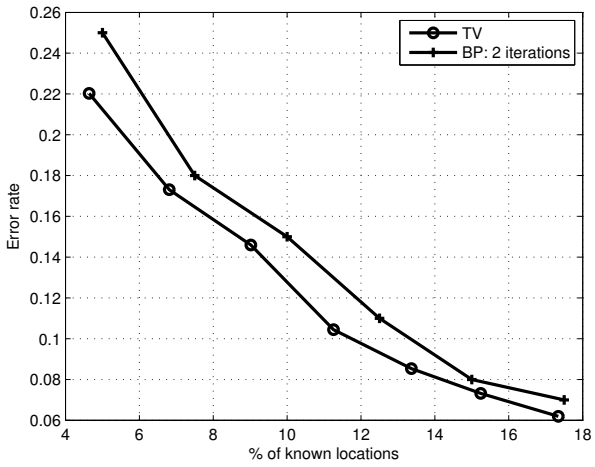

Figure 1.14 Performance comparison between TV inpainting based algorithm and belief propagation method.

relative to the known values via a gradient descent procedure [35].

While matrix completion is widely used for collaborative filtering applications, it may not be as useful for high dimensionality cases, where SVD and nuclear norm minimization may be less efficient. The method also does not take advantage of a priori information about the states of the neighbor elements of the matrix and relies solely on singularity of the matrix [27].

Keshevan et al stipulate in [25] that a condition for matrix completion is that the limit on the rank, r, is

$$r \leq n^{\frac{1}{2}} \tag{1.7}$$

where n is the number of matrix columns. In our experimentation with matrix completion, we found that the rank of the matrix of sampled channel state values was typically too high, i.e. $r > n^{\frac{1}{2}}$, to get an acceptable error rate to compare to total variation inpainting performance.

1.3.5 TV inpainting with low-pass filter

In order to evaluate the performance of the TV inpainting algorithm to time-series spectrum sensing data, the 3-D TV inpainting algorithm is implemented with the low-pass filter to better predict the spectrum status. Assuming that the traffic of the PUs

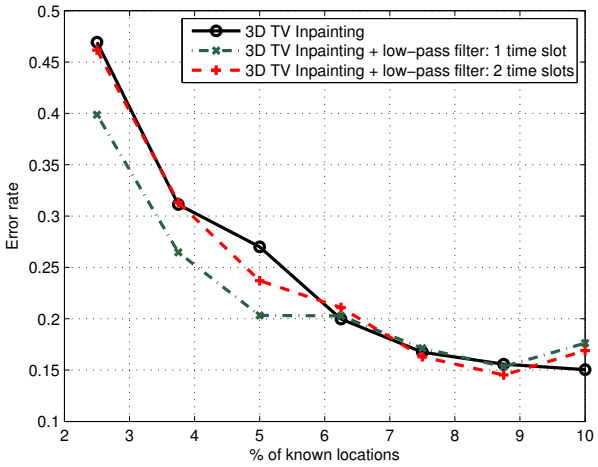

Figure 1.15 Performance of the 3-D TV inpainting algorithm with the low-pass filter.

follows a Poisson process, with arrival rate 1.0 and expected service time of 6 time units, a 10 time-unit spectrum sensing data was generated and used as input to the proposed algorithm. The result is shown in Fig. 1.15. It is observed that in general the error rate by using the low-pass filter is lower than that without considering temporal correlations among samples when the density of the CR users is low. However, when the density of the CR users reaches a certain level (6.3% in this case), the gain vanishes. This is because the CR users cover most of the locations when their density is high and the current measurement gives more accurate information on spectrum occupancy without considering the history. It is also interesting to notice that using one-slot history performs better than using two-slot history. This is because the PUs are very actively changing their channel usages in this simulation scenario. The observation suggests that it is not always better to consider more historical data, and that the amount of history that should be included would be affected by the parameters of the traffic process of the PUs as well as the density of the CR users.

1.3.6 Performance of TV inpainting under spectrum sensing error

The performance of the TV inpainting algorithm under spectrum sensing error is tested. The reconstruction error rate under no noise, 10% spectrum sensing error and 20% spectrum sensing error, are compared in Fig. 1.16. It is observed that the

reconstruction error rate increases with the higher spectrum sensing error, as expected. However, the error rate decreases very fast with more available measurements, e.g., the reconstruction error rate is below 20% when only 15% of locations are sensed and the spectrum sensing error is 10%. Furthermore, the performance gap between the no-error case and error case also decreases with more available measurements, e.g., the performance gap between the no-error case and the 10% error case decreases from 18% to about 5.6%.

Additionally, in Fig. 1.17, we show the TV inpainting error breakdown into false alarms, which is the interpretation that a channel is occupied by a PU when it is not, and missed PU detection, which is the interpretation that a channel is available when it is not. For a low number of known locations, e.g. 5%, the overall error rate is driven by the false alarm error rate. This is due to the inpainting of pixels as occupied, while the algorithm has relatively little information with which to base its decisions on. As the number of known locations increases, the false alarm rate decreases dramatically between 5% and 10% of known locations, thus improving the overall error rate proportionately. The missed detection rate remains in the 5% to 10% range until approximately 20% of the locations are known, and after 30% of the locations are known the missed detection rate monotonically decreases to a final value of 0.8% with 42.3% known locations. The overall error rate is the sum of the missed detection errors and the false alarms and reaches a low of 7.8%. Since missed detection errors can cause interference with PUs, it is very important that they are minimized, even at the expense of increased numbers of false alarm errors. The false alarm errors decrease the efficiency of the SU transmission capability, but it is observed that once enough SUs are present to provide approximately 12% of known locations, the false alarm and missed detection errors are comparable as the rates decrease from 10% to below 5%. The performance of the TV inpainting algorithm then protects the PUs, even at low numbers of SUs, from excessive interference, while improving the transmission opportunity for the SUs as the number of known locations increases.

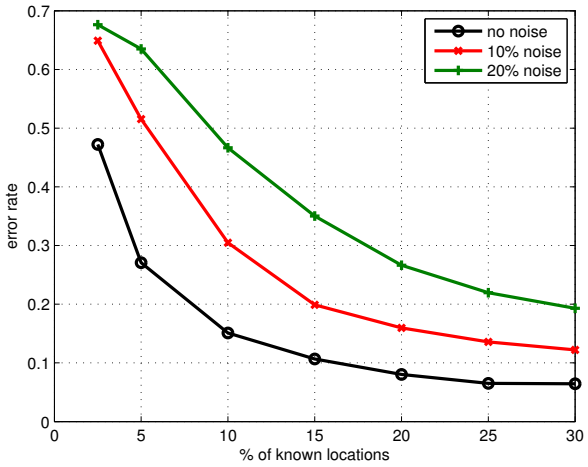

Figure 1.16 Performance of the TV inpainting algorithm under spectrum sensing error.

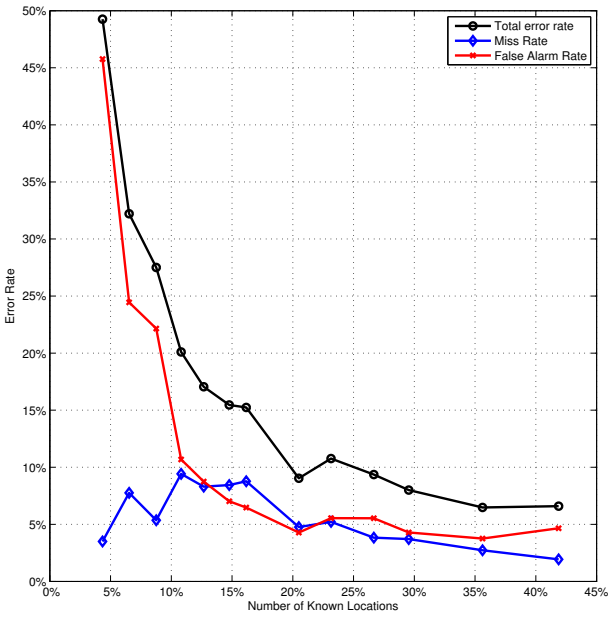

Figure 1.17 Performance of the TV inpainting algorithm showing false alarm and missed PU detection error.

1.4 Related Work and Discussion

There are several recent works using image processing techniques for spectrum occupancy reconstruction in wireless networks. A method based on image processing techniques for the characterization of homogeneous radio-electrical regions is proposed in [36] where certain frequencies can be detected. The authors further improve their method in [37] by using object-based reconstruction technique to combine a number of sensed samples at different geographical positions to build a map of estimated locations and coverage areas of primary transmitters.

For a single spectrum sensor, combining space and time correlation of received signal samples is considered in [19]. The authors conclude that space-time joint signal processing not only improves the sensing performance but also solves the noise uncertainty problem to some extent. Significant work has been done on collaborative/cooperative spectrum sensing when there are multiple spectrum sensors distributed in different locations, and they cooperate to achieve higher sensing reliability. This includes [38], which exploits spatial diversity in multi-user networks to improve the spectrum sensing capabilities. The focus is on the fusion (either data fusion or decision fusion) from distributed cognitive sensors [19], rather than determination of wide-area spectrum status from limited measurements. Furthermore, existing decision fusions have mostly assumed that decisions of different users are independent, which may not be accurate because many users actually receive signals from some common sources.

Compressive sensing provides a means to recover sparse signals and images from a limited number of linear measurements or samples [39]. This method depends on the sparsity of the signal of interest and the incoherence of the sensing modality [40, 41]. However, for effective compressive sensing, it is important that the solution signal be sparse, that is, have relatively few large coefficients in a chosen basis. It is also important that the coherence, or correlation on elements, of the sensing basis and solution basis be low, or largely incoherent. In total variation inpainting, these constraints are not encountered in the effective performance of the algorithm.

The wireless channels considered in this work basically follows the large-scale fading

model. Note that small-scale fading is important for wireless channel modeling, and thus for channel sensing as well. Closed form expressions for probability of detection under AWGN and fading (Rayleigh, Nakagami, and Ricean) channels have been derived [53]. Average probability of detection for energy detector based sensing algorithms under Rayleigh fading channels is derived and the effect of log-normal shadowing is obtained via numerical evaluation in [42]. It is observed that the performance of energy-detector degrades considerably under Rayleigh fading. In this work, the detection results from SUs are considered as input to the proposed algorithm, and our focus is on inference of spectrum status, rather than spectrum detection itself.

In this work, we targeted a large CR network that covers large geographical area and has heterogeneous spectrum usage across the network. The proposed TV inpainting algorithm is centralized in that it requires all the information from the SUs gathered at a central data fusion center. In the case of a CR network that has centralized infrastructure, such as in IEEE 802.22, such information can be gathered readily by the controlling base station. However, for ad hoc CR networks, a mechanism should be put in place to collect such information at a CR network manager node as discussed in [48].

Another requirement on practical fusion algorithms is that they should be robust to data errors due to channel impairment, interference, and noise. The proposed method using TV inpainting takes advantage of correlations in the sensing data from different users, and it is resilient to noise, as demonstrated in the simulation.

1.5 Conclusions and Future Work

In this work, the spectrum status reconstruction problem is formulated in a cognitive radio network as an image determination problem. The method of Total Variation Inpainting is applied to determine the 3-D matrix representing the spectrum occupancy in the network. It is shown that the proposed algorithm outperforms the belief propagation based method. Furthermore, the spectrum status reconstruction problem was also studied using time-series measurements, and proposed to combine a 3-D Total

Variation Inpainting algorithm with a low-pass filter. Simulation results demonstrate the effectiveness of the proposed method when the density of the CR users is low, where the improvement of estimating channel availability is most needed.

Continuing efforts include studying the cases where PUs may not choose consecutive channels and when PUs and CR users are mobile rather than stationary.

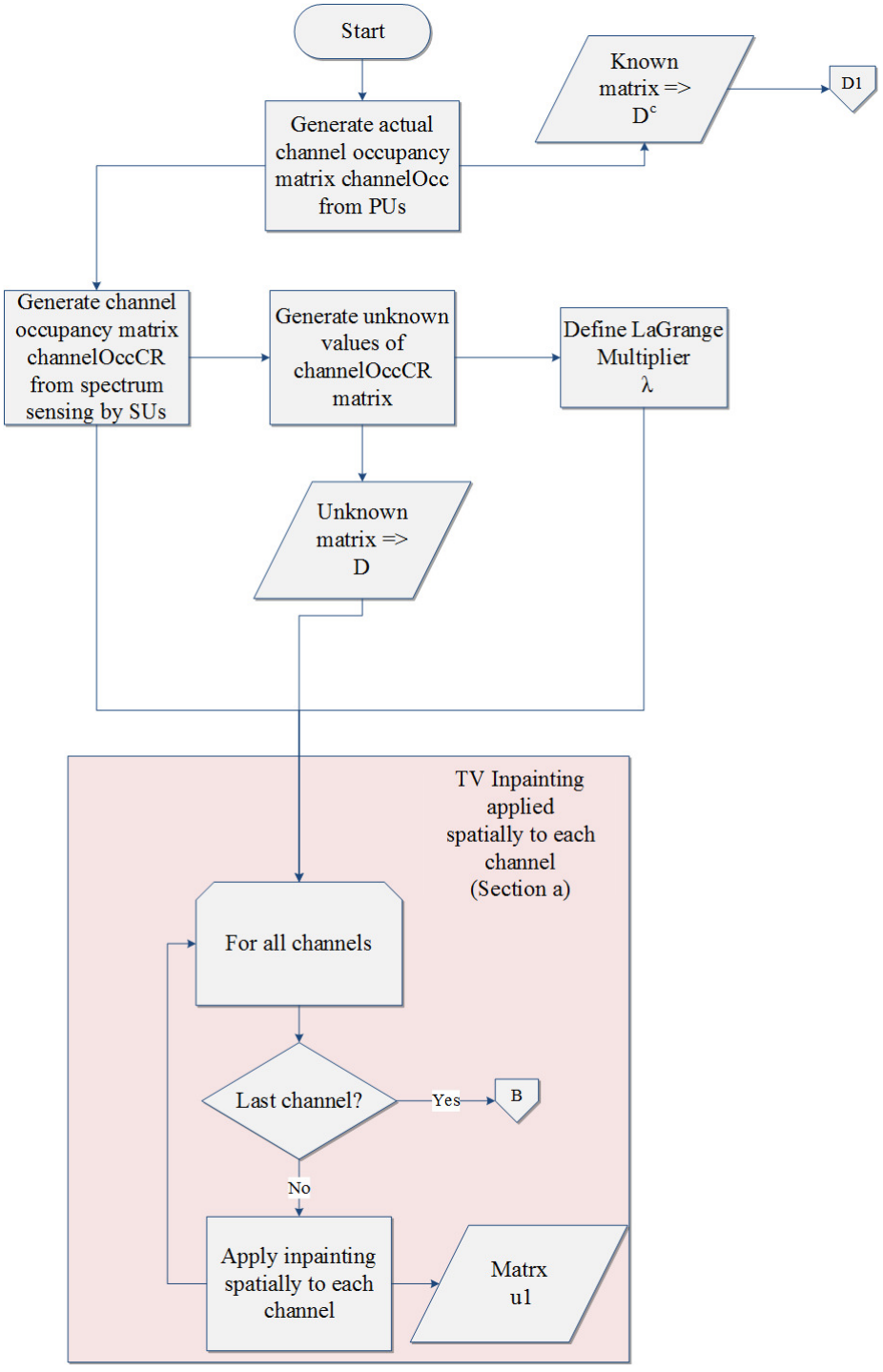

Figure 1.18 Total Variation Inpainting Flowchart 1 - This flowchart shows the initial total variation inpainting algorithm action. The algorithm acquires the channel occupancy matrix from the SU channel sensing results and the actual channel occupancy determined by the PUs. The first processing step of the algorithm is performed to inpaint each spatial plane of the 3-D matrix, where each plane represents a frequency band in the system.

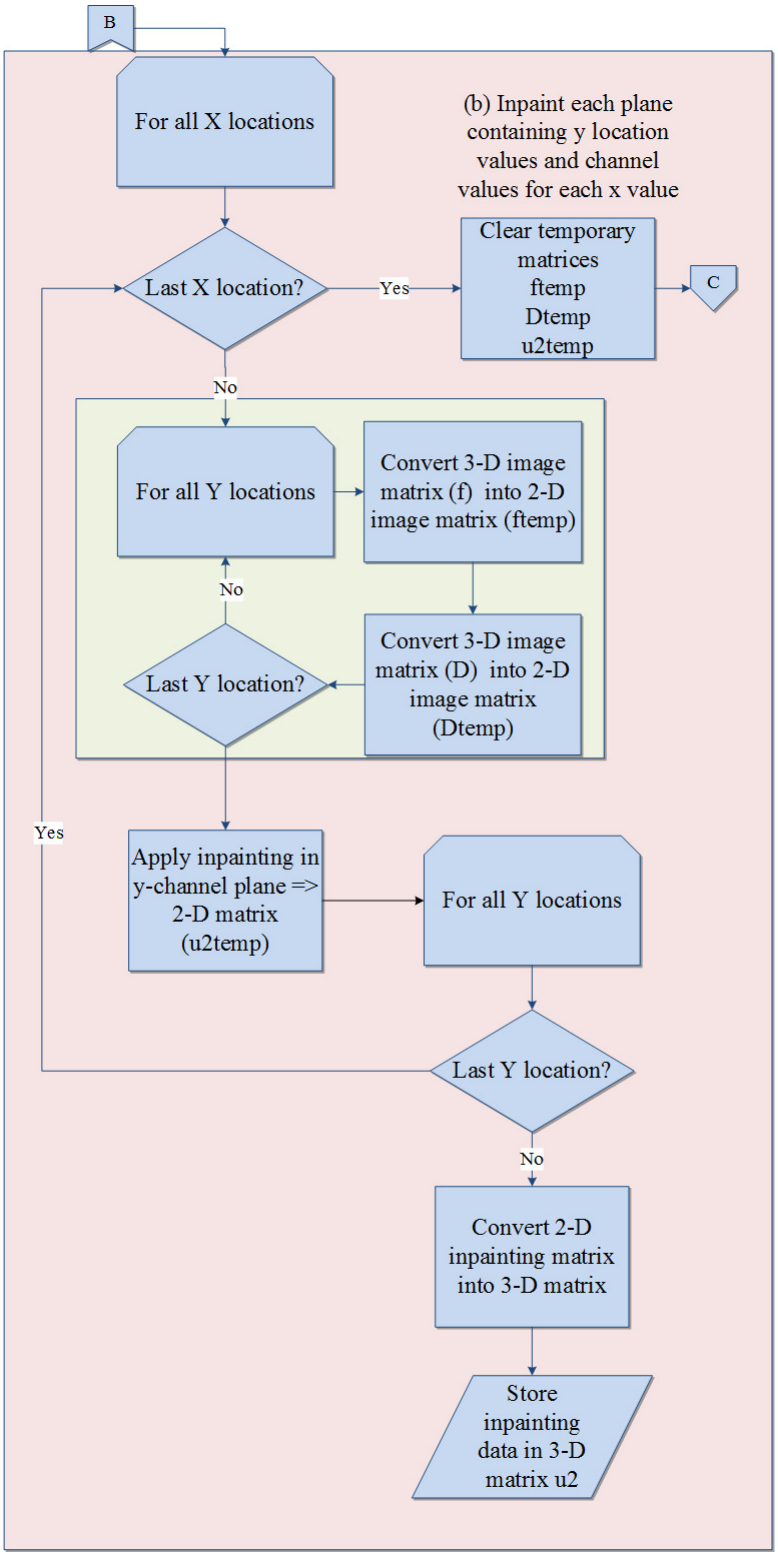

Figure 1.19 Total Variation Inpainting Flowchart 2 - The second processing action of the algorithm is shown in this flowchart. The 3-D matrix is processed in the spectral domain by holding the X direction constant while inpainting the data in the 2-D plane made up of Y spatial values and the frequency bands of the system.

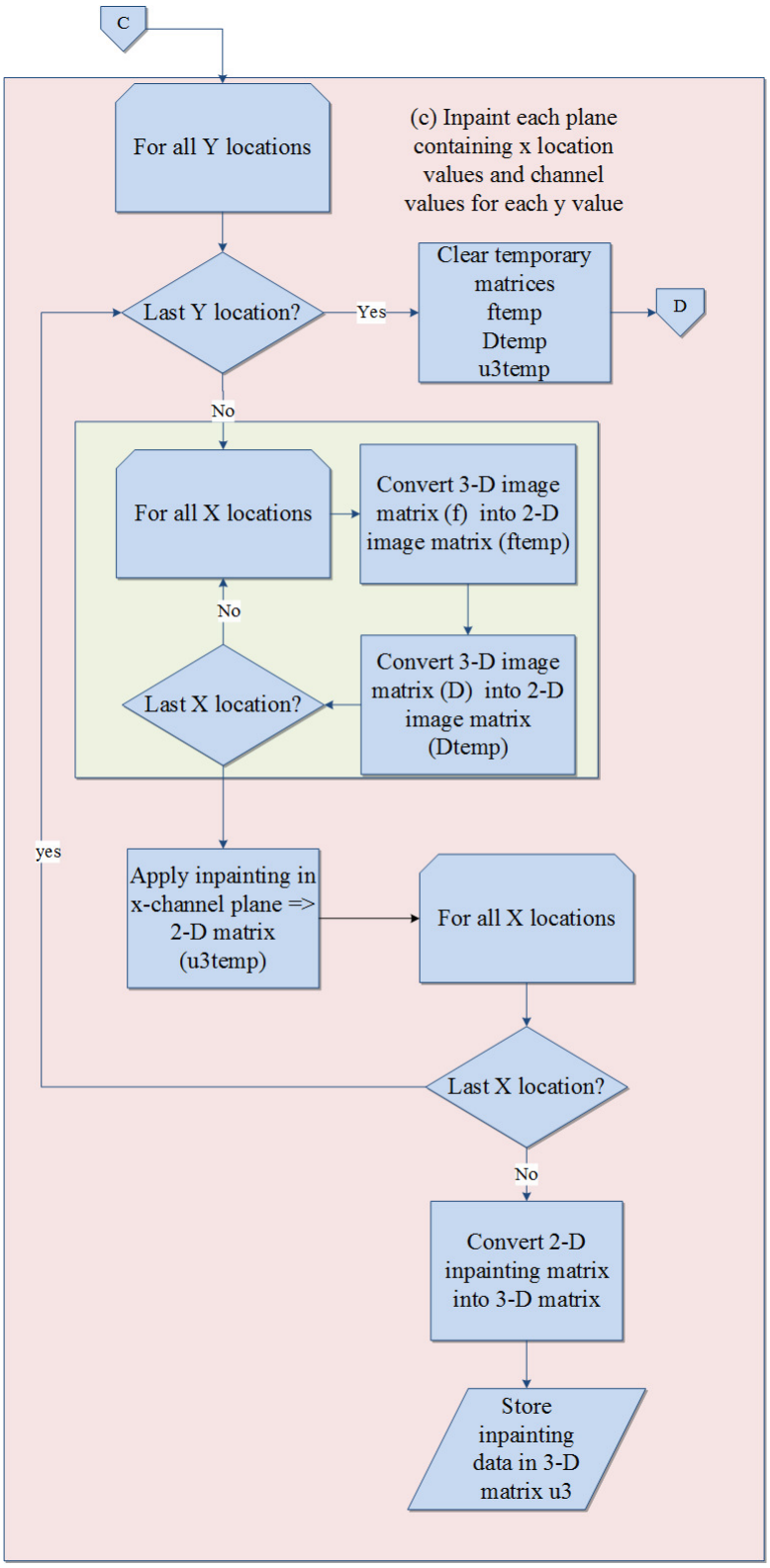

Figure 1.20 Total Variation Inpainting Flowchart 3 - In this flowchart, the same type of processing is repeated for each X location. The algorithm is applied while holding the Y spatial values constant and inpainting the 2-D plane consisting of the X spatial values and the frequency bands in the system.

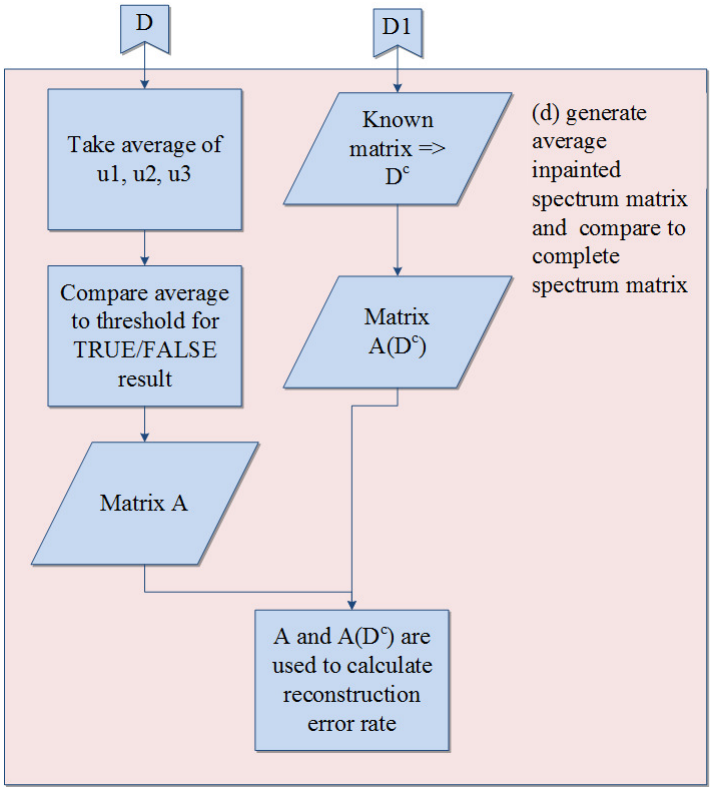

Figure 1.21 Total Variation Inpainting Flowchart 4 - The final portion of the algorithm in this flowchart takes the average of the values for each coordinate of the 3-D matrix from the three values generated in the previous processing. That average is then stored in Matrix A, which is the reconstructed estimate matrix of the values contained in the true channel status Matrix, $A\,(D^c)$. In the algorithm the values of the estimated matrix and the true channel status matrix are compared to determine the amount of error in the estimated matrix.

Chapter 2

Cross-network Spectrum Awareness

In this chapter, the cross-network spectrum sensing is considered for future mission-critical wireless networks employing cognitive radio technology. In military operations and disaster relief efforts, multiple cognitive radio networks may be deployed in the same geographical area for different organizations to access the spectrum collaboratively and provide much needed interoperability enabled by a software radio platform. In this context, cross-network collaboration based spectrum sensing in cognitive radio is studied. Because of security requirements among different organizations, different co-existing networks can only communicate through certain gateway nodes. The limited communication capability of gateway nodes incurs significant challenges for the collaboration. We propose to apply the technique of Belief Propagation for the cross-network collaboration with the assumption of Markov random field for the spectrum occupancies. The cross-network information is embedded into the Belief Propagation framework as *a priori* probabilities. The cross-network messages are also compressed due to the limited communication bandwidth. The effectiveness of the proposed algorithm is demonstrated by extensive simulations.

2.1 Introduction

In military operations, many heterogeneous network elements may be deployed to the same geographical area on a mission. An example is shown in Figure2.1, where many troops and UAVs are deployed in the battlefield. With the advancement of Cognitive Radio (CR) technology, it is expected that many of the network elements will have cognitive capability for providing spectrum awareness and dynamic spectrum access, as well as interoperability enabled by a software defined radio platform, such as the

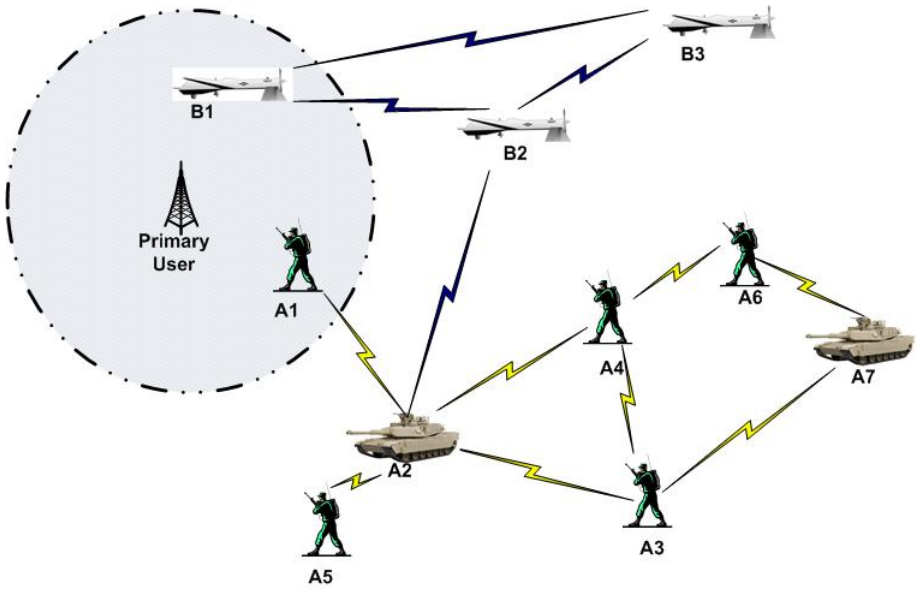

Figure 2.1 An illustration of multiple co-existing cognitive radio networks with gateways (A2 and B2).

Joint Tactical Radio System (JTRS) program being a prime example with its software communication architecture (SCA). As a result, they are able to collaborate and share critical information for maintaining reliable and efficient communications to maximize survivability and efficiency in a harsh environment.

In order to achieve such a vision, spectrum awareness across multiple heterogeneous wireless networks is a must. Cognitive radio has attracted plenty of studies in recent years [88]. In cognitive radio systems, users can search for available spectrum bands and efficiently utilize the opportunities in spectrum. A key procedure is spectrum sensing, which identifies the available spectrum resources and facilitates the subsequent data transmission. Due to the existence of noise, interference and shadowing, the spectrum sensing by a single user may be unreliable. Therefore, many collaborative spectrum sensing schemes are proposed, e.g., [82][83][84][87][93][94], just name a few, in which users exchange information with each other and enhance the reliability of spectrum sensing. Substantial studies on the collaborative spectrum sensing have demonstrated its validity.

Although the collaborative spectrum sensing has been studied intensively, most studies make an implicit assumption, i.e., there is only one network within the area and

nearby users can always communicate with each other for the collaboration in spectrum sensing. However, this assumption may not be valid in many mission-critical systems. Below are two examples:

- Military networks: In a battlefield, there exist multiple heterogeneous wireless networks which may belong to different organizations such as the army and the air force. Different organizations may have different equipment and organizational constraints (such as security), which forbid all the users from different networks to communicate with each other directly.

- First responder networks: When disaster occurs, wireless networks from different departments like fire fighter, emergency medical service and police may co-exist in the same area. Due to different hardware implementations and/or different security levels, users in different networks may not be able to communicate with each other directly.

The lack of mutual communications among different co-existing networks significantly reduces the possibility of collaboration. Therefore, some gateway nodes with powerful communication and computing capabilities can be placed as interpreters/bridges among different networks. An illustration is shown in Figure2.1, in which two networks A and B can communicate with each other via the gateway nodes A2 and B2. The collaboration for spectrum sensing among different networks can be achieved by the gateways.

If the gateway nodes have a very strong capability of communications and the messages from different networks can be disseminated immediately, then the multiple networks can be considered as a single network for the task of spectrum sensing and all existing collaborative spectrum sensing algorithms can be applied. For example, in Figure 2.1, gateway B2 can send the spectrum sensing observations of nodes B1 and B3 to network A. However, gateway nodes may not have such a capability. When the cross-network communication capacity is limited, an intelligent mechanism is needed for the information selection and signaling design of the cross-network communication for collaborative spectrum sensing.

In this work, we *apply the framework of Belief Propagation (BP) for the cross-network collaborative spectrum sensing with gateway nodes having limited communication capability.* Belief Propagation (BP) is an effective approach to utilize the correlations among different random variables (the spectrum occupancies in the context of cognitive radio) for statistical inference. Note that BP based collaborative spectrum sensing has been studied in some existing literatures [92][98]. However, these studies do not consider the case of multiple networks and limited capability of information exchange. A new mechanism is in a pressing need for applying the BP in the more challenging scenario of cross-network collaboration, and it is the focus of this study.

The remainder of this chapter is organized as follows. The system model is introduced in Section 2.2. The BP procedure within a single network is introduced in Section 2.3, as a preliminary of the case of multiple networks. The challenges in the cross-network BP and the proposed method are addressed in Section 2.4. Numerical results and conclusions are provided in Sections 2.5 and 2.6, respectively.

2.2 System Model

In this section, we introduce the system model used in this work. First, we explain the configuration of co-existing networks. Then, the probabilistic relationship between observations and spectrum occupancies is detailed. Finally, we propose a random field model for the spectrum occupancies at different nodes.

2.2.1 Networks

We assume that there are N co-existing networks equipped with cognitive radio. For notational simplicity, we assume that each network has J nodes[1], denoted by n_1, ..., n_J for network n. Each network can be represented by a graph in which each vertex represents a node and each edge represents a communication link between two nodes. Each network has G gateway nodes (included in the J nodes) which can directly communicate to the gateway nodes of other networks, as well as neighboring nodes in

[1]It is straightforward to extend to the case of different numbers of nodes in different networks.

the same network. Therefore, the gateway nodes form an overlay network. We assume that all networks, including the overlay gateway network, are fully connected, i.e., there is only one component in the corresponding graph. For simplicity, we only consider the single channel case in this work. We will extend the algorithm to the multiple channel case in a future study[2].

2.2.2 Observation and Spectrum Occupancy

The spectrum occupancies at different nodes may be different, thus forming a heterogeneous spectrum situation. We denote by a binary random variable X_{n_j} the spectrum occupancy at node n_j. When $X_{n_j} = 1$, the spectrum is busy; otherwise, the spectrum is idle. The observation of spectrum sensing at node n_j is denoted by Y_{n_j}, which could be the measured receive power or estimated cyclostationary features depending on the spectrum sensing methods. We assume that there is a hidden variable Z_{n_j} such that $X_{n_j} - Z_{n_j} - Y_{n_j}$ form a Markov chain. The physical meaning of Z_{n_j} could be the true value of the receive power or the true value of the cyclostationary features. Y_{n_j} is a version of Z_{n_j} contaminated by noise or other random factors. We assume that when $Z_{n_j} \geq \gamma_{th}$, where γ_{th} is a threshold, $X_{n_j} = 1$. For example, when the expected receive power is larger than some threshold, the spectrum is considered as busy, which is the rule of energy detection based spectrum sensing. Therefore, the joint distribution of X_{n_j} and Z_{n_j} is given by

$$\begin{aligned} & P_{XZ}(X_{n_j}, Z_{n_j}) \\ = \;& X_{n_j} I(Z_{n_j} \geq \gamma_{th}) \frac{P_Z(Z_{n_j})}{\int_{\gamma_{th}}^{\infty} P_Z(z)dz} \\ + \;& \left(1 - X_{n_j}\right) \left(1 - I(Z_{n_j} \geq \gamma_{th})\right) \frac{P_Z(Z_{n_j})}{\int_{-\infty}^{\gamma_{th}} P_Z(z)dz}, \end{aligned} \tag{2.1}$$

where I is the characteristic function and P_Z is the marginal distribution of Z_{n_j}. We also assume that the conditional distribution of Y_{n_j} given Z_{n_j} is known, which is denoted

[2]We have employed Belief Propagation for spectrum awareness within one network for the multiple channel case in a previous study [86]

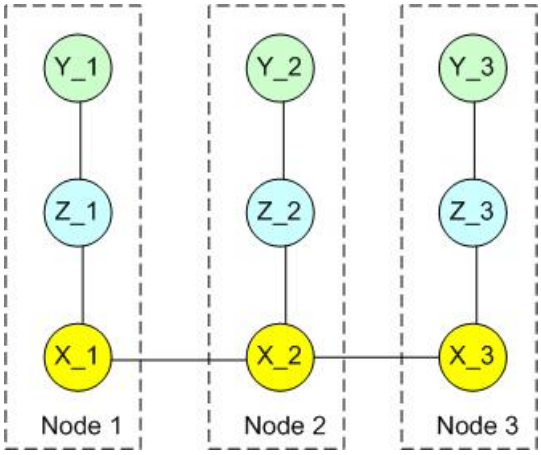

Figure 2.2 An illustration of the random field.

by $P_{Y|Z}$. Therefore, the joint distribution of X_{n_j}, Y_{n_j} and Z_{n_j} is given by

$$\begin{aligned} P_{XYZ}(X_{n_j}, Y_{n_j}, Z_{n_j}) &= P_X(X_{n_j}) P_{Z|X}(Z_{n_j}|X_{n_j}) \\ &\times P_{Y|Z}(Y_{n_j}|Z_{n_j}). \end{aligned} \tag{2.2}$$

For simplicity, we assume that all these probabilities are identical for all nodes in all networks.

2.2.3 Random Field

We assume that the spectrum occupancies at nearby nodes are correlated, which is validated by the measurements in [96]. In practice, the correlation could be very complicated and different for different nodes. In this work, we use the Markov random field model for the spectrum occupancies, which facilitates the application of BP and the cross-network information exchange. *Note that the model is assumed only in the algorithm. We used more practical spectrum occupancies when we test its validity in the simulations.*

In this section, we consider only the random field for one network, which will be extended to the multiple network case later. Therefore, we use j instead of n_j as the node index. In the random field, each spectrum occupancy variable X_j is connected to the hidden variable Z_j, as well as the spectrum occupancy variables of neighboring nodes. An example is given in Figure 2.2, in which the random field model is shown

for network B in Figure 2.1. We assume that the random field is Markovian, i.e., *each random variable is independent of the non-neighboring nodes given the true values of the neighboring nodes*. For example, for X_1, we have

$$P(X_1|\text{all other nodes}) = P(X_1|Z_1, X_2). \tag{2.3}$$

We further assume that the joint probability can be factored into the following way:

$$P(\mathbf{v}) \quad = \quad \prod_r \phi_r(r) \prod_{s\sim r} \psi_{s,r}(s,r), \tag{2.4}$$

where $\mathbf{v}$ means all random variables, $\sim$ means the relationship of neighboring in the random field and ϕ and ψ are called local and compatibility functions, which will be specified later.

Then, our essential goal of spectrum sensing is to compute the marginal probability of the spectrum occupancy given the observations, i.e.,

$$P(X_j|\mathbf{y}) = \sum_{X_i, i\neq j} \sum_{Z_k} P(\mathbf{v}|\mathbf{y}), \tag{2.5}$$

where $\mathbf{y}$ is the vector of all observations. The final decision rule of spectrum sensing is given by

$$\text{decision} = \begin{cases} 1, & P(X_j|\mathbf{y}) \geq P_{th} \\ 0, & P(X_j|\mathbf{y}) < P_{th} \end{cases}, \tag{2.6}$$

where P_{th} is a predetermined threshold.

2.3 Single-network BP

In this section, we discuss the BP in a single network, which provides a foundation for the problem of cross-network BP in the next section. We first introduce the message passing procedure, which is standard for BP. Then, we define the compatibility function for facilitating the message passing. Since we consider only a single network, the nodes are indexed using 1, 2, ..., J.

2.3.1 Message Passing

BP is an efficient algorithm for computing the marginal probability of the spectrum occupancy in (2.5). In the BP procedure, neighboring random variables in the random field exchange information in an iterative way. For a random variable r and a neighboring random variable s ($s \sim r$) in the random field, random variable s sends the following message to random variable r, which is given by

$$m^l_{s\to r}(r = R) = \sum_{s=S} \psi(s, r)\phi(S) \prod_{k\sim s, k\neq r} m^{l-1}_{k\to s}(s = S). \tag{2.7}$$

After sufficiently many, say L, iterations, the marginal probability at random variable r can be computed using an approximation, which is given by

$$b_r(r = R) = C\phi(R) \prod_{s\sim r} m^L_{s\to r}(r = R), \tag{2.8}$$

where C is a normalization constant making $\sum_R b_r(r = R) = 1$.

2.3.2 Compatibility Function

The previous subsection provides the general procedure of message passing in BP. In this section, we detail the messages between different types of random variables by substantiating the compatibility functions.

Y to Z within one node

When $r = Z_j$ and $s = Y_j$, the message is given by

$$m^l_{Y_j\to Z_j}(z) = \frac{P_{Z|Y}(z|Y_j)}{P_Z(z)}, \tag{2.9}$$

by assuming the compatibility function of Z_j and Y_j is given by

$$\psi_{Z_j,Y_j} = \frac{p_{Z,Y}(Z_j, Y_j)}{p_Z(Z_j)p_Y(Y_j)}. \tag{2.10}$$

Z to X within one node

When $r = X_j$ and $s = Z_j$, the message is given by

$$m^l_{Z_j\to X_j}(x) = \int_z \frac{P_{X|Z}(x|z)}{P_X(x)} p_Z(z) m^{l-1}_{Y_j\to Z_j}(z)dz, \tag{2.11}$$

which is very similar to (2.9). Combining (2.9) and (2.11), we have

$$m^l_{Z_j \to X_j}(x) = \int_z \frac{P_{X|Z}(x|z)}{P_X(x)} P_{Z|Y}(z|Y_j) dz, \tag{2.12}$$

which is computed in the first round and does not change in the following iterations.

X to X across different nodes

When $r = X_i$ and $s = X_j$, the message is sent across different nodes (note that the previous two types of messages are processed within the same node). We assume that the message is given by

$$\begin{aligned} m^l_{X_i \to X_j}(x) &= \sum_{\tilde{x}=0,1} P_X(\tilde{x}) m^{l-1}_{Z_i \to X_i}(\tilde{x}) \\ &\times \prod_{k \sim i, k \neq j} m^{l-1}_{X_k \to X_i}(\tilde{x}) P_{X,X}(x|\tilde{x}). \end{aligned} \tag{2.13}$$

Here, $P_{X,X}(x|\tilde{x})$ is the probability that the spectrum occupancy is x provided that the spectrum occupancy of a neighboring node is $\tilde{x}$. In practice, this conditional probability is dependent on different pairs of nodes. It is too complicated to estimate this probability since a large amount of training samples are needed. Therefore, we adopt the following simple definition of this probability, which is given by

$$P_{X,X}(x|\tilde{x}) = \begin{cases} \eta_1, & \text{if } x = \tilde{x} \\ 1 - \eta_1, & \text{if } x \neq \tilde{x} \end{cases}, \tag{2.14}$$

where η_1 is a constant for any pair of nodes. We assume that $\eta_1 > 0.5$, i.e., nearby nodes tend to have the same spectrum occupancies. The larger η is, the more correlated the spectrum occupancies are.

2.4 Cross-network BP

In this section, we extend the single-network BP to the cross-network one. We first explain the two new challenges in the multiple network case. Then, we address the challenges by proposing new algorithms.

2.4.1 Challenges

For the case of multiple co-existing networks, if the information exchange among nodes and networks is sufficiently fast, the multiple networks can be considered as a single network and the BP framework in Section 2.3 still applies. However, for practical case, there exist the following two challenges for the case of multiple networks:

- Limited gateway capacity: When J (recall that J is the number of nodes in each network) is large and G (recall that G is the number of gateway nodes) is small, each gateway node has to convey a lot of information if each cross-network message is from a specific node to another specific one like the messages in a single network. The communication links among gateway nodes may not be able to support all the traffic.

- Significant delay: Due to the limited communication capacity of neighboring nodes in the same network, the information from one node in a network to one node in another network may be significantly delayed. For example, in Figure 2.1, nodes A1 and B1 cannot communicate directly although they are nearby. Therefore, if nodes A1 and B1 want to collaborate, a message from A1 to B1 needs to take the path of $A1 \rightarrow A2 \rightarrow B2 \rightarrow B1$ with four hops. Therefore, a message may arrive at the destination after several spectrum sensing periods and the spectrum occupancy could have changed.

In the remainder of this work, we address the above two challenges separately.

2.4.2 Message Compression

To address the limited communication capacity among gateway nodes, the gateway nodes need to fuse and compress the messages from different nodes. In this work, we propose a heuristic approach which aggregates the messages within the same region, thus compressing the information exchange.

In the message compression scheme, the area is divided into multiple regions. The definitions of regions are common to all networks. The larger the communication capacity is, the smaller regions are defined. Suppose that, network n, nodes n_{k_1}, ..., n_{k_m}

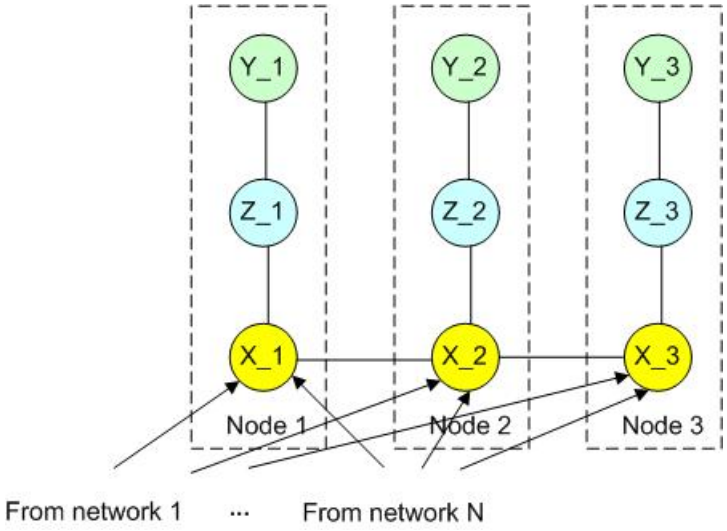

Figure 2.3 An illustration of the random field with cross-network information exchange.

belong to region R. Then, a message is generated at the end of the L iterations, which is given by

$$M_R^n(x) = \frac{1}{k_m} \sum_{i=1}^{m} \frac{b_{X_{n_i}}(x)}{P_X(X = x)}. \tag{2.15}$$

This is the average of the beliefs of the k_m nodes within the same region. Then, this message is sent to other networks via the gateway and then multicasted to the nodes within region R. Note that it is interesting to study the routing in the gateway overlay network and the routing of the compressed message in each network. However, it is beyond the scope of this work due to the limited space. For simplicity, we assume that the compressed message can reach each node within the region after D spectrum sensing periods.

The cross-network messages are directly incorporated into the computation of beliefs in (2.8), as illustrated in Figure 2.3. Note that the cross-network messages should not be used during the intra-network message passing since they are from the same source. We use the following conditional probability when incorporating the inter-network messages, which is given by

$$P_{X,X}(x|\tilde{x}) = \begin{cases} \eta_2, & \text{if } x = \tilde{x} \\ 1 - \eta_2, & \text{if } x \neq \tilde{x} \end{cases}, \tag{2.16}$$

where η_2 is a constant. We assume that $\eta_2 < \eta_1$ since the inter-network messages provide

less accurate information about spectrum occupancies due to the message compression.

2.4.3 Mitigation of Delay

If the spectrum occupancies have no correlation in time (i.e., independent in time), the delayed messages are not useful for the spectrum sensing, thus invalidating the cross-network collaboration. However, in many practical case, the spectrum occupancy does not change very rapidly (e.g., the data transmission of primary users should last for a period of time), which provides time correlations. In this work, we adopt a simple approach which changes the message $M_R^n(x)$ to $(M_R^n(x))^{\frac{\alpha}{D_n}}$, where $\alpha > 0$ is a predetermined constant and D_n is the delay (measured in spectrum sensing periods) of the cross-network message from network n. We have

$$\left(\frac{M_R^n(1)}{M_R^n(0)}\right)^{\frac{\alpha}{D_n}} \to 1, \text{ as } D_n \to \infty, \tag{2.17}$$

which means that, when the delay is large, the cross-network messages provide little information.

Denote by $b_{X_{n_j}}(x)$ the belief obtained from the intra-network BP in (2.8). Incorporating the above discussions, we refine the belief using the cross-network messages, which is given by

$$\tilde{b}_{X_{n_j}}(x) = C' b_{X_{n_j}}(x) \left(\prod_{m \neq n} M_R^m(x)^{\frac{\alpha}{D_m}}\right), \tag{2.18}$$

where C' is a new normalizing constant.

2.4.4 Summary of Algorithm

The cross-network collaborative spectrum sensing algorithm is then summarized in the following procedure.

2.5 Numerical Results

In this section, we use numerical simulations to demonstrate the performance of the proposed algorithms.

Procedure 1 Cross-network Collaborative Spectrum Sensing

```
Initializing the parameters α and η.
for Each spectrum sensing period do
    Each node receives cross-network messages.
    for Each BP iteration do
        Each node computes the messages using (2.12) and (2.13).
        Neighboring nodes exchange messages.
    end for
    Each node computes the belief using (2.18).
    Each node makes the decision using (2.6).
    Gateway nodes aggregate the beliefs of individual nodes and propagate to other networks.
end for
```

2.5.1 Configuration

In the simulations, three primary users are randomly located within a 5km×5km area. Meanwhile, 10 secondary networks, each having 100 nodes, are co-located in the same area. We assume that the maximum communication range of normal secondary users is 100m while that of the gateway nodes is 200m. The impact range of a primary user is 1km.

The communication path loss is given by $l = 26.5 + 35 \log_{10} d(\text{dB})$, where d is the distance measured in meters. We assume that the observation Y is the received power in dB scale, which is impacted by shadow fading, fast fading and noise. The hidden variable Z is the expected received power in dB scale, which is determined by only the path loss. Similarly to [82][83], we assume that Y is Gaussian distributed with expectation Z and variance σ_n^2. We also assume that Z is uniformly distributed within a very large range. Therefore, the conditional probability is given by

$$\begin{aligned} P_{Z|Y}(z|y) &= \frac{P_{Y|Z}(y|z)P_Z(z)}{\int P_{Y|Z}(y|z')P_Z(z')dz'} \\ &\approx \frac{1}{\sqrt{2\pi\sigma_n^2}} \exp\left(-\frac{(z-y)^2}{\sigma_n^2}\right), \end{aligned} \tag{2.19}$$

i.e., the conditional probability of Z can be approximated by the Gaussian distribution with expectation Y and variance σ_n^2. Five iterations are used for each BP procedure. We did not optimize the parameters η_1 and η_2, which are simply set to 0.8.

The performance of spectrum sensing is measured using the receiver operation characteristic (ROC) curves, in which the detection probabilities and false alarm probabilities are plotted. A ROC curve closer to the upper left corner implies a better performance. Each ROC curve is obtained from using 10 different thresholds in the decision rule of (2.6) with 20 random deployments of the primary and secondary users.

2.5.2 Stationary Spectrum

We first assume that the spectrum is stationary or changes very slowly. Then the delay of the inter-network messages does not impact the performance much. However, the individual beliefs of the secondary users in different networks cannot be delivered to other networks due to the limited communication capacity.

In Figure 2.4, the performance is compared for the cases of no collaboration, only intra-network collaboration and inter-network collaboration (also including the intra-network collaboration). For the inter-network collaboration, the size of each region is 250m×250m. We observe that the intra-network collaboration can improve the performance. However, the performance gain is limited. The inter-network collaboration can further improve the performance of spectrum sensing. For example, when the false alarm rate is 10%, the miss detection probability dropped from 20% to 10%.

We also tested the impact of the number of nodes within each network. In Figure 2.5, we show the performance of inter-system collaboration and intra-system collaboration when there are 100 or 400 nodes within each network. We observe that the performance is improved when the number of users within each network is increased. Even when there are 400 nodes within each network, the performance gain of the inter-system collaboration is still significant.

2.5.3 Dynamic Spectrum

In Figure 2.6, we assume that one of the primary users changes its activity with time. The dynamic of this time-varying primary user is assumed to be a two-state, busy (B) and idle (I), Markov chain with state transition probability $Q_{s_1 s_2}$. We set $Q_{BB} = 0.95$ and $Q_{II} = 0.9$. We also assume that the cross-system messages incur the

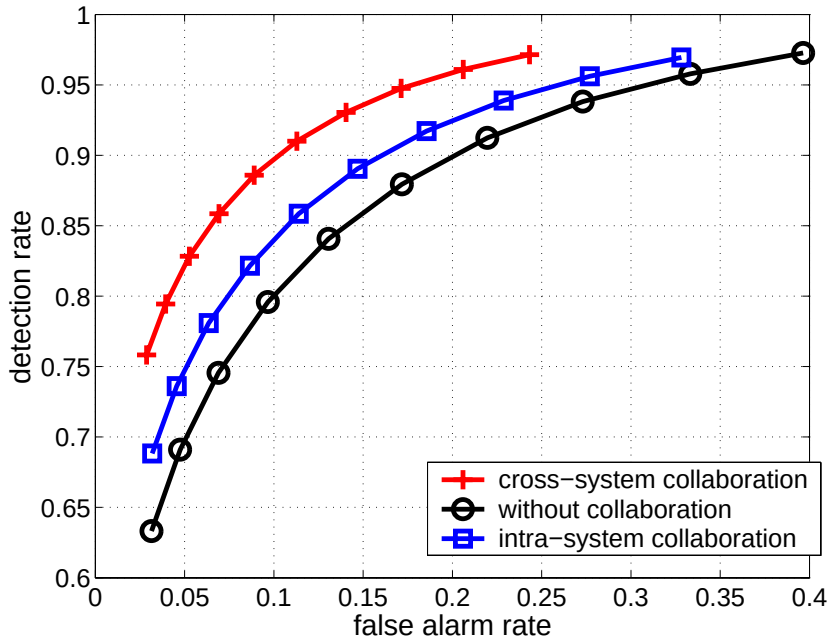

Figure 2.4 ROC curves for the case of no delay when there are 200 nodes in each network.

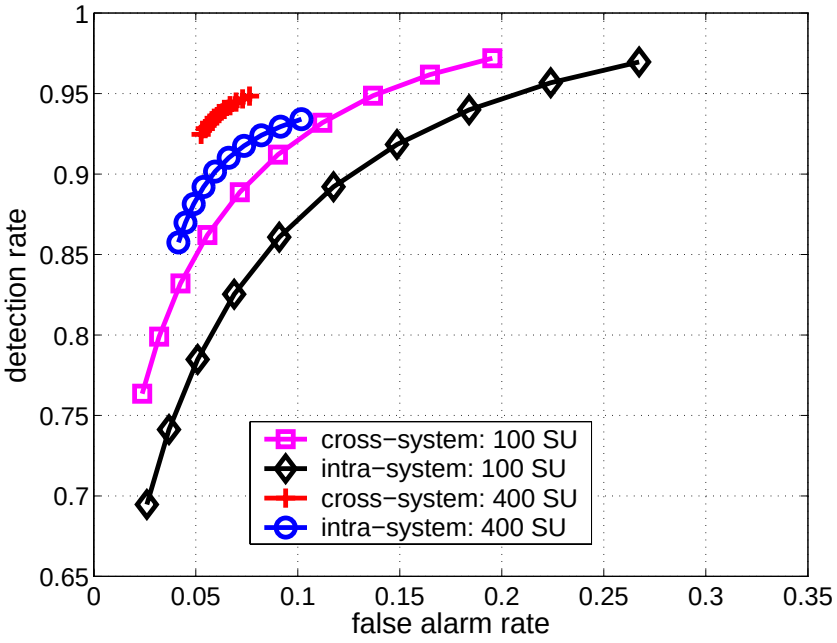

Figure 2.5 ROC curves for the case of no delay when there are 200 / 400 nodes in each network.

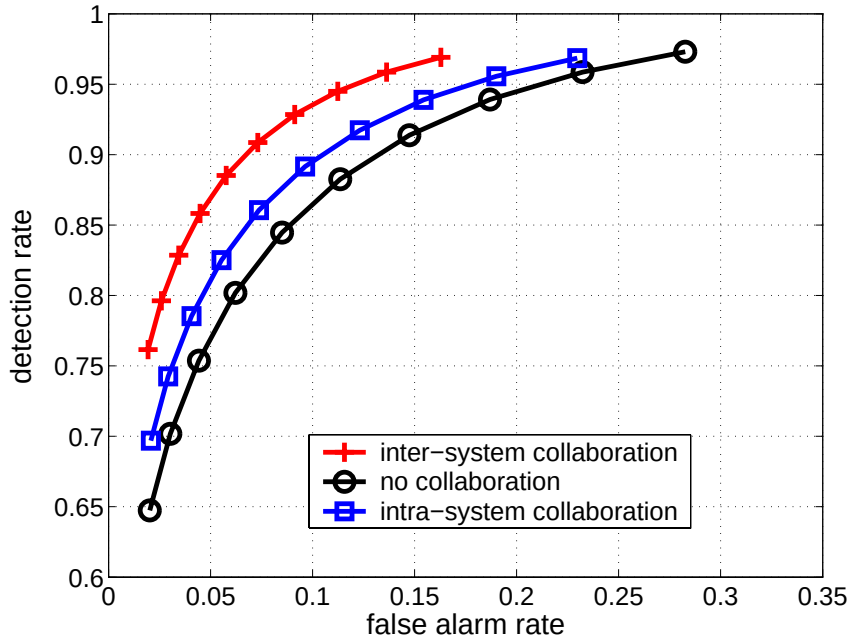

Figure 2.6 ROC curves for the case of one time slot delay when $Q_{II} = 0.95$ and $Q_{BB} = 0.9$.

delay of one spectrum sensing period. All other configurations are the same as those in Figure 2.4. We observe that, despite the delay of the cross-system messages, the cross-system collaboration achieves significantly better performance than other approaches.

In Figure 2.7, we assume that two primary users change their activities with time. The state transition probabilities are given by $Q_{BB} = 0.6$ and $Q_{II} = 0.7$ for both users. Therefore, the spectrum occupancies are much more dynamic than that in Figure 2.6. We observe that the performance gain of the cross-system messages is reduced. However, it still attains an obviously better performance than the cases of intra-system collaboration and no collaboration.

2.6 Conclusions

In this work, the collaboration of spectrum sensing across multiple co-deployed networks is investigated in the context of future mission-critical systems employing cognitive radio technology. The framework of belief propagation has been applied for the spectrum sensing information exchange within each network. Among different networks,

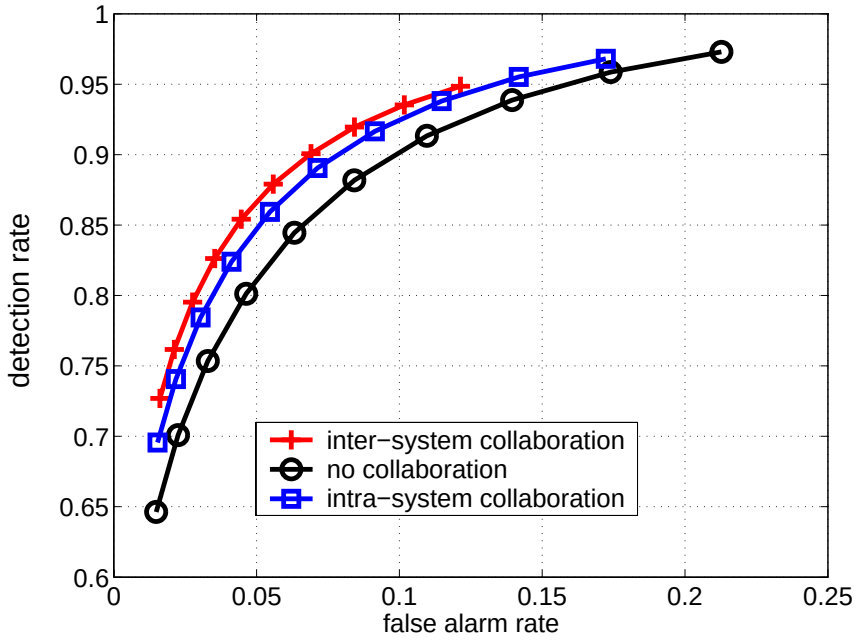

Figure 2.7 ROC curves for the case of one time slot delay when $Q_{II} = 0.7$ and $Q_{BB} = 0.6$.

we have proposed to use gateway nodes for the inter-network communications because of the requirements for maintaining organizational structure. The challenges of limited communication bandwidth among gateways and possible delays have been addressed and efficient heuristic algorithms are proposed to reduce the complexity and aimed for potential implementation. The proposed algorithms have been demonstrated using extensive simulations and the results show that collaborations across multiple networks provides significant gain. The proposed framework is critical for achieving collaborative intelligence for future cognitive radio networks to maximize efficiency and survivability. Currently we are in the process of extending the proposed method to multi-channel multi-network scenarios.

Chapter 3

Joint Congestion Control and Routing Subject to Dynamic Interruptions in Cognitive Radio Networks

In this chapter, we consider joint congestion control and routing in cognitive radio networks for robustness enhancement. Cognitive radio networks suffer from dynamic interruptions from primary users. The joint congestion control and routing are tackled using stochastic control techniques. Centralized dynamic programming is applied for the primal optimization, which provides a performance upper bound. Q-learning is applied when the primary user knowledge is unknown. Dual optimization based decomposition is used to decentralize the stochastic control. A heuristic scheme based on the limited lookahead policy (LLP) and binary pricing is proposed to tackle the prohibitive difficulty in the dual optimization. Numerical simulation shows that the proposed algorithms achieve the optimal or near-optimal performance.

3.1 Introduction

Cognitive radio networks, illustrated in Figure 3.1, are attracting more and more studies in recent years due to its capability of alleviating the problem of spectrum underutilization. The fundamental change of spectrum access incurs significant challenges to all layers in cognitive radio networks. Researchers have proposed new algorithms and protocols to combat the new challenges, e.g. Quality of Service (QoS) aware scheduling [110][111], spectrum-aware routing [106][108][113], distributed resource allocation [109] and a new TCP protocol incorporating the activities of primary users [102].

As the new scheme of spectrum access incurs significant impacts on all layers, it yields a better performance to design the network across different layers of cognitive radio networks. Note that the cross-layer design has been considered for scheduling

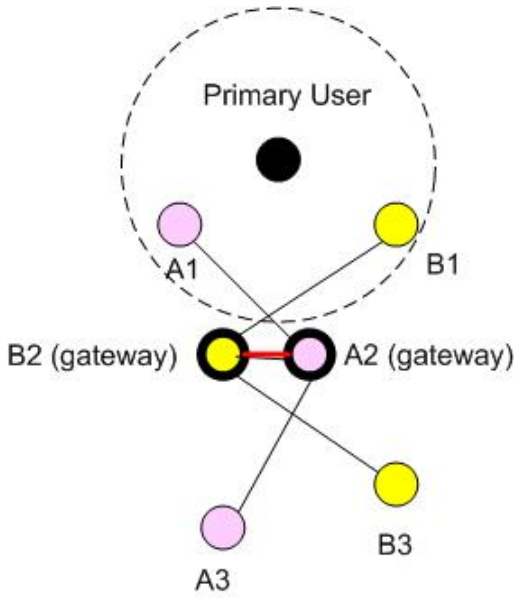

Figure 3.1 Illustration of cognitive radio network subject to interruptions.

[110] and routing [108] in cognitive radio networks. However, no uniform mathematical framework is proposed in these studies. Note that the cross-layer design framework has been widely used for analyzing and designing networks in the first decade of this century [101][104][105]. For example, the joint congestion control and routing (TCP/IP) has been studied in [112]. However, the corresponding studies are mainly focused on stationary networks, i.e., the link qualities do not change dynamically and the optimization problem is for only one snapshot. It is straightforward to extend these techniques to cognitive radio networks operating in relatively stationary spectrum bands, like TV band. However, for spectrum bands with dynamic occupancies of primary users, we face the following two new challenges:

- *Dynamic Interruptions*: Since a secondary user must quit the corresponding frequency band, each emergence of a primary user causes an interruption to the data traffic of secondary users within its interruption range. Even if the secondary users can look for new channels, the procedure of channel switching and sensing new channels also incurs a significant overhead. If the traffic of primary users is bursty, the interruptions are dynamic and random, thus necessitating the stochastic control of the cognitive radio network.

- *Medium Time Scale*: In many situations, the time scale of interruptions from primary users is medium, which incurs trouble to the strategy optimization. For small time scale (say, a few milliseconds), similar to fast fading, the randomness can be alleviated in the physical layer, e.g. using channel coding to correct errors. Therefore, the negative effect can be smoothed out with time and there is no need for re-routing. For large time scale (say, ten minutes), the optimal route and the transport layer rate can be used for a long period of time. A re-routing or adjustment of transmission rate is infrequent and incurs little overhead. However, for a medium time scale, it is impossible to alleviate the interruptions using approaches like channel coding and it is inefficient to stick to the same transmission rates and routes.

In this work, we tackle the problem of joint congestion control and routing in cognitive radio networks subject to the above problems. The procedure of congestion control (i.e., adjusting data rate) and routing (i.e., the decisions of re-routing and path selection) are coupled with each other. Therefore, a joint optimization is needed. Due to the dynamic interruptions and the medium time scale, a stochastic control framework is applied to the joint congestion control and routing. Then, the challenge is *how to derive the optimal or near-optimal strategy in various situations*. For the centralized case, dynamic programming and Q-learning are both applied for the cases with and without primary user information, respectively. For the decentralized case, the stochastic control is decomposed to individual controls via Lagrange pricing. In sharp contrast to one-stage optimizations in stationary networks, the strategies of individual data flows are still coupled even though the capacity constraint has been decoupled via pricing. A heuristic scheme based on a limited lookahead policy and binary pricing scheme is then proposed to break the coupling. Note that the study in this work does not concern the detailed design of protocols. However, it provides insights and tools for the design of practical cognitive radio networks.

The remainder of this chapter is organized as follows. The system model for cognitive radio networks will be introduced in Section 3.2. The elements of control, primal

optimization and dual optimization are discussed in Sections 3.3, 3.4 and 3.5, respectively. Numerical results and conclusions are provided in Sections 3.6 and 4.6, respectively.

3.2 System Model

We consider a cognitive radio network, in which there are L cognitive radio links and N data flows. We denote by $x_s(t)$ the rate of data flow s at (discrete) time t. The rates are stacked into one vector $\mathbf{x}(t) = (x_1(t), ..., x_N(t))$. The utility of flow rate x_s is given by $U_s(x_s)$, where U_s is the utility function of data flow s. The time is divided into routing periods. We assume that each routing period is sufficiently long such that the rate allocation can be completed within one routing period. The routes of different data flows at routing period t are represented by a matrix $\mathbf{R}(t)$, where the rows stand for links and columns mean data flows. Data flow j passes through link i if the element $R_{ij}(t)$ equals 1. Otherwise, $R_{ij}(t) = 0$. We assume that there are N_s possible routes for data flow s. We assume that the capacity of link i is given by c_i. We use one vector, $\mathbf{c} = (c_1, ..., c_L)$, to denote the capacities of all links. For simplicity, we consider the thermal-limited regime and ignore the coupling of interference. When the interference is strong, we can consider joint congestion control, routing and scheduling. However, it is beyond the scope of this work.

We use a vector $\mathbf{m} = (m_1, ..., m_L)^T$ to represent primary users' activities. When $m_i = 1$, link i is not occupied by primary users and can be used by secondary users; otherwise, $m_i = 0$. For simplicity, we assume that the spectrum occupancy is constant within each routing period. The activity of each primary user is modeled as a two-state Markov chain. The two states are busy (B), i.e., occupied by primary users, and idle (I), i.e., not occupied by primary users. The state transition probabilities are denoted by $P_{s_1 s_2}$, where s_1 and s_2 are two consecutive states.

The re-routing procedure may be activated by the emergence of primary user, which may block the corresponding data flow for a long period of time. However, the re-routing may incur unnecessary overhead if the primary user's interruption is actually

short. We assume that each re-routing procedure takes T_{rr} routing periods, i.e., only after T_{rr} routing periods can the data flow resume operation. We also assume that each re-routing incurs a penalty P_{rr} since a lot of information exchange is needed for the re-routing procedure.

3.3 Basic Elements of the Stochastic Control

For the joint congestion control and routing in cognitive radio networks subject to dynamic interruptions of primary users, we adopt the framework of optimization based cross-layer design [101][104][105]. For simplicity, we consider only single-channel case here. For multi-channel case, we can extend the action space to incorporate channel selection. In this section, we explain the three elements in the joint congestion control and routing, namely reward function, state space and action space.

3.3.1 Reward Function

We consider the discounted sum of all data flows from routing period 1 to routing period T. The optimization problem is thus given by

$$\begin{aligned} &\max \sum_{t=1}^{T} \beta^{t-1} r_t \\ &s.t. \qquad \mathbf{R}(t)\mathbf{x}(t) \leq \mathbf{c} \odot \mathbf{m}(t), \end{aligned} \tag{3.1}$$

where r_t is the network-wide reward obtained at routing period t, which is given by

$$r_t = \sum_{s=1}^{N} U_s(x_s(t))\phi_s(t) - P_{rr} \sum_{s=1} \theta_s(t). \tag{3.2}$$

where $0 < \beta < 1$ is a discounting factor, $\theta_s(t)$ is the characteristic function of the event that re-routing begins at t, the function $\phi_s(t)$ indicates whether the data flow is in active state and $\odot$ means elementwise multiplication, i.e., the capacities of all links are modulated by the spectrum occupancy vector $\mathbf{m}(t)$. Obviously, the first term in the reward function is the reward of data flow and the second term is the penalty for re-routing.

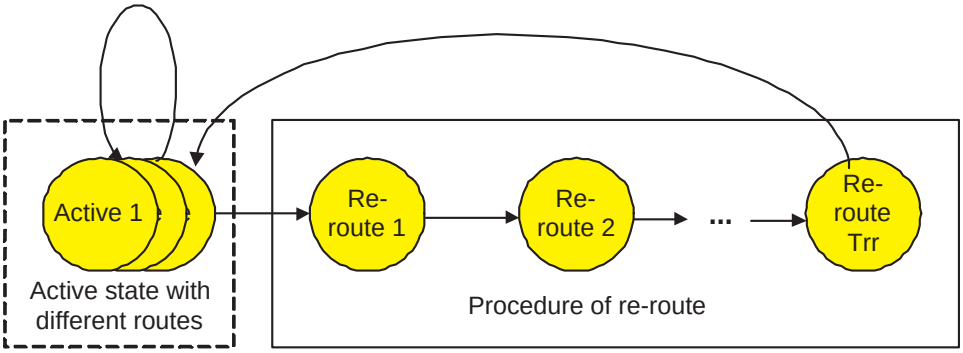

Figure 3.2 Illustration of local state transitions.

3.3.2 State Space

The system state contains the states of spectrum occupancies of all links and the local states of data flows. For data flow s, there are $N_s + T_{rr}$ states, namely N_s active states, denoted by $\{\mathbb{A}_p\}_{p=1,\ldots,N_s}$ ($\mathbb{A}_p$ means that data flow is active and is using route p), and T_{rr} re-routing states, denoted by $\{\mathbb{R}_t\}_{t=1,\ldots,T_{rr}}$ (t means the number of routing periods that have been passed for re-routing). The local state transition of a data flow is illustrated in Figure 3.2.

3.3.3 Action Space

Each data flow can choose different actions for the following two local states: (a) Active $\mathbb{A}_p$: when the current state is active, each data flow can either adjust its data rate x_s, or the data flow can choose re-routing, thus entering local state $\mathbb{R}_1$; (b)Re-routing $\mathbb{R}_t$: if $t < T_{rr}$, the data flow can do nothing but resuming the re-routing procedure; when $t = T_{rr}$, the data flow should choose the corresponding routing path p and then enter the local active state $\mathbb{A}_p$. Note that the states of spectrum occupancies of all links cannot be changed by the actions of data flows since they are affected by only primary users. The actions can change only the local states of data flows.

3.4 Centralized Primal Optimization

In this section, we discuss the centralized primal optimization problem by using dynamic programming and Q-learning. We suppose that the optimization is carried

out by a control center.

3.4.1 Dynamic Programming

We assume that the knowledge of primary users, i.e., the transition probabilities of the two-state Markov model, is perfectly known. It is well known that the optimal strategy of the stochastic control can be obtained via dynamic programming. Define the value function to be

$$V_t(\mathcal{S}_t) = \max_{\mathbf{R}(t)\mathbf{x}(t)\leq \mathbf{c}\odot\mathbf{m}(t)} \sum_{\tau=t}^{T} \beta^{\tau-1} r_\tau, \tag{3.3}$$

where $\mathcal{S}_t$ is the overall system state at routing period t. Then, the value functions are given by the Bellman's equation, which is given by

$$V_t(\mathcal{S}_t) = \max_{\mathbf{a}} E\left[\max_{\mathbf{R}(t)\mathbf{x}(t)\leq \mathbf{c}\odot\mathbf{m}(t)} r_t + \beta V_{t+1}(\mathcal{S}_{t+1})\right], \tag{3.4}$$

where the expectation is over the the randomness of the next system state and $\mathbf{a}$ means the decisions of re-routing of all data flows. Since the allocation of data flow rate $\mathbf{x}$ does not affect the state transition, it is independent of $V_{t+1}(\mathcal{S}_{t+1})$ and is used to optimize the instantaneous reward r_t. We can use either centralized or decentralized approaches, e.g. pricing based optimization decomposition, to obtain the optimal $\mathbf{x}$ within one routing period. The optimal strategy is then obtained by solving (3.4), beginning from time T.

3.4.2 Q-learning

Note that dynamic programming requires perfect knowledge about primary users. When such a knowledge is unknown, we can apply Q-learning. We set Q-values for each data flow s, system state $\mathcal{S}$ and action a, denoted by $Q_s(\mathcal{S}, a)$. Then, the learning procedure of different data flows is given by

$$\begin{aligned} Q_s^{t+1}(\mathcal{S}_t, a) &= (1-\alpha(t))Q_s^t(\mathcal{S}_t, a) \\ &+ \alpha(t)\left(r_s(t) + \max_u \beta Q_s^t(\mathcal{S}_{t+1}, u)\right), \end{aligned} \tag{3.5}$$

where $\alpha(t)$ is a learning factor. The probability of using action a is given by the following Boltzman distribution:

$$P_s^t(\mathcal{S}, a) = \left(e^{\frac{Q_s^t(\mathcal{S},a)}{T}}\right) / \left(\sum_u e^{\frac{Q_s^t(\mathcal{S},u)}{T}}\right). \tag{3.6}$$

3.5 Dual Optimization and Decomposition

In this section, we discuss the dual optimization and propose a heuristic algorithm based on Limited Lookahead Policy (LLP) and binary pricing. We assume that the *a priori* information about primary users is perfectly known.

3.5.1 Dual Optimization

In order to decompose the stochastic optimization problem, we convert the primal optimization problem into the dual one:

$$\Lambda^* = \arg\min_{\Lambda} \sum_{s=1}^{N} \max \sum_{t=1}^{T} \Bigg(U_s(x_s(t))\phi_s(t) - P_{rr}\theta_s(t) - x_s(t) \sum_{l} R_{ls}(t)\lambda_l(t) \Bigg) + \sum_{t=1}^{T} \sum_{l} c_l m_l(t)\lambda_l(t), \tag{3.7}$$

where $\lambda_l(t)$ is the Lagrange factor (price) of link l at time t and Λ is the set of link prices at different routing periods.

Eq. (3.7) can be rewritten as

$$\Lambda^* \quad = \quad \arg\min_{\Lambda} G(\Lambda) \tag{3.8}$$

where

$$G(\Lambda) = \sum_{s=1}^{N} V_s(\Lambda, T) + \sum_{t=1}^{T} \sum_{l} c_l m_l(t)\lambda_l(t), \tag{3.9}$$

and

$$V_s(\Lambda, T) = \max \sum_{t=1}^{T} \Bigg(U_s(x_s(t))\phi_s(t) - P_{rr}\theta_s(t) - x_s(t) \sum_{l} R_{ls}(t)\lambda_l(t) \Bigg). \tag{3.10}$$

Obviously, $V_s(\Lambda_s, T)$ means the optimal strategy of data flow s, given link prices Λ. In stationary systems, $V_s(\Lambda, T)$ can be optimized by data flow s without coupling with other data flows. However, *in the dynamic environment due to interruptions from primary users, the decomposition is no longer valid since the action taken by a data flow depends on the current system state, which couples with the actions of other data flows.* Therefore, the dual optimization based decomposition in traditional cross-layer design does not apply in the stochastic control of cognitive radio networks. Although there

exist some approaches to decompose stochastic control into subproblems, e.g. scenario tree based stochastic programming [107] and Uzawa-based heuristic algorithm [100], the former is mainly used to decompose large scale linear programming problems instead of tackling utility privacies, while the latter needs a predetermined function to describe the change of price without a general expression. A systematic approach to decompose the stochastic control with utility privacy is still an open problem. Therefore, we consider only a heuristic suboptimal approach in the next subsection.

3.5.2 LLP Strategy and Binary Pricing

When each secondary user knows only its local state, it is difficult for secondary users to optimize its strategy since the expected payoff is dependent on the system state, as well as other secondary users' strategies. In this case, we let secondary users adopt a LLP strategy, i.e. looking ahead for only limited steps.

When all links of a data flow are not interrupted by primary users, there is no need to carry out re-routing. When one (or more) link in the data flow is interrupted by primary users, the data flow needs to consider whether carry out a re-routing procedure. Due to the LLP strategy, the data flow compares the actions of keeping current route and changing the route, respectively. If a re-routing procedure is initiated, the loss is given by

$$L_1 = P_{rr} + T_{rr}\bar{U}, \tag{3.11}$$

where $\bar{U}$ is the expected utility of traffic in each routing period. We use the utility of traffic averaged over all previous routing rounds to approximate $\bar{U}$. If no re-routing procedure is carried out and the data flow waits for the recovery of the whole path, the expected loss is given by

$$L_2 = \bar{T}\left(\sum_{i\in R_i}\lambda_i + \bar{U}\right), \tag{3.12}$$

where $\bar{T}$ is the expected time needed for primary users to quit the spectrum, which can be obtained from P_{BI}.

It is quite challenging to find the optimal pricing since it is coupled with all secondary data flows. Therefore, we use a simple binary pricing strategy, i.e. for link i, the price λ_i is 0 when the link is available; otherwise, it is λ_h, which is common for all links. Numerical simulation will show that such a simple pricing strategy achieves near-optimal performance.

3.6 Numerical Results

We consider the network illustrated in Figure 3.1, in which the nodes are labeled using their coordinates, e.g. A1 or B2. We assume that there are two data flows, namely A1→D3 and A3→D1. Each data flow has two possible routes, each having 5 hops:

- Path 1 for data flow 1: A1→B1→C1→D1→D2→D3.
- Path 2 for data flow 1: A1→B1→B2→B3→C3→D3.
- Path 1 for data flow 2: A3→B3→B2→B1→C1→D1.
- Path 2 for data flow 2: A3→B3→B2→C2→D2→D1.

We assume that a re-routing procedure has penalty $P_{rr} = 1$ and duration $T_{rr} = 5$. Therefore, each data flow has 7 local states. The channel capacity of each link is set to 1 except for the link between D1 and D2, which is set to 2. Obviously, the optimal scheme is to let data flow 1 choose path 1 and data flow 2 choose path 2, which yields throughput 1 for both data flows. We assume $T \to \infty$, i.e. we consider an infinite time horizon.

Suppose that there are two primary users co-existing with the cognitive radio network. Their locations and the ranges of interruptions are illustrated in Figure 3.1. We consider the following two cases of the primary users' activity: (a) Case 1: for primary user 1, $P_{IB} = 0.01$ and $P_{BI} = 0.05$; for primary user 2, $P_{IB} = 0.02$ and $P_{BI} = 0.1$; (b) Case 2: for primary user 1, $P_{IB} = 0.1$ and $P_{BI} = 0.25$; for primary user 2, $P_{IB} = 0.15$ and $P_{BI} = 0.3$.

Obviously, in Case 1, the channel occupancy is more stationary and each interruption from primary users is much longer than that of Case 2. Since the primary users have 4 states and each data flow has 7 states, there are totally 196 system states.

We consider the data throughput as the utility U. Therefore, the objective is to maximize the discounted total throughput, subtracting the penalty of re-routing. When the routes are fixed and the spectrum occupancy is known, the optimal rate assignment $\{x_s\}$ can be efficiently obtained via linear programming.

3.6.1 Optimal Strategies via Dynamic Programming

We used dynamic programming to compute the optimal strategies for cases 1 and 2. The optimal actions of some key system states are listed in Table 3.1 for case 1. The results for case 2 are omitted due to the limited space and the similar conclusions. The notation of actions is explained as follows: A (continue re-routing), B (begin re-routing), C (keep current route), D (choose route 1), E (choose route 2) and F (stay in the active state).

From both results, we find the following strategy differences which coincide with intuitions: (a) In Case 1, whenever one or more primary user emerges, the corresponding data flow begins re-routing, since the duration of primary user occupancy is long. (b) In Case 2, the data flows do not respond to the primary users' emergence. Re-routing is carried out when the data flows are not using the optimal path, e.g., when data flow 1 is using Path 2 and data flow 2 is using Path 1.

3.6.2 Q-Learning

For both cases 1 and 2, we applied Q-learning to learn the optimal strategy without the knowledge of P_{IB} and P_{BI}. The results are provided in Figure 3.3, in which each epoch means 200 routing periods and the rewards are computed using the 200 instantaneous rewards in the corresponding epoch. We observe that, in both cases, the Q-learning can effectively improve the performance. The learning speed of Case 2 is faster since the primary users emerge more frequently, thus providing more experience for learning. Anyhow, both learning procedures are slow, which implies the importance

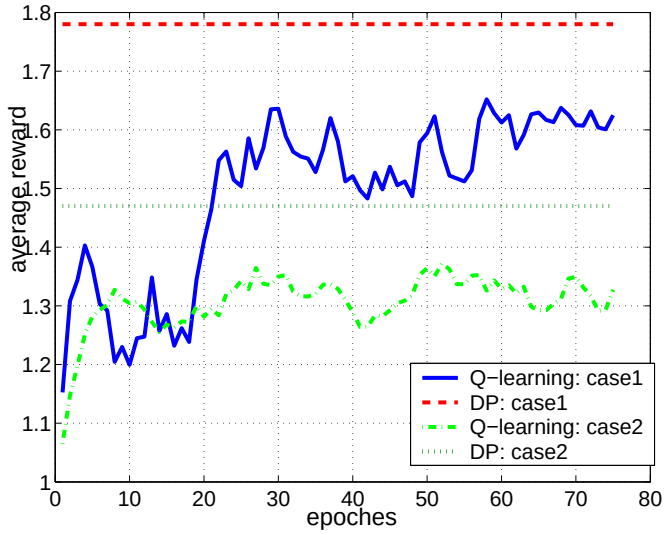

Figure 3.3 Comparison of performances of dynamic programming and Q-learning.

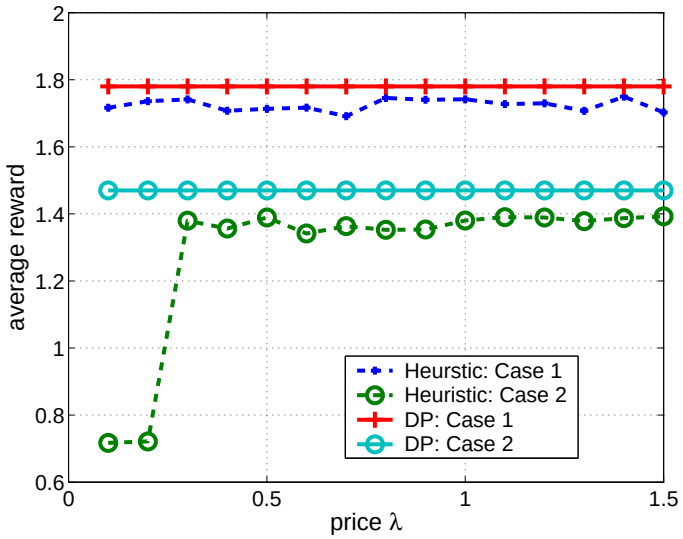

Figure 3.4 Comparison of performances of dynamic programming and LLP strategy/binary pricing.

Table 3.1 The Optimal Strategy for Typical System States in Case 1

	(0,0)	(0,1)	(1,0)	(1,1)
(1,1)	(B,B)	(B,B)	(C,B)	(C,B)
(1,2)	(B,B)	(B,C)	(C,B)	(C,C)
(1,3)	(B,A)	(B,A)	(C,A)	(C,A)
(1,7)	(B,E)	(B,E)	(C,E)	(C,E)
(2,1)	(B,B)	(C,B)	(B,B)	(B,C)
(2,2)	(B,B)	(B,C)	(B,B)	(B,C)
(2,3)	(B,A)	(C,A)	(B,A)	(C,A)
(2,7)	(B,E)	(C,E)	(B,E)	(C,E)
(3,1)	(A,B)	(A,B)	(A,B)	(A,C)
(3,2)	(A,B)	(A,C)	(A,B)	(A,C)
(3,3)	(A,A)	(A,A)	(A,A)	(A,A)
(7,1)	(D,B)	(D,B)	(D,B)	(D,C)
(7,2)	(D,B)	(D,C)	(D,B)	(D,C)
(7,7)	(D,F)	(D,F)	(D,F)	(D,F)

of the *a priori* knowledge of primary users.

3.6.3 LLP Strategy and Binary Pricing

For both cases 1 and 2, we test the performance for both cases 1 and 2 using different prices, ranging from 0.1 to 1.5. The results are provided in Figure 3.4. We observe that, for Case 1, the LLP strategy achieves almost perfect performance, regardless of the price; for Case 2, when the price is properly chosen, the performance of the LLP is also close to that achieved by dynamic programming. This demonstrates that the proposed LLP approach is near-optimal.

3.7 Conclusions

We have studied the joint congestion control and routing in cognitive radio networks suffering from the dynamic interruptions of primary users. Due to the time variation of spectrum occupancy, stochastic control is applied for the strategy of congestion control and routing. Multiple approaches like dynamic programming, Q-learning and pricing based algorithm, have been applied to obtain the stochastic control strategies in various scenarios. Their performances have been demonstrated by numerical simulations.

Chapter 4

Management of Cognitive Radio ad hoc Networks using a Congestion based Metric

In this work, we propose a new network management protocol to address the unique challenges of managing cognitive radio ad hoc networks that have distributed, multi-hop architectures with dynamic spectrum availability. We focus on performance management for these networks, and address the problem of network congestion for secondary users, because of its significant impact on data throughput. Specifically, we define a performance metric, the average congestion level of the network, and derive it analytically as a function of the primary users' activities and the secondary users' strategy. For practical implementation, we further propose a cluster based management architecture that utilizes a designated central manager and cluster heads that function as distributed managers. The cluster heads collect information from multiple layers of the protocol stack using new MIB variables to capture the characteristics of cognitive radio ad hoc networks, such as the location dependent spectrum availability. The objective of the management action is to utilize a network level view of the congestion situation in the network by directing the secondary users to select the highest quality links available and avoid congested clusters. This hierarchical network management design allows us to take advantage of its scalability to achieve near real time management. Numerical results demonstrate the effectiveness of the proposed scheme.

4.1 Introduction

With the increased use of radio frequency devices competing for scarce spectrum resources, the U.S. Federal Communications Commission (FCC) has indicated in a 2002

report that portions of the spectrum are significantly underutilized. [44] The spectrum shortage and the inefficient usage of spectrum has encouraged the development of Cognitive Radio (CR) that is a context aware intelligent radio capable of autonomous reconfiguration by learning and adapting to the spectrum environment. [45] [46] The emergence of bandwidth demand for a host of wireless devices has motivated new spectrum allocation policies, which allow unlicensed secondary users (SU) to access the radio spectrum when it is not occupied by licensed primary users (PU). The intent is that this cognitive radio approach will improve spectrum utilization in wireless communications systems. Since the unlicensed or lower priority SUs employing cognitive radio must limit any interference to the PUs, the SUs must only transmit in the spectrum holes left available by the PUs, where a spectrum hole is a frequency band assigned to a primary user that is not being used at a particular time and geographic location. [46]

Cognitive radio networks may be composed of single hop networks, such as the fixed point to multipoint type as described by the IEEE 802.22 specification. They may also include multihop links, without a central base station, and these networks are called Cognitive Radio Ad Hoc Networks (CRAHNs).They are characterized by dynamically changing network topology and spectrum availability. The major functions of CRAHNs are described by Akyildiz et al [47], including spectrum sensing, spectrum decision, spectrum sharing and spectrum mobility.

In this work, we propose a framework for intelligent network management that was introduced in our preliminary work, [48] called Cognitive Network Management Protocol (CNMP), that will focus initially on network performance management of the SU nodes. It has been observed that network congestion is a dominant factor in dropped packets in Mobile Ad Hoc Networks (MANET). [49] Additionally, because the SU nodes must opportunistically access the spectrum only when PU nodes are idle, the network congestion is increased more due to the intermittent availability of bandwidth. Therefore, enhancing data throughput for both primary and secondary radio users depends largely on avoiding and reducing network congestion. To address this problem, we propose a metric to assess the congestion between SU nodes that is based on cross layer information from those nodes and the observation of the transmission activity of

the PU nodes.

4.1.1 Network Management Architectures

Network management architectures for wireless networks are broadly defined as three basic types.[50] Centralized network management uses a single manager station to gather information from all of the managed nodes and controls the network. While centralized management allows a global view of the network to make management decisions, there are several drawbacks. The central manager is a single point of failure if the manager is incapacitated and no backup manager is in place. The amount of management traffic from all of the network nodes in a wireless multi-hop network may be prohibitive in a CR environment to provide meaningful management functions in a timely manner.

Distributed network management uses multiple managers who each manage subnetwork of nodes. This decreases the amount of network management overhead and per manager computation compared to the centralized approach. In this architecture, the managers communicate peer to peer, with no central manager, and can provide higher reliability with more networked information among the manager peers.

Hierarchical network management uses intermediate managers, each having their own management domain, to distribute management tasks. This architecture uses a central manager and the intermediate managers communicate up or down the hierarchy. There is no direct communication between intermediate managers. However, depending on the needs of the management system, any of these architectures can be used in combination.

While the development of cognitive radio hardware and software of has been the subject of much research, comprehensive network management of CR networks is not well addressed. CR networks may be implemented as single hop networks, where network can be managed by central base stations, such as the scheme described by the IEEE 802.22 Wireless Regional Area Networks (WRAN) specification.[51] In the 802.22 specification, the Network Management System (NMS) receives information from the managed nodes, such as base stations (BS) and customer premise equipment (CPE),

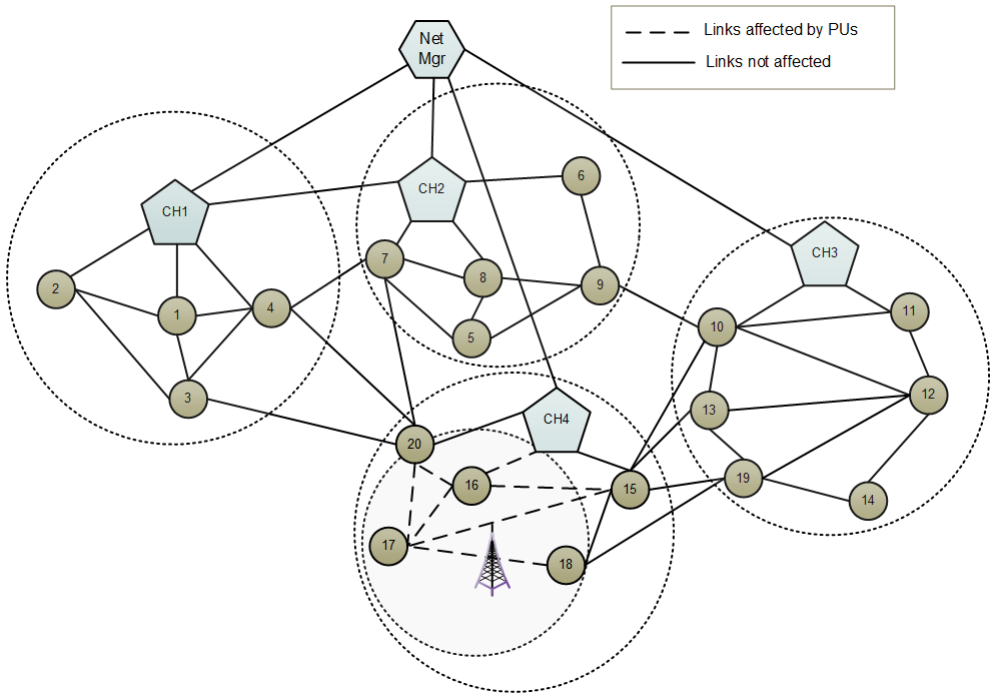

Figure 4.1 Clustered Architecture for Cognitive Radio Network Management System.

that collect and store the managed objects in a WRAN Interface MIB (e.g., wranIfMib) and Device MIB (e.g., wranDevMib) using the Simple Network Management Protocol (SNMP).

While the 802.22 network configuration uses BS and CPE devices in a cognitive implementation, the operation of those networks is controlled primarily by the base stations and therefore are dissimilar to the independent spectrum sensing and channel acquisition operation of CRAHNs. Thus, the management of CRAHNs [52] is inherently different, which we address with a clustered architecture based management system in this work.

CRAHNs require management of distributed CR nodes and can be implemented with a management system based on a clustered architecture similar to the Ad Hoc Network Management protocol (ANMP) [50] model. An example is shown in Fig.4.1, where the architecture is comprised of a hierarchical three layer system which includes a central network manager, cluster head nodes and managed CR nodes. The network manager node has knowledge of the entire network by exchanging management information with cluster heads CH_1, CH_2, CH_3, and CH_4. These cluster heads communicate

management information with the CR nodes in their respective clusters. The managed nodes use SNMP that includes a modified Management Information Base (MIB), cnmpMIB, that specifically addresses the management information needed for CRAHNs.

As an example of a management scenario from Figure 4.1, consider the case where most traffic from cluster 1 to cluster 3 traverses through cluster 4. However, if the primary user *PU* becomes active and occupies a substantial number of channels, many links in cluster 4 may become unavailable to the CR network and the network manager should advise the cluster heads to redirect traffic from cluster 1 to cluster 3 traverse through cluster 2. Cognitive radio networks that are sharing spectrum with very active PU networks may have to frequently move their communication data to new channels (spectrum handover) or through a different geographical area to avoid interference with the PUs. Thus, we propose an autonomous management system by distributed management network nodes in near real time that capitalizes on the capabilities of the CR nodes to perform basic functions such as spectrum sensing [53] [54] and channel acquisition [52] in order to optimize overall network throughput.

4.1.2 Outline of Work

In this work, we focus on the performance management aspect of CNMP. Specifically, the congestion management issue is examined and the overall flow is shown in Figure 4.2. We consider a CRAHN of secondary users overlaid on a primary user system that senses spectrum holes to provide transmission opportunities. The SU network with assigned nodes monitors the average PU ON and OFF activity in addition to spectrum sensing done by the remaining SU nodes. This PU information, together with the SU sensing, transmission, and idle times are used to determine the steady state probability of channel availability.

The channel availability is then estimated based on a threshold probability and is used in the assessment of the probability of successful channel contention for each active SU link. Together with the probability of packet error, the probability of successful transmission per link is used to determine the probability of packet drop (PPD). We then compare the PPD to a congestion threshold to determine whether the link is

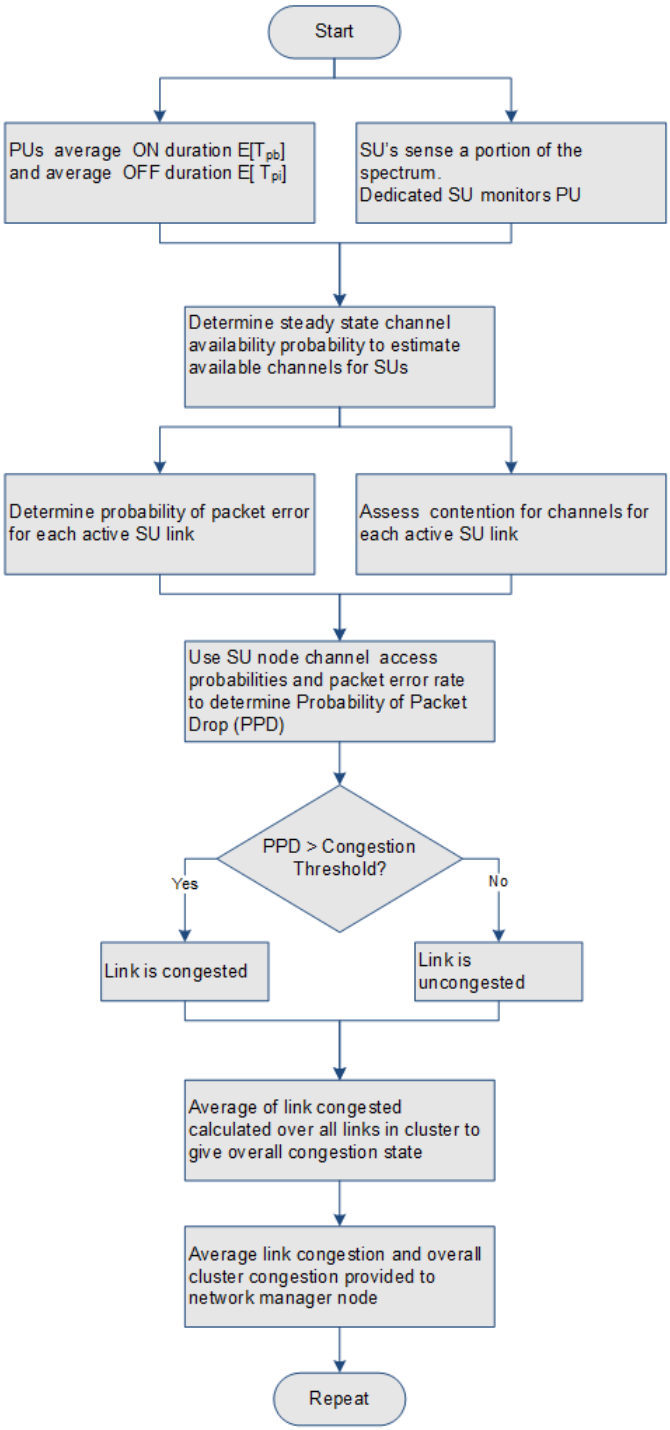

Figure 4.2 Overview of Congestion Metric Development.

considered congested. In our hierarchical cluster scheme, the average congestion of the links in each cluster are calculated. Additionally, the overall cluster congestion is determined by comparing the average congestion to a cluster level congestion threshold value. The average link congestion and the overall cluster congestion are then reported to the CR network manager, which can be used to influence adaptive routing or other management tasks.

This chapter is organized as follows: Section 4.2 provides a review of the related works. Section 4.3 discusses the problem formulation and the proposed network congestion indicator. The proposed procedure for acquiring the management data is given in Section 4.4, and our numerical results are reviewed in Section 5.4. Finally, we provide our conclusions and future research plan in Section 4.6.

4.2 Related Work

4.2.1 Comparison with Classic Network Management

We start by providing an overview of the inherent differences between managing traditional networks and cognitive radio ad hoc networks (CRAHNs). [48] Traditional network management of wireline networks is divided into five areas: performance management, fault management, security management, configuration management and accounting management.[55] These areas as applied to telecommunications can be generally described using the Bellcore-GR2869 Generic Requirements for Operations Based on the Telecommunications Management Network (TMN) Architecture [56] and the ITU-T Recommendation M-3400 TMN Management Functions. [57] In Table 4.1 we contrast the traditional functions to those required by CRAHNs. Managing a CRAHN poses a unique set of problems which include the availability and stability of channels in the wireless CRAHN environment, and in particular the potential channel interruptions due to PU activities.

1. *Performance management*: Performance management involves measurement of network performance, with metrics such as overall throughput, packet loss and delay. Baseline performance levels are then established, based on acquired data,

and performance thresholds are set for various monitored parameters. Network tuning is accomplished by throttling network devices as required to maintain network throughput.[55] In a CRAHN, performance management also should consider the 'exploit vs. explore' tradeoff, which applies to the amount of time the SUs sense the spectrum. Longer sensing time possibly finds more available bandwidth, but leaves less time for data transmission. Spending less time sensing allows more time to transmit data, but possibly using a smaller bandwidth. The optimization of this parameter is considered by Kim and Shin,[58] and leads to the acquisition of additional or better performing channels to meet Quality of Service (QoS) objectives.

2. *Fault management*: Fault management includes identifying, isolating and potentially correcting abnormal conditions that adversely affect services in the network.[59] Deciding which faults to manage will be influenced by the scope of control desired over the network, which affects the amount of data gathered from network devices and also by the size of the network.[55] The sub areas of fault management include detecting alarms, localizing faults, performing diagnostic tests, and fault correction. Fault management in a CRAHN environment can be very complex, due to dynamically changing spectrum availability, which can cause severe difficulties to perform fault identification and isolation. Communication alarms that include loss of signal or frames, must take into account the resumption of communication in an alternate channel if there is spectrum handover of the communication flow due to PU interruption.

3. *Security management*: Security management ensures that network users are authenticated and authorized by controlling network access points. It also prevents unauthorized users from spoofing the network, or tampering with network operation.[55] CRAHNs, in addition to these traditional security functions, must handle spectrum congestion; where attacks may be waged by malicious jammer nodes to occupy all channels in a geographic area.[60] This denies channel availability to SU users, who sense that it is PU activity, and affects both transmitting

and receiving CR nodes.

4. *Configuration management*: Configuration management traditionally involves locating and setting up the parameters and versions of network devices for operation. Additionally, it includes network planning and engineering, installation, service planning, provisioning and control.[56] However, in CRAHNs, nodes may be mobile, or may power off intentionally to save power, or die from battery discharge. Also, during PU or malicious node activity, there may be no channels available to reach some of the CR nodes, effectively altering the topology of the network. In a hierarchical CR network model, methods for cluster head selection and managed node affiliation that can be applied to configure a CR network is discussed by Chen, et al.[50].

5. *Accounting management*: Accounting management monitors the network usage of users and groups and provides the measurement method for compliance to a service level agreement. The management system also keeps records of the usage metrics for charging and billing. Managing a QoS agreement on a CRAHN is more complex than using traditional management because the service is not solely dependent on the CR network, but also on the activity of the PU network, which can hamper throughput or completely interrupt service. This provides a potential application of accounting management to track quantities such as bandwidth usage, average throughput and spectrum handovers due to PU activity, as spectrum markets and brokering systems are developed. Markets based on primary to secondary users and also between secondary users, as discussed in work by Xu, [61] will require accounting management.

4.2.2 Comparison with Related Network Management Protocols

While the literature describes various approaches to managing CR networks, we should distinguish between network management and radio resource or spectrum management. There has been significant research for spectrum management, such as those

Network Management Component	**Wired Traditional Network**	**Wireless Cognitive Radio Ad Hoc Network**
Performance Management	Monitor performance and throttle resources	Proactive and reactive performance control with dynamic bandwidth allocation
Fault Management	Identify, isolate and clear faults	Manage highly variable link quality, channel acquisition after PU interruption
Security Management	Control network access, Protect against intrusion, tampering, spoofing	Control network access and routing, mobility handling. Protect against intrusion, tampering, spoofing
Configuration Management	Setup equipment configuration, Update software versions	Update network for nodes that move, power-off or die, Spectrum sensing and utilization
Accounting Management	Track resource utilization, Allocate resources per Service Level Agreements	Accounting/billing used with Performance Management for Quality of Service agreement

Table 4.1 Traditional versus Cognitive Radio Network Management System Functions

discussed in the survey done by Akyldiz, et. al [62] However, these studies do not provide solutions for a comprehensive network management system.

The Ad Hoc Network Management Protocol[50] is fully compatible with SNMP and has created a set of MIBs that are more germane to wireless than wireline networks, such as power usage, agent information and topology maintenance groups of information records. ANMP also uses a clustering concept to simplify management of the network by reducing management messaging overhead. However, ANMP was intended for fixed spectrum access and the network management message overhead was not dependent on spectrum availability. We note that for CR networks, in addition to grouping CR nodes by geolocation or number of hops proximity to each other, we must also take into account that they should also be clustered by a set of common potentially available channels.

Policy-based management was initially proposed as an approach to automate the

management of large-scale networks and distributed systems. However, the conventional policy-based management systems cannot be directly applied to CR networks. [63]

Clearly, the unique network management needs of CRAHNs demand a new approach. To address this problem, our contribution builds on the concepts reviewed and includes the following:

1. The CR network is implemented as a hierarchical cluster with a network manager, cluster heads (distributed managers) and managed nodes.

2. The manager uses average network congestion indicator as one of it's tools to manage the CR network nodes.

3. The proposed average network congestion indicator is derived as a function of PUs' activities and SUs' strategy, which is based on a two state markov model, and in turn provides grounds for setting control parameters for SUs to relieve network congestion if needed.

4. Thirteen new Management Information Base (MIB) variables are introduced to facilitate the calculation of the new management metric.

Several network management and performance metrics for CR networks are shown in Table 4.2, where we observe that the existing metrics in the literature do not directly address network congestion based on PU activity as interference to SU channel access. However, the new metrics presented in this chapter will address the need for the congestion awareness.

4.3 Problem Formulation & the Proposed Network Congestion Indicator

Given the uncertainty of spectrum availability for CRAHNs as we have discussed above, we now propose a model from which we will develop our network management platform. Initially, we determine the probability of packet drop, which is a key indicator

Metric	Explanation
Signalling load	Number of bytes required for signalling as an indicator of the amount of management traffic [64]
Spectrum utilization	Sum of network throughput or goodput, network available time, and throughput of secondary (CR) system [65]
Power efficiency	Measure of active time and battery efficiency [65]
Communication cost	Communication cost for end users [65]
Link Reliability	Link reliability with respect to Bit Error Rate (BER), Frame Error Rate (FER), and Packet Drop Ratio (PDR) [65]
Average packet delay	average amount of delay experienced by primary network due to secondary (CR) network [65]
Application Quality of Service	Voice quality measured by Mean Opinion Score (MOS), Video quality measured by Media delivery index (MDI), distortion and peak signal to noise ratio (PSNR) [65]

Table 4.2 Comparative Network Management & Performance Metrics and Explanations

for network congestion that the network manager can use to influence the overall routing behavior determined by the cluster heads and managed nodes.

In order to model the channel usage patterns of primary users, various approaches have been proposed in the literature, such as the Hidden Markov Model (HMM) [66], and multivariate time series [67], to learn the primary user characteristics and predict the future occupancy of channels. For practical implementation considerations, a binary scheme (empty or occupied) can be used to reduce the complexity and storage requirements. It is also noted in Geirhofer et. al [68] [69] based on real-world measurement data that the statistical model of a primary user's behavior should be kept simple enough to be able to design optimal higher order protocols. On the other hand, the model would be useless if the primary user's behavior could not be predicted well. In order to strike a balance between complexity and effectiveness, in this work, we have used a Markov model of PU's activities, adjusted by the SU's perceptions. This is very important since the channel availability the SU perceived would be what actually matters in terms of actions taken by the SU. The periodic spectrum sensing/data transmission based MAC layer model is the de-facto choice for CR networks, and it is also

general enough to cover most of the proposed MAC structures proposed in the literature [70]. As a result, the model used in this work represents realistic implementations of real-world CR ad hoc networks.

In this work, we assume that there exists a radio network consisting of a set of Z licensed primary users, $\mathcal{Z} = \{1, \ldots, Z\}$ and a set of S unlicensed secondary users, $\mathcal{S} = \{1, \ldots, S\}$ employing cognitive radio devices. To simplify the metric development, we assume that both the PU and SU devices are stationary but randomly distributed. The CR nodes are connected via a set of L links, $\mathcal{L} = \{l_{jk} | j \in \mathcal{S}, k \in \mathcal{S}\}$, where each link is defined by the nodes on either end of the link. The set of channels used is $\mathcal{C} = \{1, \ldots, C\}$ where C is the total number of channels in the system. Each link, l_{jk}, uses a subset of available channels obtained by spectrum sensing. As various source and destination nodes communicate across the network, they will establish a set of F data flows, $\mathcal{F} = \{1, \ldots, F\}$, to occupy some or all of the available channel bandwidth on the links. We define the total flow across a given link as the set of individual flows traversing the link, $\mathcal{F}_{jk} = \{f_{jk} | f \in \mathcal{F}, j \in \mathcal{S}, k \in \mathcal{S}\}$. Similarly, the set of channels in use on a particular link, l_{jk}, are specified by $\mathcal{C}_{jk} = \{c_{jk} | c \in \mathcal{C}, j \in \mathcal{S}, k \in \mathcal{S}\}$. And for the specific set of channels that are used by the total flow $\mathcal{F}_{jk}$ on link l_{jk}, we define the set $\mathcal{C}_{jk}^{\mathcal{F}} \subset \mathcal{C}_{jk}$.

Each channel, $c \in \mathcal{C}$, will have a data rate of b_c. The aggregate data rate of a link can then be expressed as

$$\beta_{jk}^{\mathcal{C}} = \sum_{c \in \mathcal{C}_{jk}} b_c \tag{4.1}$$

and the data rate of the flow per link as

$$\beta_{jk}^{\mathcal{F}} = \sum_{c \in \mathcal{C}_{jk}^{\mathcal{F}}} b_c \tag{4.2}$$

4.3.1 Primary User Activity Model

It is assumed that the PU's activity follows a Markov model, where the ON or OFF intervals of each PU are completely independent and determine the availability of the channels for the SUs in the interference range of any PU. We assume that the ON and OFF durations are exponentially distributed. We will consider the channel availability

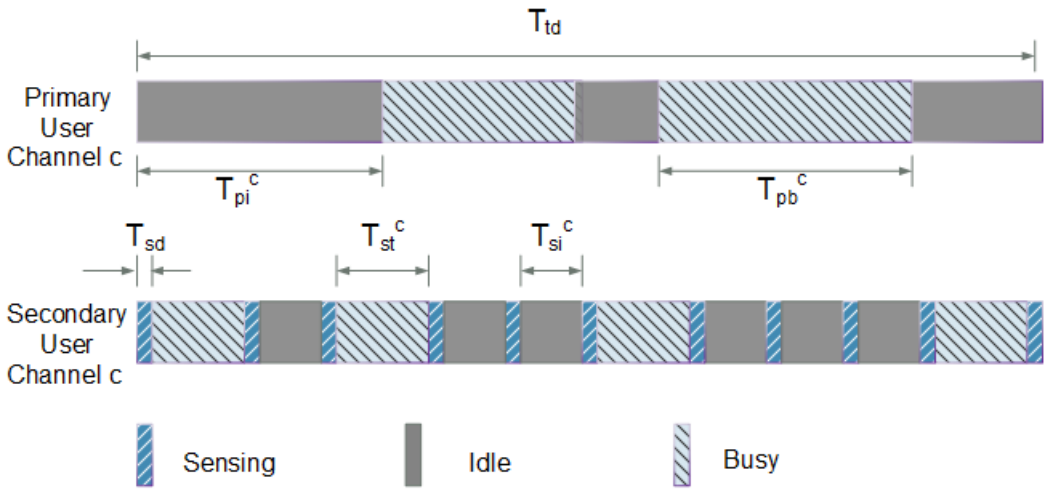

Figure 4.3 Time durations for channel access

as perceived by the SUs, given that their spectrum sensing may include some probability of error. Referring to Figure 4.3, let T_{st}^c be a random variable representing the time duration that the SU transmits in channel $c \in \mathcal{C}$, after sensing that the channel is idle. We also let T_{si}^c be a random variable representing the time duration that the SU is idle in channel c after sensing that the channel is busy. Since the SU may not always sense the channel state accurately, P_{ef}^c represents the probability of false alarm, and P_{em}^c is the probability of missed detection. With respect to the PU, the duration of the busy period from a PU transmission on channel c is T_{pb}^c, and the complimentary idle period duration for the PU on the channel is T_{pi}^c. The SU will attempt to acquire the channel, c, for the overall time duration of interest, T_{sd}.

As discussed by Kim and Shin,[58] we define channel utilization, u^c, as the fraction of the total time duration of interest in which channel c is in the busy state as

$$u^c = \frac{E[T_{pb}^c]}{E[T_{pb}^c] + E[T_{pi}^c]} \tag{4.3}$$

Additionally, we define the average number of arrivals of a channel going into a busy state as

$$\lambda_b = \frac{1}{E[T_{pb}^c]} \tag{4.4}$$

and the average number of arrivals of a channel going into an idle state as

$$\lambda_i = \frac{1}{E[T_{pi}^c]} \tag{4.5}$$

which then allows the channel utilization, u^c, to be expressed as

$$u^c = \frac{\lambda_i}{\lambda_i + \lambda_b} \tag{4.6}$$

Referring to Fig.4.4, as noted earlier, we model the state of the channel activity as a Markov process to determine the transition probabilities of the channel states. The transition probability of changing from the idle state, S_{idle}, to the busy state S_{busy}, at any time instant, t, is shown by Kim and Shin[58] as

$$P_{ib}^c(t) = u^c - u^c e^{-(\lambda_i+\lambda_b)t} \tag{4.7}$$

and from the busy state to idle state is

$$P_{bi}^c(t) = (1 - u^c) - (1 - u^c)e^{-(\lambda_i+\lambda_b)t} \tag{4.8}$$

The probability of the idle state transitioning back to itself is given by

$$P_{ii}^c(t) = (1 - u^c) + u^c e^{-(\lambda_i+\lambda_b)t} \tag{4.9}$$

and similarly the probability of the busy state transitioning to itself is

$$P_{bb}^c(t) = u^c + (1 - u^c)e^{-(\lambda_i+\lambda_b)t} \tag{4.10}$$

These equations represent the *actual* channel state transition probabilities based on the activity of the PUs. To reduce the complexity of our numerical results, we will consider the network state at a specific value of t, thus allowing the actual transition probabilities to be treated as static quantities.

Since the secondary user nodes may not always correctly sense channel availability, we note that the *perceived* transition probabilities must account for the probability of missed PU activity or false alarm for the time interval under consideration. There are four cases to consider regarding the correct or incorrect sensing of the channel.

1. The SU correctly senses the channel and transmits
2. The SU incorrectly senses the channel and transmits
3. The SU correctly senses that channel and is idle

4. The SU incorrectly senses the channel and is idle

We can define the percentage of the total duration that the SU senses the channel and transmits as

$$\alpha_{st} = \frac{T_{sd} + T_{st}}{T_{td}} \tag{4.11}$$

and the percentage of the total duration that the SU senses the channel and is idle as

$$\alpha_{si} = \frac{T_{sd} + T_{si}}{T_{td}} \tag{4.12}$$

Then the perceived transition probability by the SU of the channel moving from the idle state to the busy state uses case 1 and case 2 as

$$\gamma_{ib}^{c} = P_{ib}^{c} P_{ef}^{c} \left[\alpha_{si} - \alpha_{st} + \frac{\alpha_{st}}{P_{ef}^{c}} \right] \tag{4.13}$$

and conversely, the perceived transition probability of the channel going from the busy state to the idle state uses case 3 and case 4 as

$$\gamma_{bi}^{c} = P_{bi}^{c} P_{em}^{c} \left[\alpha_{st} - \alpha_{si} + \frac{\alpha_{si}}{P_{em}^{c}} \right] \tag{4.14}$$

To complete the set of perceived transition probabilities, we see that the self-returning transition probabilities are

$$\gamma_{ii}^{c} = 1 - \gamma_{ib}^{c} \tag{4.15}$$

and

$$\gamma_{bb}^{c} = 1 - \gamma_{bi}^{c} \tag{4.16}$$

From these transition probabilities, we can determine that the perceived steady state probability that channel c is in the idle state is

$$\pi_{i}^{c} = \frac{1}{1 + \frac{\gamma_{ib}^{c}}{\gamma_{bi}^{c}}} \tag{4.17}$$

which can be represented as a function of the component probabilities and time duration intervals as shown in Eq. 4.18.

$$\pi_{i}^{c} = 1 / \left\{ 1 + \left[\frac{P_{ib}^{c} P_{ef}^{c} \left(\alpha_{si} - \alpha_{st} + \frac{\alpha_{st}}{P_{ef}^{c}} \right)}{P_{bi}^{c} P_{em}^{c} \left(\alpha_{st} - \alpha_{si} + \frac{\alpha_{si}}{P_{em}^{c}} \right)} \right] \right\} \tag{4.18}$$

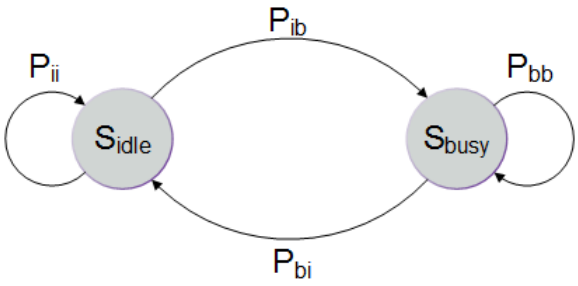

Figure 4.4 Markov 2-state Channel Diagram

4.3.2 Derivation of the Proposed Metric

We will model the state of the network as either *congested* or *uncongested* . It is also assumed that the SU network will be managed for near optimum throughput over time by a network manager SU node. Given the low latency requirements of delay sensitive applications such as video or other multimedia data, the network manager concept here does not attempt to precisely control all SU nodes in each PU observation period. The time required for node to manager communication could be prohibitive for such applications, as pointed out by Shiang and van der Schaar. [71] Instead, the network manager operates based on the average congestion of all the links, by instructing the cluster heads (distributed managers).

In order to determine the channels perceived by the SUs as available, we use the perceived channel idle probability, π_i^c, as the probability of success in a binomial model. Here the random variable, ρ_{jk}, represents the number of available channels on link l_{jk}, and x represents a number of channels that we use in the binomial model to evaluate the probability. We test the probability for a specific number of channels against a threshold, Θ, to provide a level of confidence for the estimated channel availability.

To accomplish this, we find x^*, such that

$$x^* = \arg\max\{x\} \text{ , subject to } \{1 - P\left[\rho_{jk} \leq x\right]\} > \Theta \tag{4.19}$$

We solve the inequality by evaluating the expression with a range of values for x, $(0 \leq x \leq C)$, until the criteria is satisfied. The total number of channels perceived by the transmitting and receiving nodes on link l_{jk} as being available can be set to the

number of channels meeting the probability threshold

$$C_{jk} = x^* \tag{4.20}$$

This number of available channels provides the cardinality of the set of channels that are used by the SUs on link l_{jk}, which we defined earlier as $\mathcal{C}_{jk}$.

In our study, we assume that all of the channels used by each PU are contiguous and have the same ON and OFF durations. Hence, we can use the same probability, π_i^c, for each channel and treat the probability of finding a specific number of channels as a binomial distribution. In this case, we define a success as the channel being idle with probability π_i^c, or a failure otherwise. We then consider the representation of the probability in Equation 4.19 as

$$P\left[\rho_{jk} > x\right] = 1 - \sum_{\delta=0}^{x} \binom{C}{\delta} \left(\pi_i^c\right)^{\delta} \left(1 - \pi_i^c\right)^{C-\delta} \tag{4.21}$$

where δ represents the number of channels in each trial, and C is the total number of channels in the network.

The system model bases its metric of congestion on the probability of packet drop (PPD) since the packets of incoming and outgoing queues on the CRs may be dropped in anticipation of filling, as in Random Early Detection (RED), [72] or when the queues have already filled to capacity.

Referencing Figure 4.5, the uni-directional flow load $\mathcal{F}_{jk}$ on link l_{jk}, is defined as the flow from the transmitter of link l_{jk}, (T_j), to the receiver of link l_{jk}, (R_k). The transmitting node on link l_{jk} has a coverage range, Γ_j^T, which contains a subset of the SUs that are within that area. Similarly, the receiving node on link l_{jk} has a sensitivity range, Γ_k^R, which contains the subset of SUs whose transmissions reach node R_k.

In order to calculate PPD, without loss of generality, we use a Carrier Sensing Multiple Access (CSMA) Media Access Control (MAC) scheme. We assume that all flows from a particular node may be accommodated by the use of Orthogonal Frequency Division Multiplexing, (OFDM),with adaptive and selective allocation of OFDM subcarriers such that any subset of channels, $c \in \mathcal{C}$ may be transmitted simultaneously.

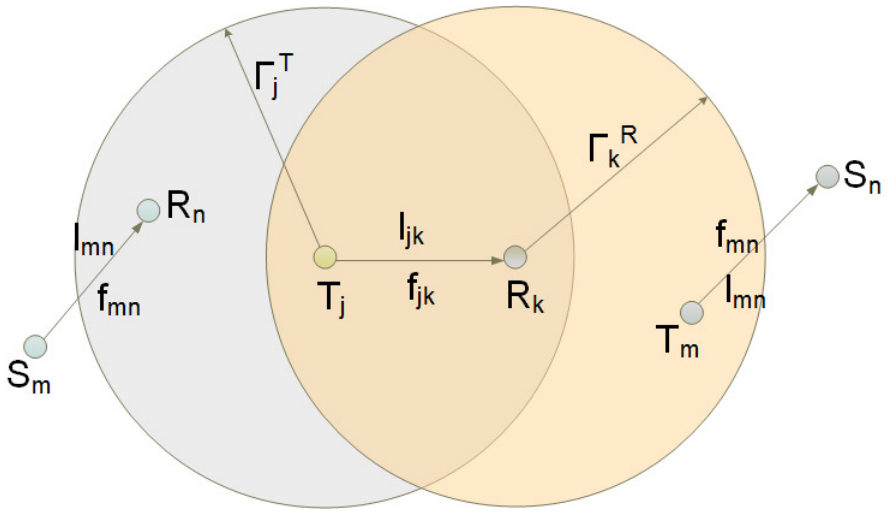

Figure 4.5 Secondary User node and link configuration

Here, we note that OFDM is well suited for CR because it is agile in selecting and allocating subcarriers dynamically and it facilitates decoding at the receiving end of each subcarrier [73]. In multiuser OFDM systems, the subcarrier allocation to users can be done adaptively as well. By using OFDM, any subset of channels is a group of OFDM subcarriers, which can be allocated to a certain traffic flow. It is also shown that simultaneous transmission on a set of OFDM subcarriers is feasible [73].

Then we calculate the probability that the transmitting node, T_j, of link l_{jk} is able to obtain the bandwidth required, $\beta_{jk}^{\mathcal{F}}$, that is shared with other neighboring nodes, for transmitting the total flow, $\mathcal{F}_{jk}$,. That probability is

$$P_{TX}^{jk} = \prod_{R_n \in \Gamma_j^T} \left(1 - \frac{\beta_{jk}^{mn}}{\beta_{jk}^{\mathcal{C}}}\right) + \left(1 - \prod_{R_n \in \Gamma_j^T} \left(1 - \frac{\beta_{jk}^{mn}}{\beta_{jk}^{\mathcal{C}}}\right)\right) \frac{\beta_{jk}^{\mathcal{F}}}{\left(\sum_{R_n \in \Gamma_j^T} \beta_{jk}^{mn}\right) + \beta_{jk}^{\mathcal{F}}}. \quad (4.22)$$

Here, Γ_j^T is the interference range of T_j, and R_n is a receiver of link l_{mn}, $(l_{mn} \neq l_{jk})$, that is within the interference range of T_j. $\beta_{jk}^{\mathcal{C}}$ is the data rate on link l_{jk} that uses the channels in $\mathcal{C}_{jk}$. The channels used by the flow on link l_{mn} for it's data rate that are contained in the set of channels, $\mathcal{C}_{jk}$, in use on link l_{jk}, are represented by the data rate

$$\beta_{jk}^{mn} = \sum_{c \in (\mathcal{C}_{mn}^{\mathcal{F}} \bigcap \mathcal{C}_{jk})} b_c \quad (4.23)$$

In other words, we implicitly assume that nodes firstly perform frequency division multiple access (FDMA) (first term in Eq. 4.22), then if not possible to accommodate all

flows by FDMA, determine the probability of winning the contention between competing nodes for channel access (second term in Eq. 4.22).

Similarly, we calculate the probability that the receiving node, R_k, of link l_{jk} is able to obtain the bandwidth needed for receiving the flow from T_j, that is shared with other neighboring nodes as

$$P_{RX}^{jk} = \prod_{T_m \in \Gamma_k^R} \left(1 - \frac{\beta_{jk}^{mn}}{\beta_{jk}^{\mathcal{C}}}\right) + \left(1 - \prod_{T_m \in \Gamma_k^R} \left(1 - \frac{\beta_{jk}^{mn}}{\beta_{jk}^{\mathcal{C}}}\right)\right) \frac{\beta_{jk}^{\mathcal{F}}}{\left(\sum_{T_m \in \Gamma_k^R} \beta_{jk}^{mn}\right) + \beta_{jk}^{\mathcal{F}}} \quad (4.24)$$

where T_m is the transmitter of link l_{mn},

Again, we implicitly assume that nodes firstly perform FDMA (first term in Eq. 4.24). Then if it is not possible to accommodate all flows by FDMA, the node competes for channel access with other neighboring nodes (second term in Eq. 4.24).

Then the probability that the transmission is not successful on link l_{jk} in a single time period can be calculated as

$$P_{fail}^{jk} = 1 - (1 - P_e^{jk})^N P_{TX} P_{RX} \quad (4.25)$$

where P_e^{jk} is the probability of bit error at the PHY layer on link l_{jk}, and N is the total number of bits in the packet. We assume that all packets are of uniform length.

The probability of packet drop D_{jk} for each flow on link l_{jk} can then be determined by using the maximum number of retransmissions, q, such that

$$D_{jk} = \left(P_{fail}^{jk}\right)^{q+1} \quad (4.26)$$

We may now define a congestion indicator, I_{jk}, for the unidirectional link l_{jk} as

$$I_{jk} = \begin{cases} 1 & \text{if } D_{jk} > \nu \\ 0 & \text{otherwise} \end{cases} \quad (4.27)$$

where ν is a pre-defined congestion threshold that may be based on a Quality of Service (QoS) target.

Since there are L links in the system, we define the overall system state as *congested* or *uncongested*, per the average of the link congestion indicator value, $\bar{I}$

$$\bar{I} = \frac{\sum_{j=1}^{L} \sum_{k=1}^{L} I_{jk}}{L} \quad (4.28)$$

which is used to calculate the system state, S

$$S = \begin{cases} 1 & \bar{I} \geq \tau \\ 0 & \text{otherwise} \end{cases} \tag{4.29}$$

where $S = 1$ corresponds to the network being congested and $S = 0$ as the uncongested case. The threshold percentage value for congestion is τ.

4.4 Management Procedure

This section describes how the parameters are received from the network nodes, processed and transmitted back to the nodes, as required. We assume that there is a Common Control Channel (CCC) that is out of band for the primary users and can be used freely by the SUs for management communication. A CCC in CR networks facilitates a variety of operations from transmitter receiver handshake, neighbor discovery, channel access negotiation, topology change and routing information updates, to cooperation among CR users [47]. The CCC design in CR networks is originated from the medium access control (MAC) in multi-channel wireless networks. Although the concept of CCC is not new, the CCC design in CR networks faces two new challenges: PU activity and spectrum heterogeneity [74]. A thorough review of CCC design in CR networks is given in a CCC survey paper by Lo [74]. For instance, adaptive multiple rendezvous control channel (AMRCC) based on frequency hopping [75] can be used by dynamically adapting the hopping sequences to the detected PU activity. We also assume that the SUs are synchronized such that a short quiet period for sensing is reserved. Initially, the PUs may be active on a number of contiguous channels in the set of $\mathcal{C}$ channels.

Referring to Figures 4.16, 4.17, and 4.18,[1] for a more detailed description of the management process, we see that the management procedure begins with observation of the primary users activity on the network channels by the regular SUs and one or more dedicated SUs or sensors. The reason for the dedicated units is to have uninterrupted monitoring of the PU busy and idle behavior for a complete SU time duration interval,

[1]The figures are in the Appendix at the end of the chapter.

T_{td}. However, to preserve node power, the network manager may choose to assign a different SU node for the next PU monitoring period, based on the amount of transmit and receive activity and remaining battery life. The monitoring SU collects and calculates information about the chosen PU monitored, including the new cnmpMIB variables cnmpPuMonitorTime, cnmpPuOnTime, and cnmpPuOffTime. Descriptions of these variables are listed in Table 4.3.

Once these variables have been recorded, the monitoring SU may send a trap to it's cluster head (CH) to inform the CH the PU variables are available. This is an implementation of trap-directed polling,[59] which provides timely notification that PU data is ready for processing, such that the cluster head can choose to poll the SU for data when it is ready to do so. This minimizes unnecessary polling and decreases network management channel congestion.

Simultaneously, the normal communicating SU nodes will perform spectrum sensing and determine whether channels are available for SU transmission. The SUs will calculate and populate the cnmpMIB with the variables, cnmpSuSensingTime, cnmpSuTransmitTime, and cnmpSuIdleTime, based on the most recent transmission, idle time and sensing activity, respectively. Since the cnmpMIB is fully compatible with SNMPv3, and SMNP 'get' command can be issued by the cluster head node to gather the values of these elements via the SNMP management agents in the SU nodes. This information is used by the cluster head to calculate the average number of arrivals of transitions of a channel going into a busy or idle state, λ_b or λ_i, respectively. It also calculates the channel utilization, u^c, and actual transition probabilities of the channel state to idle or busy, P^c_{ib}, P^c_{bi}, P^c_{ii}, and P^c_{bb}, as described earlier. Further, the cluster head calculates the probability of false alarm, P^c_{ef}, the probability of missed detection, P^c_{em}, and the channel state transition probabilities as *perceived* by the SU nodes, γ^c_{ib}, γ^c_{bi}, γ^c_{ii}, and γ^c_{bb}. These transition probabilities provide the basis to calculate the perceived steady state probability, π^c_i, that channel c is in the idle state.

The cluster head then queries the SU nodes in it's cluster for the cnmpMIB variables, cnmpNumChannelsAvailable, and cnmpChannelIndicesAvailable, from which it calculates the probability, P_{jk}, that each SU will meet or exceed a particular channel

MIB	MIB Variable	MIB Variable Description
cnmpMIB(1)	cnmpNumChannelsAvailable(1)	"The number of channels available on the node interface."
	cnmpChannelIndicesAvailable(2)	"The indices of the channels available on the node interface."
	cnmpNumFlowsAvailable(3)	"The number of flows available on the node interface."
	cnmpFlowIndicesAvailable(4)	"The indices of the flows available on the node interface."
	cnmpSuSensingTime(5)	"The time duration in seconds used by the node for spectrum sensing."
	cnmpSuTransmitTime(6)	"The time duration in seconds used by the node for a transmission sequence of packets."
	cnmpSuIdleTime(7)	"The time duration in seconds used by the node during which no packets are transmitted."
	cnmpPuOnTime(8)	"The time duration in seconds used by the primary user for a transmission sequence of packets."
	cnmpPuOffTime(9)	"The time duration in seconds used by the primary user during which no packets are transmitted."
	cnmpPuMonitorTime(10)	"The time period duration in seconds used by the secondary user node to monitor the activity of the primary user."
	cnmpAvgLinkCongestionInd(11)	"The value of the average link congestion metric for one or more secondary user nodes. The value range is continuous from zero to one, with zero being uncongested, and one being highly congested."
	cnmpSysCongestionState(12)	"The value of the system congestion state for one or more secondary user nodes. The value range is either zero, being uncongested, or one, being highly congested."

Table 4.3 Cognitive Network Management Protocol MIB

availability per the threshold, Θ.

We have also developed a process to increase the spectrum channel awareness of the SUs by treating the sensed channels over a geographic area as an image processing problem. The method used is total variation inpainting and the result of the process is an estimate of the complete channel availability over a geographic region.[76] The accuracy of the inpainting algorithm in determining the idle or busy state of the channels is proportional to the amount of correctly sensed data from the SUs. The inpainting error rate then can be a factor in the estimation of the error probabilities, P_{ef}^{c} and P_{em}^{c}.

Flow per link information is also queried from each SU node by the cluster head using the SNMP 'get' command for the cnmpMIB variables, cnmpNumFlowsAvailable and cnmpFlowIndicesAvailable. Additionally, standard MIB II variables are queried by the cluster head to calculate the probability of packet drop at the SU. Those variables are ifInUcastPkts, ifInNUcastPkts, ifInDiscards, ifInErrors, and ifInUnknownProtos.

The cluster head assigns a value of one to the link congestion indicator variable if the packet drop probability is greater than the assigned threshold, ν. Otherwise the value for the particular link is set to zero. Each SU link in the cluster is assigned a congestion value and the average of all of the congestion values in calculated and stored into the cnmpMIB variable, cnmpAvgLinkCongestionInd. This average value is then compared to a cluster congestion threshold value, τ, and the cnmpMIB variable cnmpSysCongestionState is assigned the value one if the average congestion indicator value exceeds τ. Otherwise, cnmpSysCongestionState is set to zero.

The values of cnmpAvgLinkCongestionInd and cnmpSysCongestionState are then available for query by the Network Manager to determine coarsely whether the overall cluster is considered to be congested, or more finely, how much average link congestion is present. This can be used to influence the routing protocol to select a less congested path from source to destination, if possible. Congestion adaptive routing protocols have been proposed by Tran and Raghavendra, [77] and Kumaran and Sankaranarayanan,[78] which could possibly be adapted to use this metric as a predictive factor in the routing determination. Here, we see a key contribution of this metric is that it provides a probabilistic estimate of network congestion taking into account the dynamic spectrum

Numerical Study Parameter	**Explanation**
Geographic Area Grid	500 x 500 meters
PU interference range	150 meters
Number of PUs	1, 2, or 5
Number of SUs	18
Total number of channels	30
Number of active PU channels	1 to 25
System congestion threshold, τ	50%
Packet drop rate threshold, ν	5%
Probability of false alarm error, P_{ef}^{c}	10%
Probability of missed detection error, P_{em}^{c}	10%

Table 4.4 Numerical Study Parameters and Explanations

characteristics of a cognitive radio network using a combination of standard SNMP MIB II and custom cnmpMIB variables.

4.5 Numerical Results

The numerical study examines how capturing the information to determine the system congestion state can be used to influence the network behavior towards greater throughput by avoiding congested links where possible. The model for the study was developed using MATLAB for numerical computation. We consider a square area defined by 500 x 500 meters in which we randomly place a number of primary users and a number of secondary users. For our results, we've used 1, 2, or 5 PUs and 18 SUs over the area. A table of important study parameters is included in Table 4.4. The node locations and coverage areas for the PUs and cluster heads are shown in Figure 4.6. The PUs are active on the available channels per a Poisson distribution. The interrupt range of each primary user is defined by the distance within which the channels used by the primary user are not available and in this case is set to 150 meters.

The number of channels used by the primary users is contiguous, but the number of channels and the starting channel are random, unless otherwise noted, such that the PUs do not interfere with each other on the same channels. To simplify the interaction of the effect of the PUs on the SUs, we used the sum of the log distance path loss from

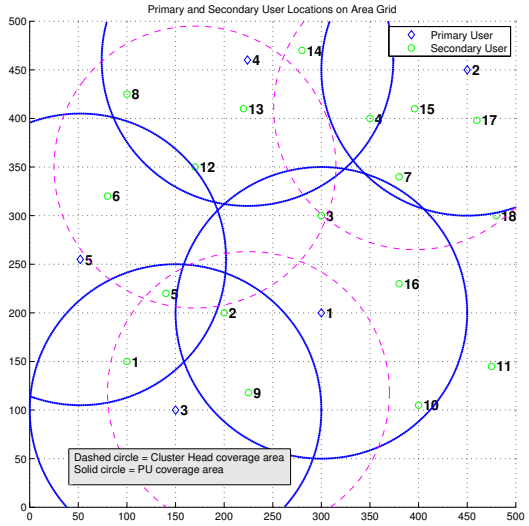

Figure 4.6 Distribution of PU and SU node locations with coverage areas of PUs and Cluster Heads on Grid

each PU to each SU in the calculation of the probability of packet error. As an example case, we consider the Bit Error Rate (BER), for Binary Phase Shift Keying (BPSK) and an Additive White Gaussian Noise (AWGN) channel for a particular packet that can be expressed as

$$P_e = Q(\sqrt{\frac{2E_b}{N_0}}) \tag{4.30}$$

Calculations were performed using this BER model. [79]

We assume sensing error probability values for the probability of false alarm, P_{ef}^c, and probability of missed detection, P_{em}^c, are 10%. The system has 30 total channels and we included the 'genie' case, where the SUs are allowed to have full channel availability knowledge, so that the effect of the PU activity could be more directly observed on our network link graphs.

Figure 4.7 shows the effect of a single PU with 10 active channels on the SU network where several SU links in the PU coverage area have a packet drop rate greater than the threshold, ν, of 5%, showing those links as congested, as indicated by the red dashed arrows. Note, however, that the availability other links, such as link $l_{2,9}$ and $l_{10,16}$ are not affected by the PU, which are the green solid arrows. This is because the

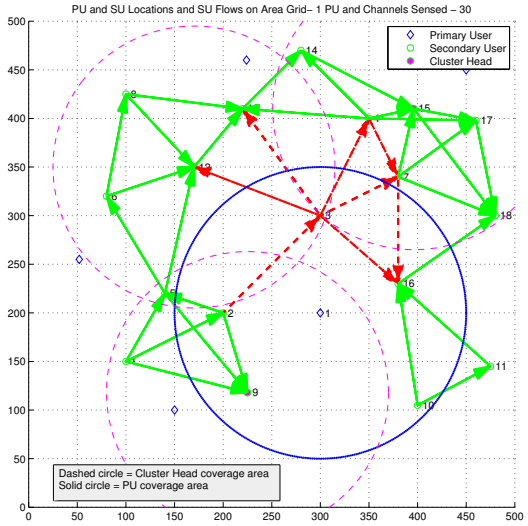

Figure 4.7 Effect of 1 Primary User with 10 Active Channels on the SU Network

assignment of channels to the SUs are random and there may be up to 20 additional available channels when the PU is active. Recall that the number of remaining available channels are dependent upon the busy and idle durations of the PU, together with the probability of sensing error, and the overall time duration that the SU nodes are attempting to access the channel.

Similarly for Figure 4.8 and Figure 4.9, we see the effects of the PU activity where each PU has 10 active channels. Consolidating the data from using 1, 2, and 5 PUs is shown in Figure 4.10, we see that increasing the number of PUs and the number of channels quickly increases the average link congestion.

The system congestion threshold, τ, is set to 50% and we see for the case of 2 PUs, the system state becomes congested when each uses 11 contiguous channels. When 5 PUs are used, the congestion threshold is exceeded at only 7 channels. The threshold can be used by the Network Manager to trigger management action and can be arbitrarily set, based on the desired network performance. The threshold can also be set adaptively depending on changing conditions, such as differing performance criteria in response to the level of PU activity, or external factors such as time of day.

In Figure 4.10 we examine the effect of how the number of contiguous channels

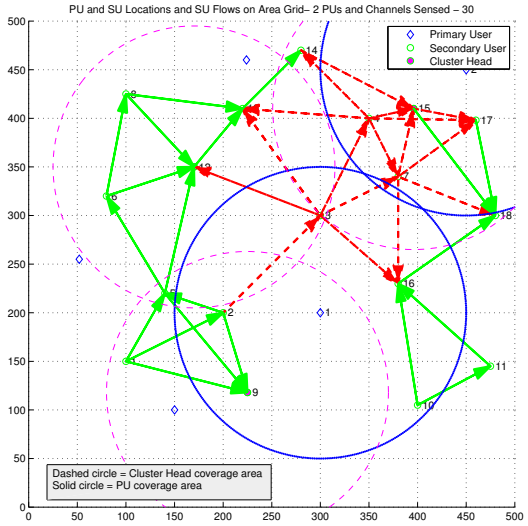

Figure 4.8 Effect of 2 Primary Users with 10 Active Channels on the SU Network

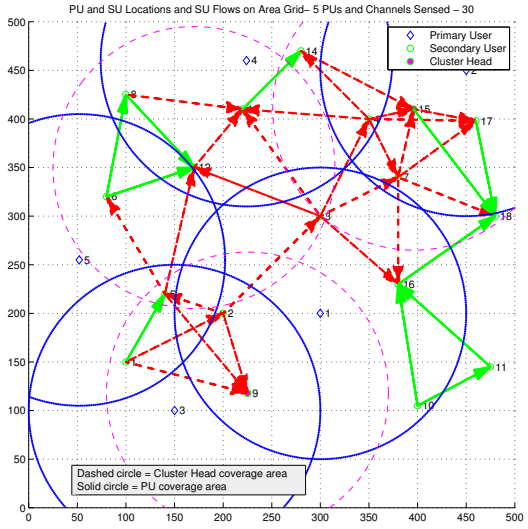

Figure 4.9 Effect of 5 Primary Users with 10 Active Channels on the SU Network

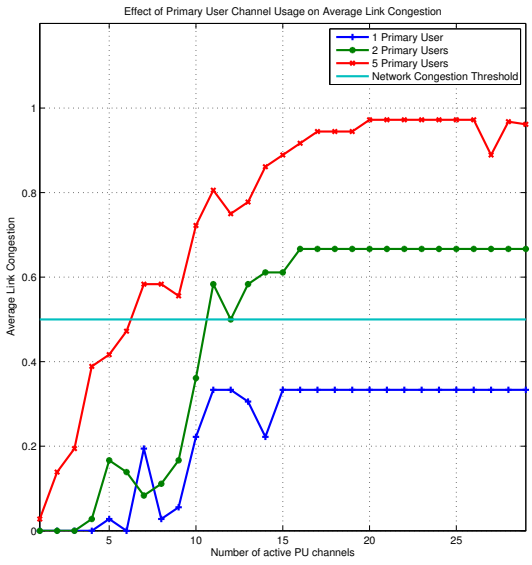

Figure 4.10 Effect of Primary User Activity on Average Link Congestion

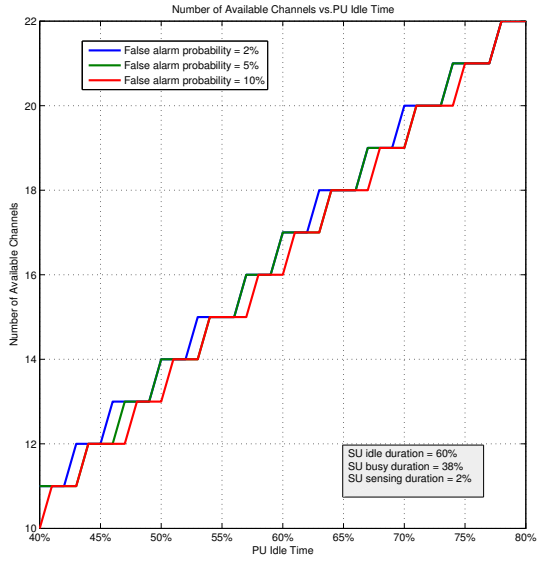

Figure 4.11 Effect of the PU Idle Time on the Number of Channels Perceived Available

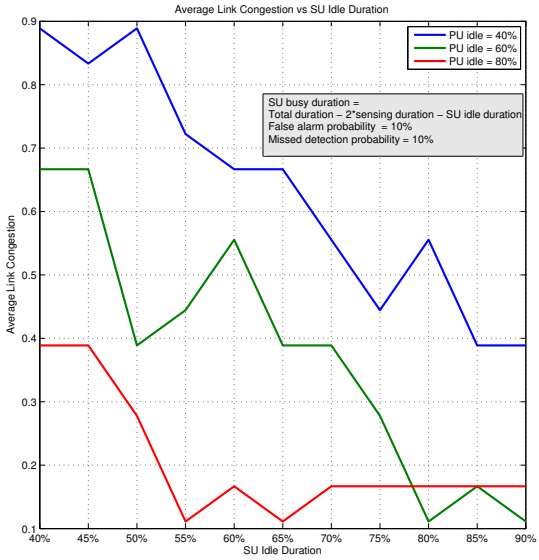

Figure 4.12 Effect of the SU Idle Duration on the Average Link Congestion

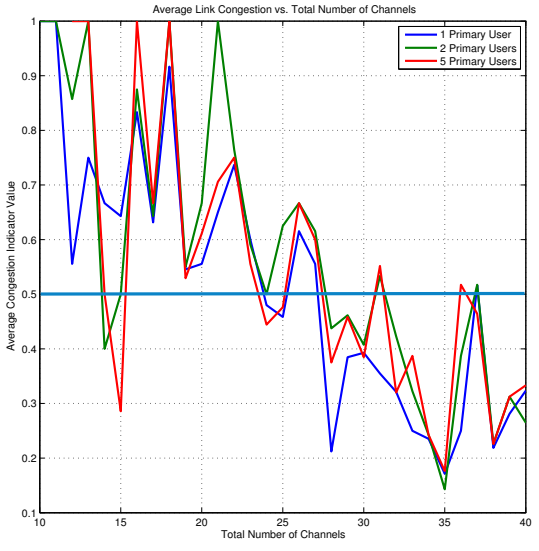

Figure 4.13 Effect of the Total Number of Channels on the Average Link Congestion

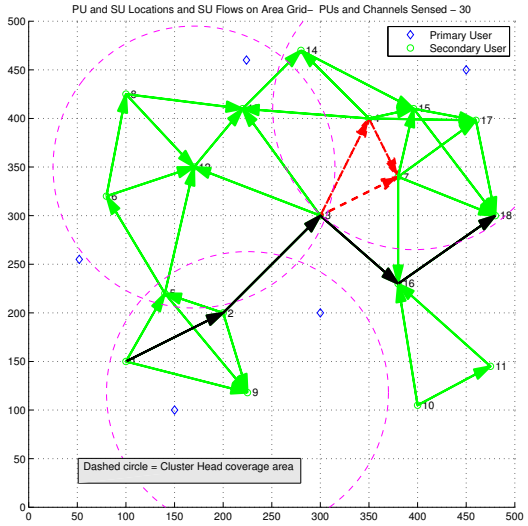

Figure 4.14 Example path without PU interference

used by the PUs affects the average link congestion. In each case of 1, 2, or 5 primary users, the congestion increases until adding more PU channels no longer increases the congestion. In our system, in each PU configuration, the congestion maximum remains basically constant after 15 to 20 channels. It does not increase further, because the total number of SU channels that have been interfered with by the PU coverage area are not further affected by additional channels used by the PUs. Hence the average congestion remains relatively constant because the ratio of unaffected to affected SU channels stabilized for this spatial configuration.

Another consideration of the PU effect on the CR network is to examine the perceived number of available channels, C_{jk}, as affected by PU idle duration in Figure 4.11. Here, we observe that as the perceived number of channels increases with increasing PU idle duration, we see also that the increasing false alarm probability delays the recognition of possible available channels. For example, when the PU idle duration is at 45%, the lowest false alarm of 2% shows the channel increase from 12 to 13 prior to false alarm probabilities of 5% and 10%. Intuitively, we would expect this result, since a lower error probability indicates more correct sensing, and therefore a more accurate perception of the channel availability for a given amount of average PU idle time per

observation period.

However, in Figure 4.12, we see that for increasing SU idle duration, the average link congestion decreases. This is due to less contention for the links by the SUs. The figure shows curves for PU idle values of 40%, 60%, and 80%, which also demonstrate that increasing idle duration decreases the link congestion, whether applied to SU nodes or the PU nodes. This observation allows the use of a possible network management control action to relieve congestion by regulating SU idle duration when necessary to reduce congestion. Additionally, cross layer control could include throttling of the data to be transmitted at the application layer.

Figure 4.13 shows the effect of the total number of channels in the system on the average congestion value. Here we examine how 1, 2, or 5 PUs impact the average congestion as the number of channels in the system increases from 10 to a maximum of 40 channels, and each PU can access up to 10 available channels. The figure shows that the congestion response shape is similar for each set of PUs, in that the congestion is generally not reduced below the 50% threshold until the system contains 27 or more channels. That the congestion generally reduces as the number of channels increases is intuitive, given the increased connectivity available to the SU nodes.

When the number of channels is below 25, because the available channels to SUs are usually small due to the occupancy of the channels by the PUs, the congestion will not monotonically change with the number of PUs. When a sufficient number of channels are available, the number of PUs play a more important role in determining the average congestion of the channels for the SUs. The randomness exists in the figure because in our simulation, the channels sensed by the SUs are randomly chosen, as may happen in a practical system [76], which in turn affects the success probability of the SUs acquiring the channels needed for data transmission. This again demonstrates the major role of the perception of channel availability to the SUs, which could be a decisive factor for the performance of the SUs in the secondary network.

Considering another potential control action, we see in Figure 4.14 an example of a source to destination SU path without PU interference after applying the congestion metric to the active links. Then, as a result of the congestion information, the Network

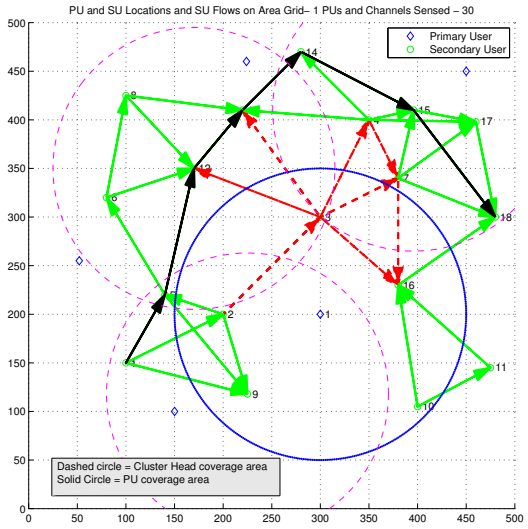

Figure 4.15 Example path avoiding PU interference

Manager can direct the path to be rerouted around the congestion caused by emerging PU activity to maintain similar throughput, as shown in Figure 4.15.

4.6 Conclusion and Future Work

In this chapter, we have investigated the need to adapt and extend the traditional network management concepts to cognitive radio ad hoc networks. We have shown that by creating a model framework to introduce new metrics that are available to a network manager with a total system view, such as the network congestion index, the network manager can influence network performance. This can be done, for instance, by directing the cluster heads (distributed managers) to avoid potentially troubled areas, and route paths with higher channel availability and throughput. This management action can reduce the interference to the primary users.

This work created probabilistic congestion metrics that are specifically intended for application to CRAHNs. These are the average link congestion indicator and overall network (or cluster) congestion indicator as components of a tool set utilized by a network manager node to manage the CR network. Thirteen new cnmpMIB variables have been created to aid in the metric calculations. The average network congestion

indicator is derived as a function of PUs' activities and SUs' strategy per a 2-state Markov model, and in turn provides grounds for setting control parameters for SUs to relieve network congestion if needed.

As highlighted in a recent NSF report, [80] Section 4.5 states, "Most currently available approaches towards measurement provide coarse-grained counters such as SNMP variables, or long timescale flow-based summarizations. From an architectural standpoint, research is needed to determine what finer-grained currently-hidden information (e.g., wireless channel characteristics, MAC protocol and routing information) can be exposed to the user, to network management functions, and to others (e.g., carried in protocol headers) to help manage (e.g., diagnose and (auto-)configure) a network". Our proposed congestion indicator can be considered as an attempt to relate finer-grained information such as channel availability and MAC protocol to a network level metric used by a network manager to make decisions. This work is preliminary and we intend to further investigate network control that can take advantage of the network management process.

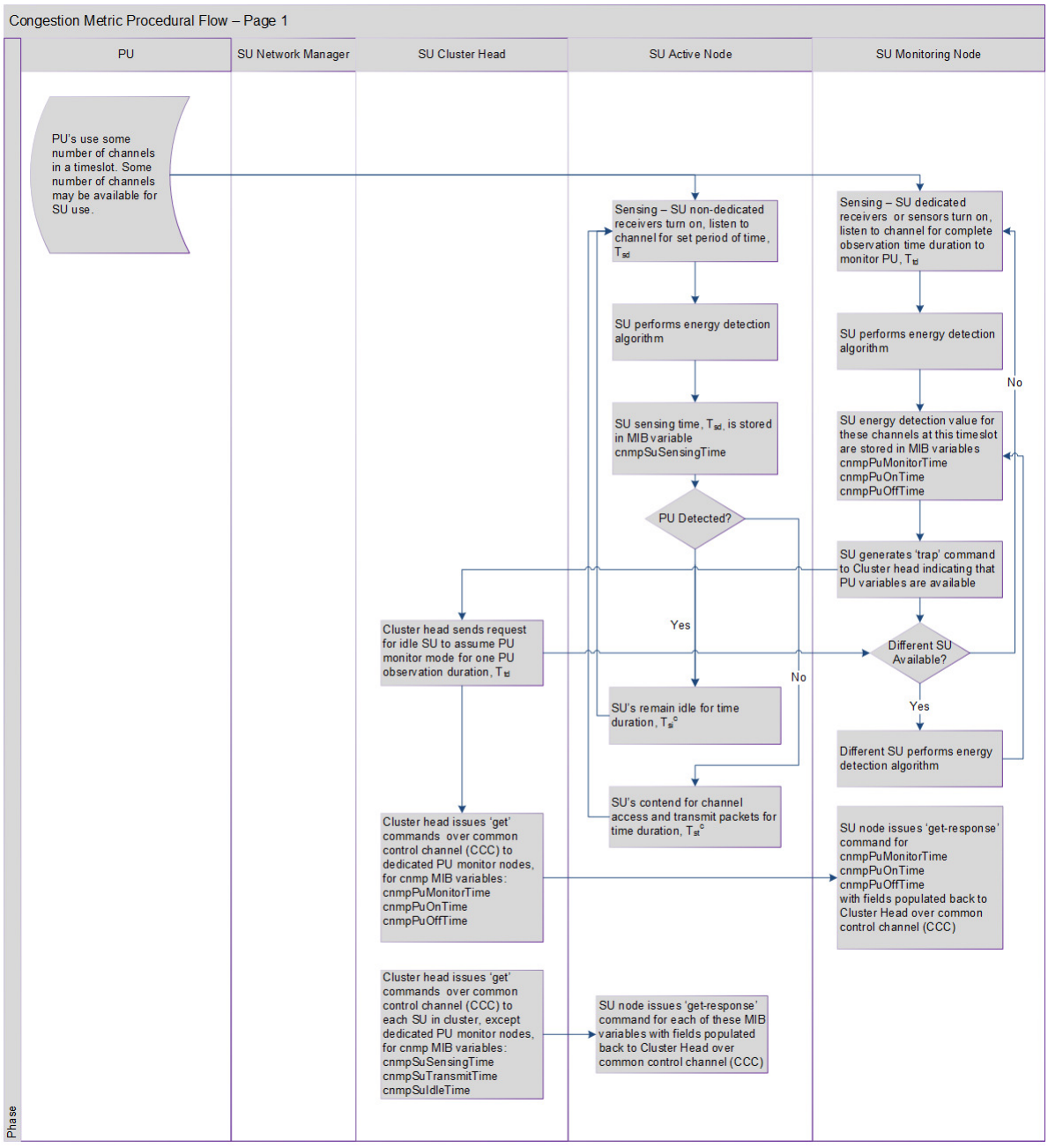

Figure 4.16 Management Procedure Flowchart - Page 1

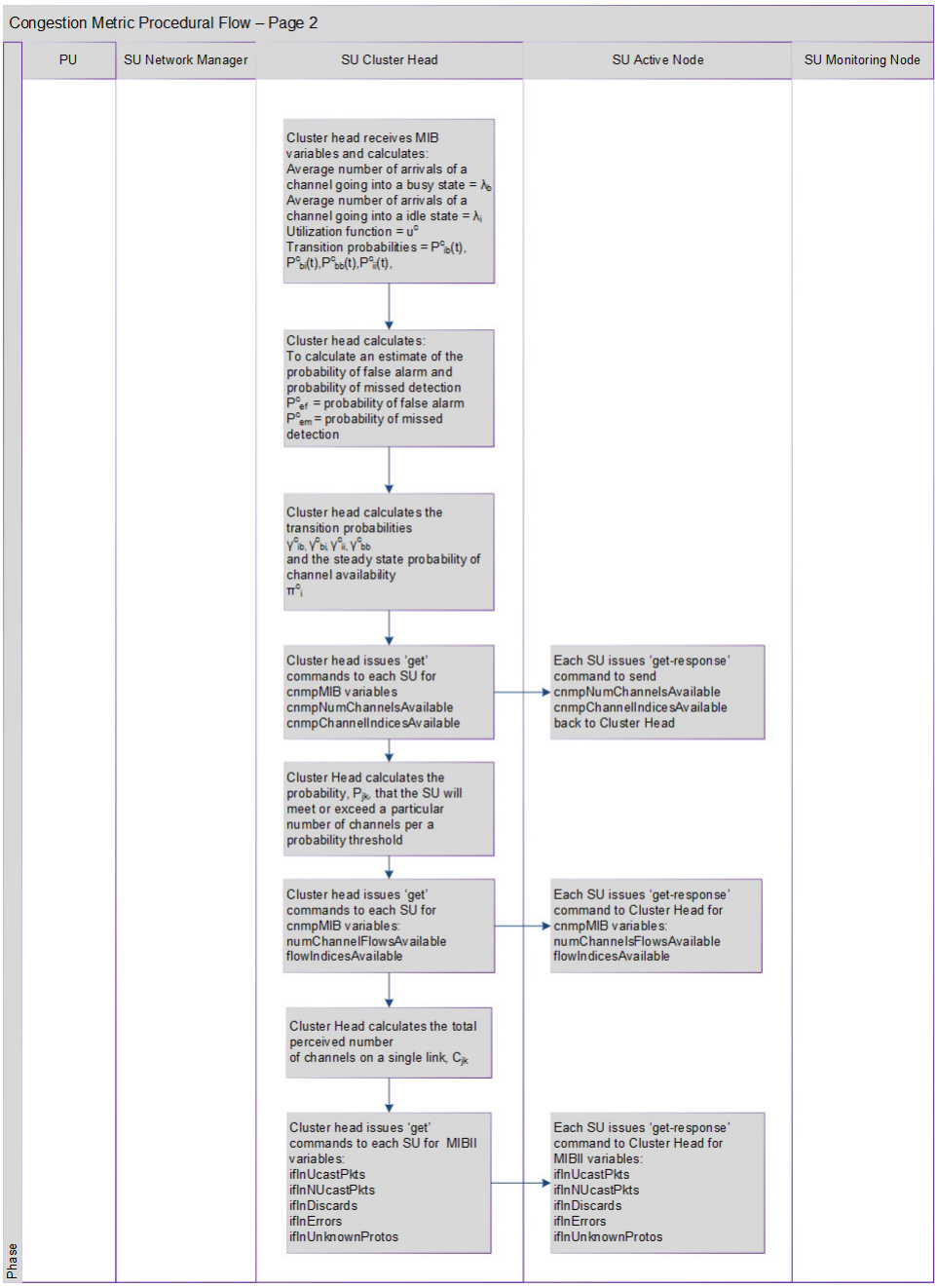

Figure 4.17 Management Procedure Flowchart - Page 2

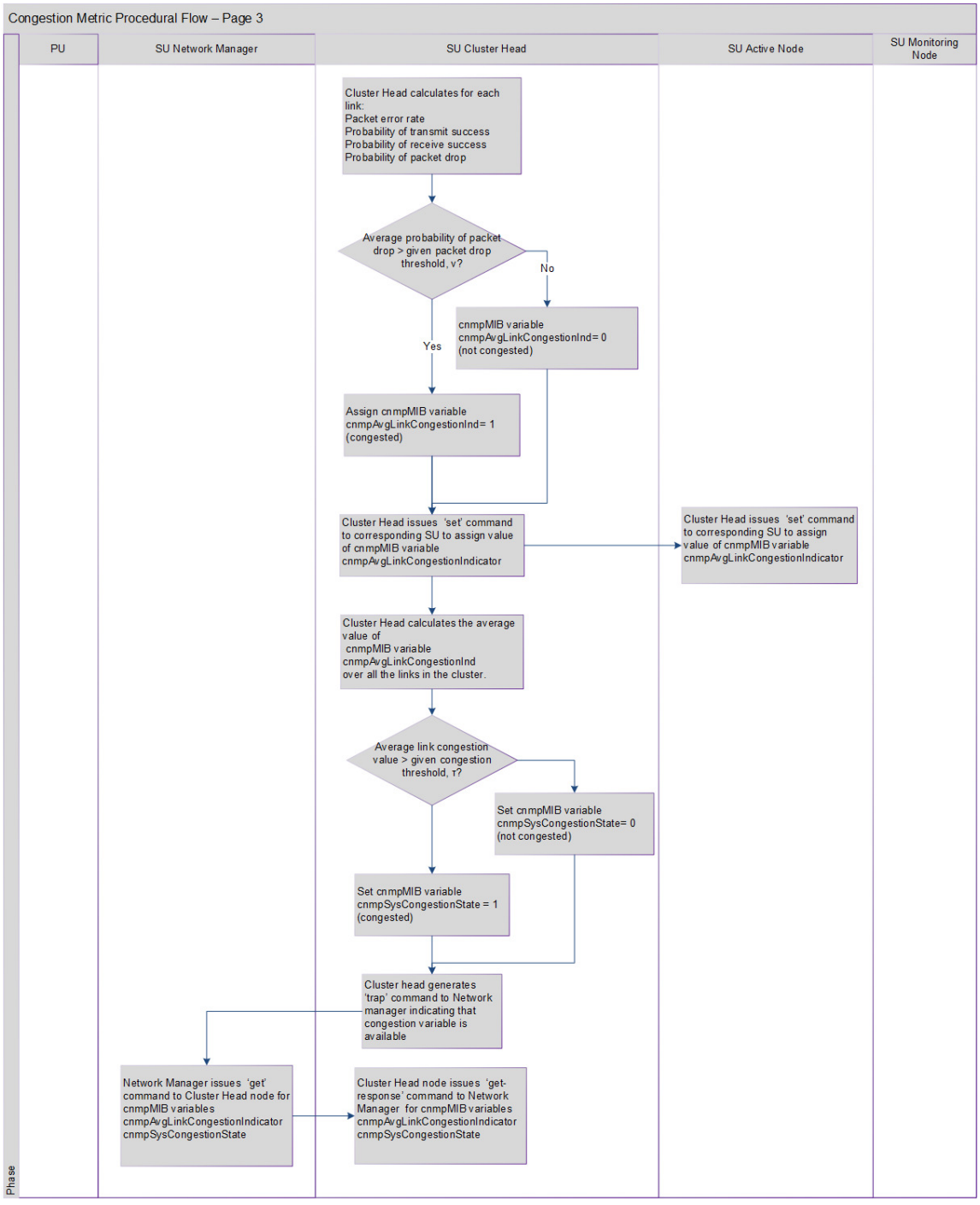

Figure 4.18 Management Procedure Flowchart - Page 3

Chapter 5

Per-Node Throughput Performance of Overlapping Cognitive Radio Networks

In this chapter, we study multiple Cognitive Radio (CR) networks coexist in the same spatial domain. As a start, we consider two uncoordinated and geographically overlapping CR networks coexisting together with a primary network. We specifically study the achievable per-node throughput performance of the CR networks. Firstly, an interference model is specified which models the situation. By using this model we derive the per-node throughput for overlapping CR networks. Furthermore, the upper bound for the probability of false alarm, which is required to achieve a certain throughput, is deduced. The results of this work illustrates how the different CR network parameters, such as network density, transmission probability, and sensing performance, impacts the achievable per-node throughput in overlapping CR networks. This can be served as guidance for the deployment of multiple CR networks.

5.1 Introduction

Cognitive Radio (CR) is a revolutionary technology aiming to increase spectrum utilization through dynamic secondary spectrum access. In many practical scenarios, multiple CR networks (CRNs) may coexist in the same geographical area. One example is disaster relief effort, where different organizations such as police, fire fighters, and emergency medical services are all deployed in the disaster area at the same time. All of these participating organizations use CRs to sweep a wide range of spectrum and find suitable spectrum for communications. Another example is in battlefield communications, where multiple wireless networks may coexist. These networks may belong to different military branches or organizations such as the army and the air force. With

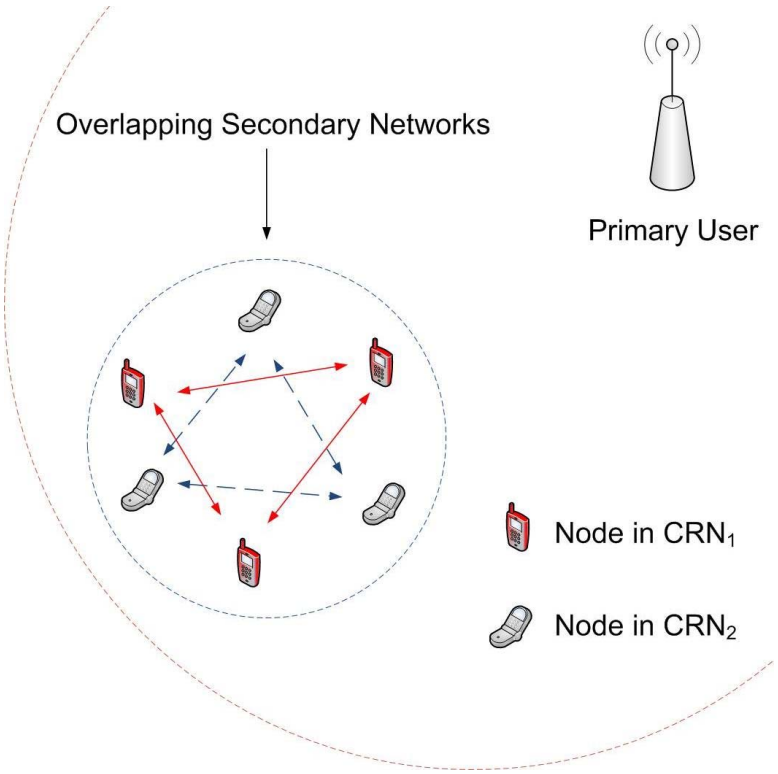

Figure 5.1 An example network scenario, where two overlapping CR networks are within the range of a primary user.

the advancement of CR technology, it is expected that many of the network elements will have cognitive capability enabled by a software defined radio platform, such as the Joint Tactical Radio System (JTRS) program being a prime example.

The network scenario for the case of two overlapping CR networks is demonstrated in Figure 5.1. The figure shows two coexisting CR networks, CRN_1 and CRN_2, that are operating in the same spatial domain and on the same frequency with a Primary User (PU). The main problem is that secondary networks will interfere with each other in such situations, in addition to yielding to the PUs. In this work we specifically study the impact of the interfering CR network on the performance of a given CR network.

There are rich literatures on the coexistence of heterogeneous wireless networks on the ISM bands. Research work in this field has been focused on the coexistence of WiFi (802.11) and Zigbee (802.15.4) radios, see, e.g., [114, 115, 116]. IEEE 802.11 b/g networks may interfere with IEEE 802.15.4 sensor networks and thereby introduce significant coexistence problems for low-power sensor nodes. Although intensive research has been carried out on CR technology and single CR networks, only a few studies

address the coexistence of multiple CR networks [117, 118, 119, 120]. Furthermore, none of the existing works discuss the fundamental per-node throughput of a CR user when multiple CR networks coexist with the PUs.

The main objective of this work is to find out how much throughput a node in a CR network can achieve in the presence of another CR network and a PU. The main contributions of this work are as follows. We firstly derive an interference model for overlapping CR networks which takes into account spectrum sensing performance. This model is then used to deduce the probability that the received Signal to Interference and Noise Ratio (SINR) is larger than the required threshold for successful reception of a packet. These results are used to find out the per-node throughput and the bound for the probability of false alarm in case of coexisting CR networks. This bound determines whether it is feasible to deploy multiple CR networks in the same region with the required quality-of-service, say, the minimum throughput. We analyze the performance of a node in detail by considering the effects of various CR network parameters such as transmission probability, performance of spectrum sensing (false alarm and detection probabilities), etc. This work provides fundamental insights on the dominant factors of the per-node throughput in case of overlapping CR networks.

This chapter is organized as follows. First, the used system model is defined in Section 5.2. Then, we derive the interference model, the probabilistic per-node throughput, and the performance bound for a CR node in overlapping CR networks in Section 5.3. Theoretical results are verified by simulations. Fundamental results and detailed analysis on the performance of a CR node in coexisting CR networks are presented in Section 5.4. Section 5.5 gives the concluding remarks.

5.2 System Model

In this work, we will focus on the case where two CR networks are uncoordinated and deployed in the same geographical area at the same time in addition to a PU. The presence of the PU is defined using the following hypotheses. Hypothesis H_0 denotes the case in which the PU is not present and H_1 stands for the case in which the PU is

present. We further make the following assumptions:

- Each CR network performs its own spectrum sensing and the corresponding probabilities of detection and false alarm are taken into account in this work. However, they do not coordinate their sensing nor share the sensing results. For example, although the organizations are collaborating on the disaster relief mission, each organization has its own CR network and their CR networks are not coordinated since the spectrum situation in the disaster area is not known a priori and each organization has its own administrative constraints such as security requirements.

- Since CSMA/CA is a well-established Media Access Control (MAC) protocol and has been adopted by many practical wireless networks, we assume that the CR networks use CSMA/CA as the basis of their MAC protocol. It is also assumed that CR nodes can detect others' transmissions, e.g., by using CSMA/CA, where the RTS/CTS message exchange is carried out before data transmissions.

- The secondary CR networks are homogeneous in the sense that the nodes in the CR networks have similar capabilities and behaviors, such as the transmission power.

- Channels and signals from the PU to CRs are complex and the channels experience fast and shadow fading leading to Gaussian distributed signals [121].

- CR networks are located in an urban area. Since the CR nodes are typically less powerful than the primary nodes, have smaller transmission ranges and are located closer to each other, we model the channel between CR nodes with Rayleigh fading.

- Noise is Additive White Gaussian Noise (AWGN).

In this work, we focus on CR ad hoc networks instead of CR networks with infrastructure support such as the IEEE 802.22 [122] systems.

5.3 Theoretical Modeling

In this section we first derive the interference model for overlapping CR networks which is then exploited to deduce the per-node probabilistic throughput for such scenario. Then, we enhance these results by taking into account the sensing parameters, the probability of false alarm and detection. The performance bound for the probability of false alarm is also derived. Finally, theoretical results are verified by simulations.

5.3.1 Interference Modeling and Probabilistic Throughput per node

Both of the CR networks are uniformly random networks where nodes are independently distributed in an area according to a Poisson Point Process (PPP). Node densities of CRN_1 and CRN_2 are denoted by λ_1 and λ_2, respectively. As a channel model we use deterministic distance-dependent path loss $r^{-\alpha}$, where r is the distance between the transmitter and the receiver and α is the path loss exponent. We consider Rayleigh fading, x with $E\{x^2\} = 1$.

The Cartesian coordinates of a node are denoted by X and Y. These random variables are independent of the other nodes' locations and uniformly distributed in $[-L, L]$. By setting the node density $\lambda = N/(4L^2)$, where N is the number of nodes, the probability of finding k nodes in an area A in the plane is given by

$$\Pr\{k \in A\} = \frac{e^{-\lambda A}\,(\lambda A)^k}{k!}. \tag{5.1}$$

With these assumptions we can calculate the mean μ and variance σ^2 of interference $\mathcal{I}$ for a random Poisson network with density λ as follows [123]

$$\mu = \frac{2\lambda p\pi d_0^{(2-\alpha)}}{\alpha - 2} \tag{5.2}$$

$$\sigma^2 = \frac{2\lambda p\pi d_0^{2(1-\alpha)}}{\alpha - 1}, \tag{5.3}$$

where p is the transmission probability and d_0 the near field cut-off radius. The near field cut-off radius defines the distance in which other nodes in a network cannot transmit. For a large number of interferers, the interference can be modeled as Gaussian

distributed due to the Central Limit Theorem, with parameters μ and σ^2 [124]. We call this as intra-network interference within one CR network.

In our case the problem is that nodes in the other CR network may decide to transmit as well (depending on the sensing results) and thus, create inter-network interference. We can model inter-network interference similarly as before using Equations (5.2) and (5.3). The resulting interference $\mathcal{I}$ is Gaussian distributed $\mathcal{N}(\mu_1 + \mu_2, \sigma_1^2 + \sigma_2^2)$ which gives

$$\mu = \frac{2\lambda_1 p_1 \pi d_{0,1}^{(2-\alpha)}}{\alpha - 2} + \frac{2\lambda_2 p_2 \pi d_{0,2}^{(2-\alpha)}}{\alpha - 2} \tag{5.4}$$

$$\sigma^2 = \frac{2\lambda_1 p_1 \pi d_{0,1}^{2(1-\alpha)}}{\alpha - 1} + \frac{2\lambda_2 p_2 \pi d_{0,2}^{2(1-\alpha)}}{\alpha - 1}. \tag{5.5}$$

Furthermore, the received SINR γ is calculated as follows

$$\gamma = \frac{P x^2 R^{-\alpha}}{\mathcal{I} + \sigma_n^2}, \tag{5.6}$$

where P is the transmission power, R the distance between a transmitter and a receiver and σ_n^2 is the noise power. Then, we can calculate the probabilistic throughput

$$\begin{aligned} \Pr\{\gamma > \theta\} &= \Pr\left\{\frac{x^2 P R^{-\alpha}}{\mathcal{I} + \sigma_n^2} > \theta\right\} \\ &= \Pr\left\{x^2 > \frac{\theta(\mathcal{I} + \sigma_n^2) R^{\alpha}}{P}\right\}, \end{aligned} \tag{5.7}$$

where θ is the required SINR for successful reception (threshold). By denoting $z = x^2$ this can be deduced to the following form

$$\begin{aligned} \Pr\{\gamma > \theta\} &= E\left\{F_{c,z}\left(\frac{\theta(\mathcal{I} + \sigma_n^2)}{P R^{-\alpha}}\right)\right\} \\ &= E\left\{\exp\left(\frac{-\theta(\mathcal{I} + \sigma_n^2)}{P R^{-\alpha}}\right)\right\}, \end{aligned} \tag{5.8}$$

where $F_c(.)$ stands for the Complementary Cumulative Distribution Function (CCDF). Moreover, note that z is an exponential random variable and $F_{c,z}(z) = e^{-z}$. The expectation is taken over the Gaussian distribution which gives [124]

$$\begin{aligned} \Pr\{\gamma > \theta\} &= \exp\left(-\frac{\theta(\mu + \sigma_n^2)}{P R^{-\alpha}}\right) \exp\left(\frac{\theta^2 \sigma^2}{2(P R^{-\alpha})^2}\right) \\ &\times Q\left(\frac{\theta \sigma^2}{P R^{-\alpha}} - \frac{\mu}{\sigma}\right). \end{aligned} \tag{5.9}$$

5.3.2 Simultaneous Secondary Access

In CR networks the received interference depends on the sensing results. Furthermore, in case of overlapping the operations of the other CR network also affect the performance. Consequently, we have multiple scenarios listed in Table 5.1 depending on the PU's activities and the spectrum sensing results of the CRNs. For instance, if the PU is idle (H_0), and only CRN_2 has a false alarm, then CRN_1 will be able to use that channel for transmission alone. By denoting the probability of false alarm and probability of detection as $P_{f,i}$ and $P_{d,i}$ for CRN_i, the probability of this scenario is $(1 - P_{f,1})P_{f,2}P(H_0)$. Other cases are determined using similar reasoning. The probability of miss for CRN_i is defined as $P_{m,i} = 1 - P_{d,i}$.

Table 5.1 Possible transmission scenarios

Scenarios	H_0	H_1
Idle	$P_{f,1}P_{f,2}$	$P_{d,1}P_{d,2}$
CRN_1	$(1 - P_{f,1})P_{f,2}$	$P_{m,1}P_{d,2}$
CRN_2	$(1 - P_{f,2})P_{f,1}$	$P_{m,2}P_{d,1}$
CRN_1 & CRN_2	$(1 - P_{f,1})(1 - P_{f,2})$	$P_{m,1}P_{m,2}$

By using the scenarios defined in Table 5.1 we can derive the following equation for successful packet reception for a node in CRN_1

$$\begin{aligned}\Pr\{\gamma > \theta\} &= (1 - P_{f,1})P_{f,2}P(H_0)\Pr\left\{\frac{x^2P_1R^{-\alpha}}{\mathcal{I}_1 + \sigma_n^2} > \theta\right\} \\ &+ P_{m,1}P_{d,2}P(H_1)\Pr\left\{\frac{x^2P_1R^{-\alpha}}{\mathcal{I}_1 + \mathcal{I}_p + \sigma_n^2} > \theta\right\} \\ &+ (1 - P_{f,1})(1 - P_{f,2})P(H_0)\Pr\left\{\frac{x^2P_1R^{-\alpha}}{\mathcal{I}_1 + \mathcal{I}_2 + \sigma_n^2} > \theta\right\} \\ &+ P_{m,1}P_{m,2}P(H_1)\Pr\left\{\frac{x^2P_1R^{-\alpha}}{\mathcal{I}_1 + \mathcal{I}_2 + \mathcal{I}_p + \sigma_n^2} > \theta\right\}, \end{aligned} \tag{5.10}$$

where $\mathcal{I}_1$, $\mathcal{I}_2$, and $\mathcal{I}_p$ denote the received intra-network, inter-network, and PU's interference, respectively. Then, by formulating each term of Equation (5.10) in the same way as in Equation (5.8) and solving that we can find an exact value for $\Pr\{\gamma > \theta\}$, similar to Equation (5.9).

The main problem is that the performance of CRN_1 will be determined by the operations of CRN_2 and vice versa. By using these formulas we will analyze the throughput of overlapping CR networks to see what are the suitable bounds to guarantee reasonable performance.

We define the per-node throughput such that the transmitter has a packet to transmit while a receiver is idle, i.e., the receiver does not have a packet to transmit. Moreover, the received SINR has to be larger than the threshold for successful packet reception. This can be mathematically formulated as follows

$$S = p(1-p)\Pr\{\gamma > \theta\}. \tag{5.11}$$

In practice CR users should achieve reasonable throughput to enable feasibility from the economic perspective. We denote this throughput threshold by $\hat{S}$. Next, we derive the bound of the probability of false alarm that is required to achieve the desired throughput, $S \geq \hat{S}$. By analyzing Equation (5.10) we have concluded that in practice the second and the fourth term in Equation (5.10) have negligible influence on the performance of CR users, since both the miss rate and the probability of the PU being active are small. In addition, it is not practical to design CR networks by assuming that their transmissions would overlap with the transmissions of the PU's. Thus, we use the following approximation

$$\begin{aligned} S &\geq \hat{S} \Rightarrow \\ \hat{S} &\leq p(1-p)(1-P_{f,1})P_{f,2}P(H_0)\Pr\left\{\frac{x^2P_1R^{-\alpha}}{\mathcal{I}_1+\sigma_n^2} > \theta\right\} \\ &+ p(1-p)(1-P_{f,1})(1-P_{f,2})P(H_0) \\ &\times \Pr\left\{\frac{x^2P_1R^{-\alpha}}{\mathcal{I}_1+\mathcal{I}_2+\sigma_n^2} > \theta\right\}. \end{aligned} \tag{5.12}$$

The above inequality shows the maximum achievable throughput for a node in CRN_1 given the PU's activity and the spectrum sensing performance of the two CRNs.

Moreover, let us define

$$\Omega_1 = P(H_0)\Pr\left\{\frac{x^2P_1R^{-\alpha}}{\mathcal{I}_1+\sigma_n^2} > \theta\right\} \tag{5.13}$$

$$\Omega_2 = P(H_0)\Pr\left\{\frac{x^2P_1R^{-\alpha}}{\mathcal{I}_1+\mathcal{I}_2+\sigma_n^2} > \theta\right\}, \tag{5.14}$$

and assume that both CRNs have the same spectrum sensing performance, i.e., $P_{f,1} = P_{f,2} = P_f$. Then,

$$\hat{S} \leq p(1-p)(1-P_f)[P_f\Omega_1 + (1-P_f)\Omega_2] \tag{5.15}$$

It is observed that when the false alarm probability P_f is very small, the achievable throughput approaches $p(1-p)\Omega_2$. It can be shown that as long as $\frac{\Omega_1}{\Omega_2} \leq \frac{2-P_f}{1-P_f}$, the achievable throughput will decrease when P_f increases.

If the spectrum sensing performance of CRN_2 is given *a priori*, then we can find out the maximum probability of false alarm of CRN_1 for achieving a certain throughput $\hat{S}$.

$$P_{f,1} \leq 1 - \frac{\hat{S}}{(P_{f,2}\Omega_1 + (1-P_{f,2})\Omega_2)p(1-p)}. \tag{5.16}$$

In other words, Equation (5.16) defines the upper bound for the probability of false alarm of CRN_1.

5.3.3 Simulation Verification

The correctness of the theoretical results has been verified by Matlab simulations. We use the Monte Carlo simulation method and for each simulation run we randomly generate the received interference which is then used to produce the SINR according to Equation (5.6). SINR is further exploited to find out whether a packet was received properly or not by comparing it to the threshold. Finally, we took an average over all the runs so that the results are comparable with Equation (5.10). The number of simulation runs was set as 10,000.

For each simulation run the presence of the PU is first determined randomly using $P(H_0)$. We consider only the performance of CRN_1 and hence, if a false alarm occurs in CRN_1, the secondary spectrum access opportunity is missed. However, if the PU is idle and CRN_1 senses the situation correctly, the number of nodes in CRN_1 is generated from a Poisson distribution with parameter $\lambda_1 A$. After this the nodes are positioned randomly according to the PPP and the received interference is calculated by taking into account d_0 and p. In other words, only the nodes that are outside of d_0 and have a packet to transmit will generate interference. The same procedure is repeated for CRN_2 as well.

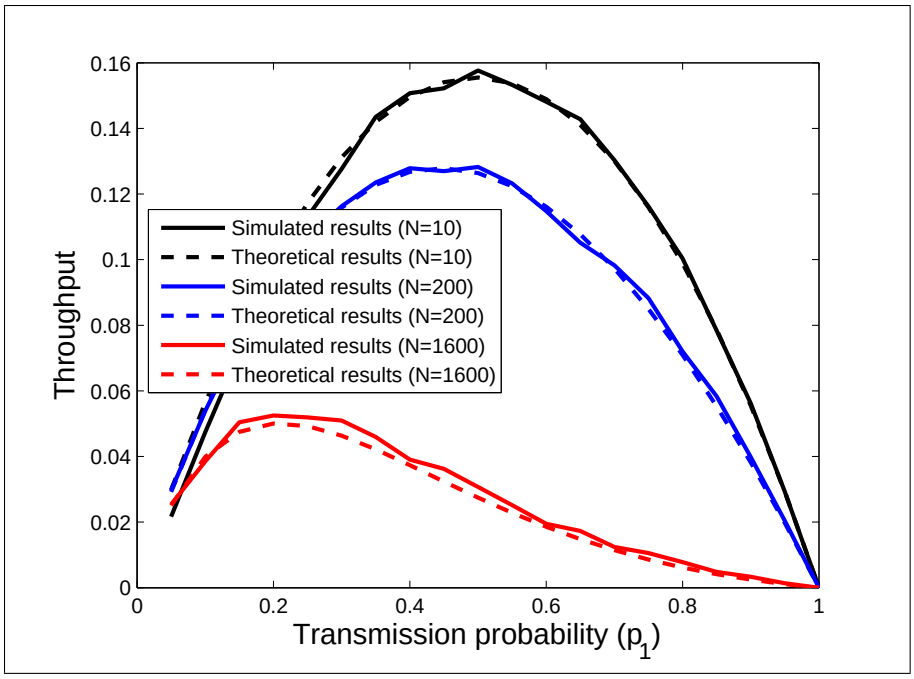

Figure 5.2 Throughput of CRN1 as a function of transmission probability.

Furthermore, if the PU transmits and CRN_1 does not detect the activity of the PU, the transmissions overlap. This happens with a small probability but still it has to be taken into account in the simulations. In this case the PPP is again used for positioning the nodes of CRN_1 and the inter-network interference is produced as in the previous case but now the PU signal is also considered. If CRN_2 also misses the transmission of the PU, interference from CRN_2 is added. Finally, we calculate the mean of probability of successful transmission over all the simulation runs and use that to estimate the throughput.

The outcomes of the simulations are displayed in Figure 5.2 together with the theoretical results. In the figure we show the results for different numbers of nodes, i.e., for various network densities since the size of the are is fixed. As the figure demonstrates, theoretical and simulated results match up well even in case of small networks ($N = 10$). The used network parameters are the same as in [123]: $d_0 = 3m$, $R = 1m$, $P = 10nW$, $\sigma_n = 5fW$, $\theta = 10dB$, $L = 40m$, $\alpha = 4$, $p_2 = 0.1$, and $N_2 = 10$. Moreover, the used CR parameters are: $P_{f,1} = P_{f,2} = 0.1$, $P_m = 0.05$, and $P(H_0) = 0.7$.

The influence of the PU's transmission power on the performance is negligible since the probabilities $P_{m,1}P_{d,2}P(H_1)$ and $P_{m,1}P_{m,2}P(H_1)$ are very small in general. On

the other hand, the interfering CR network has a significant effect on the per-node throughput of CRN_1.

5.4 Results and Analysis

Since the theoretical derivations have been verified by simulations, we show numerical results in this section. The performance of overlapping CR networks is studied by investigating the effects of different parameters on the throughput of CRN_1. Unless otherwise stated, we use the following practical values for network parameters in this section: $d_0 = 100$ m, $R = 50$ m, $P = 30$ dBm, $\sigma_n = -70$ dBm, $\theta = 10$ dB, $L = 500$ m, $\alpha = 4$, $p_1 = p_2 = 0.5$, and $N_1 = N_2 = 100$. Moreover, the used CR parameters are: $P_{f,1} = P_{f,2} = 0.1$, $P_m = 0.05$, and $P(H_0) = 0.9$. For each result figure we vary different parameters to demonstrate their impact.

First of all, we study the upper bound of false alarm probability. By exploiting Equation (5.16) it is possible to determine the maximum value for the probability of false alarm that is required to achieve a certain throughput. This is demonstrated in Figure 5.3. Within the feasible region it is possible to implement a system which achieves the desired throughput. Outside of this region it is impossible to meet the requirements set for the throughput. The black line that divides these two regions is the upper bound for the probability of false alarm from Equation (5.16). This limit naturally depends on the network and sensing parameters of CRN_2 as well.

Figure 5.4 shows the effect of sensing performance on the throughput in case of overlapping CR networks. The figure captures the fundamental nature of overlapping CR networks. As expected, the sensing performance of both networks has an effect and it seems that both networks have equal and linear influence on the throughput of CRN_1. These results imply that CR users would like to have as low probability of false alarm as possible to achieve the best performance. Whereas, the false alarm probability of the interfering CR network should be high such that the CR network in question would be able to access use the spectrum alone as often as possible.

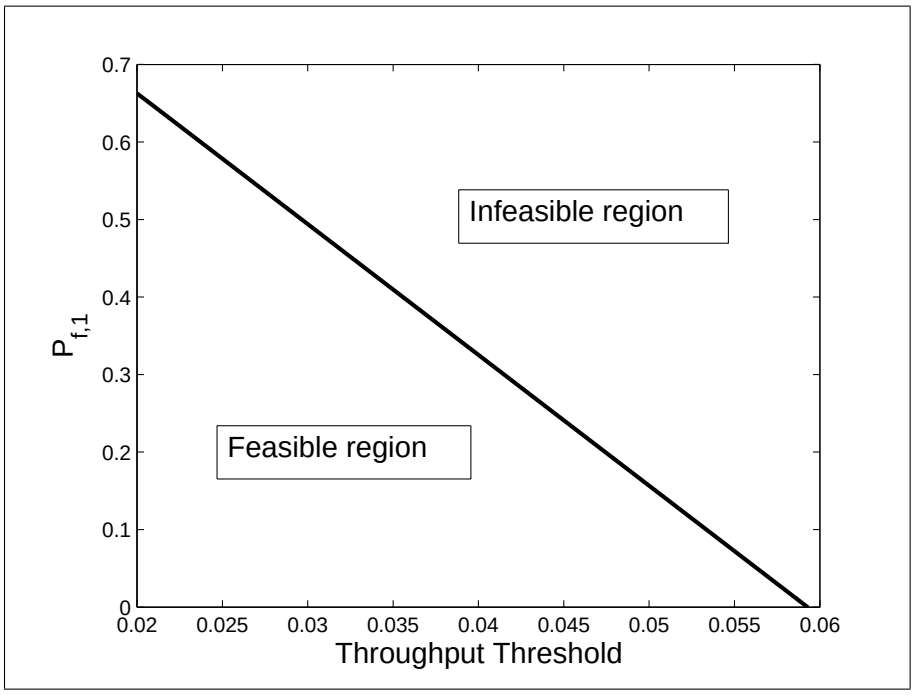

Figure 5.3 Maximum probability of false alarm as a function of throughput threshold.

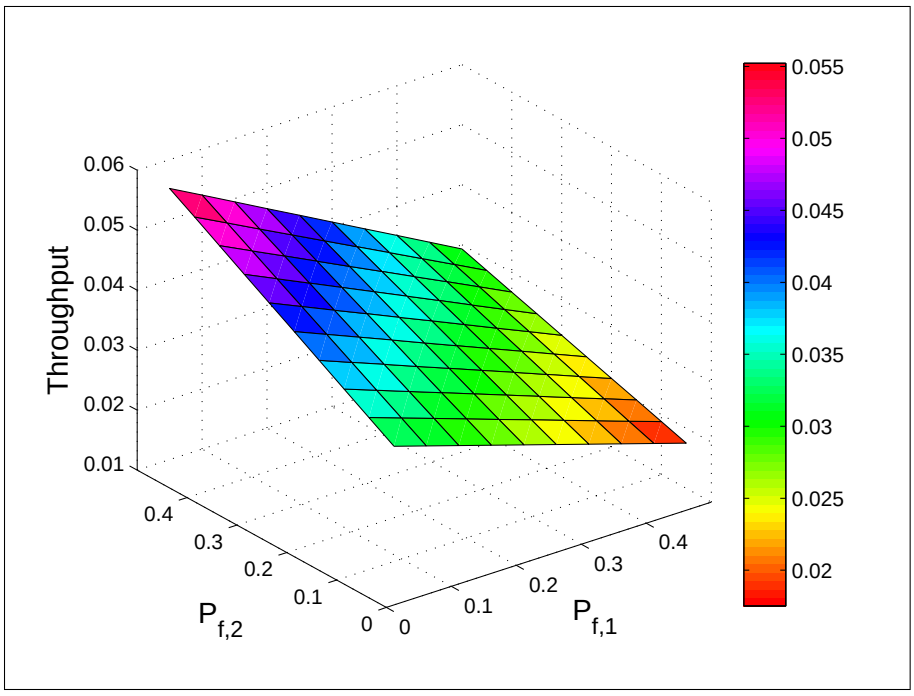

Figure 5.4 Effect of false alarm probabilities on the throughput of CRN_1.

The activity of the interfering CR network has a significant impact on the performance in case of overlapping CR networks. Figure 5.5 demonstrates the effect of the transmission probability of CRN_2 on the performance of CRN_1. From the figure it is possible to determine the optimal transmission probability for CRN_1. The results imply that the optimal transmission probability of the first network is independent of the transmission probability of the second network. However, as the network load of the second network is increased, the throughput of the first network decreases. The false alarm probability of CRN_2 ($P_{f,2}$) has a reversed effect on the performance of CRN_1 since if $P_{f,2}$ is increased, CRN_2 will transmit more rarely which means that it is not as active from the perspective of CRN_1. Thus, for CRN_1 it would be beneficial to have as low p_2 and as high $P_{f,2}$ as possible.

Nevertheless, it should be noted that the optimal value of p_1 depends on the amount of intra-network interference. With these parameters the term $p(1-p)$ in Equation (5.11) dominates the performance of CRN_1 since the throughput is maximized when $p_1 = 0.5$. Whereas, if the amount of received intra-network is larger, i.e., the network density of CRN_1 is higher, $\Pr\{\gamma > \theta\}$ becomes dominant. Consequently, smaller values of p_1 will give the best performance in that case.

In case of secondary spectrum usage, the activity of the PU determines the amount of transmission opportunities for CR users. Even though there would be large portions of available spectrum in time, high false alarm probabilities of CR users will restrict the achievable throughput. This is shown in Figure 5.6 where the throughput of CRN_1 is plotted as a function of $P(H_0)$ and $P_{f,2}$. If the PU is active for the most of the time, high probabilities of false alarm have only a minor effect on the throughput. Nevertheless, if the PU is inactive often, the probability of false alarm affects the performance significantly. In any case it is beneficial for CRN_1 to have as high $P(H_0)$ and $P_{f,2}$ as possible for throughput maximization.

Network density is another important parameter that should be taken into account when embarking on network design. In Figure 5.7 the combined effect of the network density and probability of false alarm of CRN_2 on the throughput of CRN_1 is displayed. The network density has an important impact on the achievable performance since the

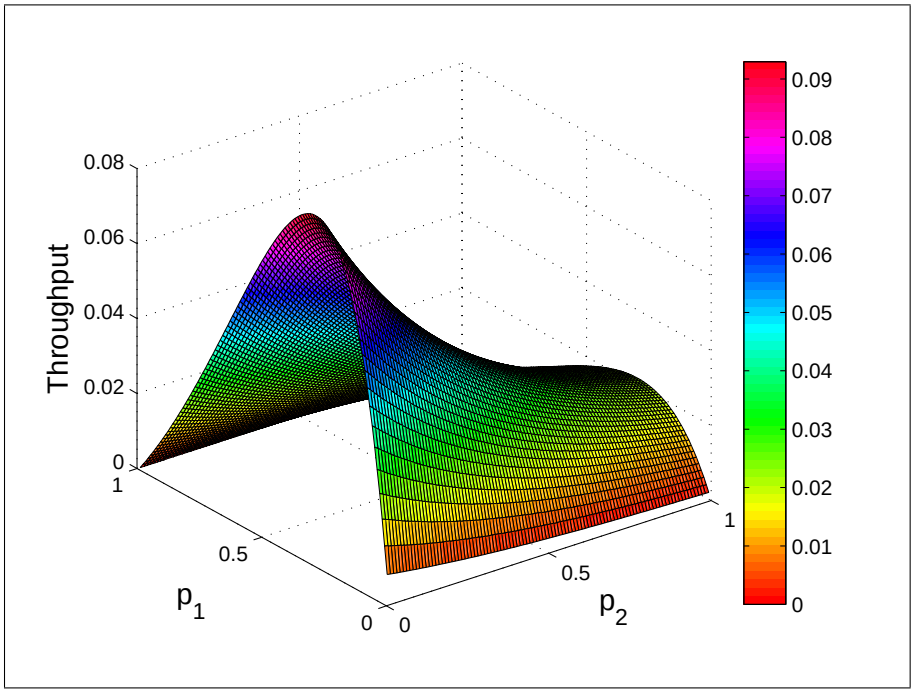

Figure 5.5 Impact of transmission probabilities of CR networks on the throughput of CRN_1.

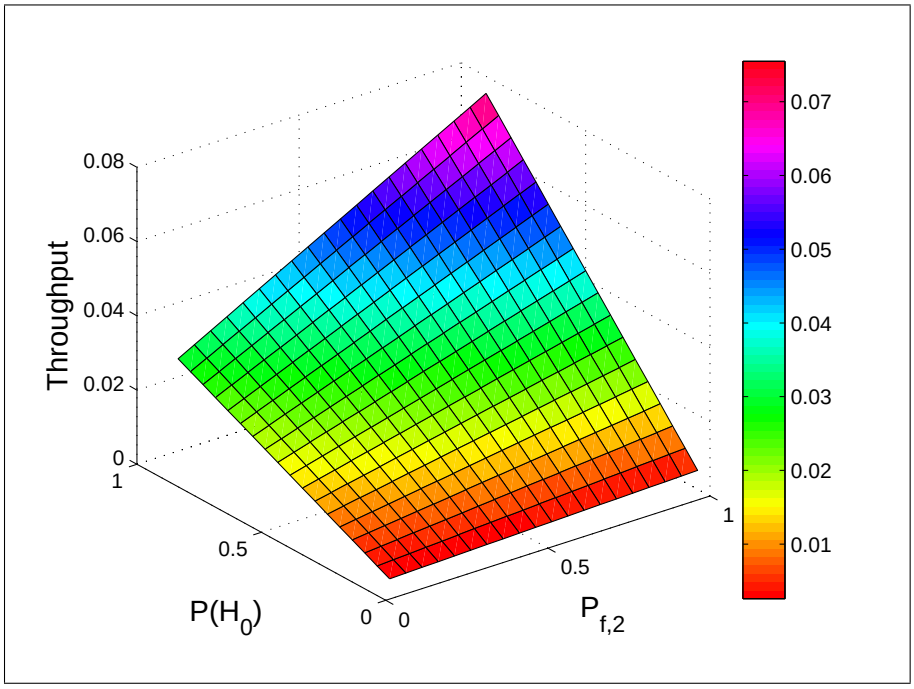

Figure 5.6 Combined effect of primary user's activity and false alarm probability of CRN_2 on the performance of CRN_1.

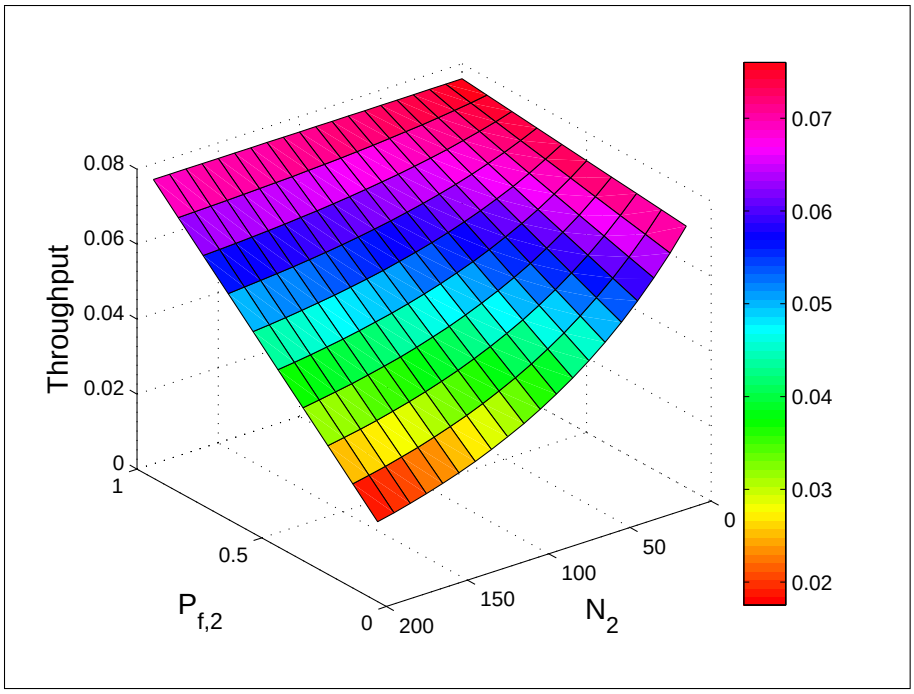

Figure 5.7 Effects of the network density and probability of false alarm of CRN_2 on the performance of CRN_1.

throughput diminishes significantly as the number of nodes within the area is increased. According to these results it seems that the effect of network density on the performance is smaller in case of high false alarm probabilities. This is due to the fact that in such cases transmissions take place rarely. To achieve high per-node throughput small networks are preferred. Nevertheless, this may not be true if the total throughput of the network would be considered but we leave this as future work since the focus of this work is on per-node throughput.

5.5 Conclusions

This work studied the performance of overlapping CR networks which coexist together with a PU. The performance of CR networks in such situations was evaluated by investigating the achievable per-node throughput. For the analysis, an interference model was derived which was then used to find out the per-node throughput. Theoretical results were verified by simulations. The results demonstrate the impact of the interfering CR network on the performance and the analysis shows how the feasibility of a CR network can be evaluated in the presence of another CR network. These results

will be extended to study the achievable throughput of overlapping CR networks in different scenarios and serve as guidance for the deployment of multiple CR networks.

Chapter 6

Distributed Spectrum Monitoring and Surveillance using a Cognitive Radio based Testbed

This chapter described the development and implementation of a distributed spectrum monitoring and surveillance testbed for identifying and locating RF signals using the Universal Software Radio Peripheral (USRP). We use a centralized RF trace collection testbed to establish the baseline, and we focus on distributed RF trace collection. Challenges associated with synchronization is identified and candidate solutions are discussed. The distributed testbed was implemented using NI USRPs (293x/295x) with LabVIEW. The complex nature of implementing the distributed case necessitate the choice of LabVIEW because of the versatile features provided. Potential applications are discussed and sample traces are demonstrated.

6.1 Introduction

Deployment and management of wireless devices and networks are often hampered by the poor visibility of PHY and MAC characteristics, and complex interactions at various layers of protocol stacks both inside a managed network and across multiple administrative domains. Conventional commercial-of-the-shelf (COTS) devices only provide selected information and control parameters to upper level, and thus greatly limit the ability for wireless surveillance and diagnosis. On the contrary, cognitive radio platforms have the advantage of greater programmability, reconfigurability and visibility compared to COTS devices. Availability of programmable platforms such as USRP/USRP2 [125] with GNU Radio [126] open up new opportunities to extract PHY-layer information beyond what is currently available in COTS wireless interfaces. Furthermore, they provide fine-grained control over a rich set of parameters that allows

faster reconfiguration of the PHY layer.

Understanding the dynamics of wireless spectrum, usage patterns, and interactions of wireless devices is pivotal to the design and evaluation of protocols and management solutions. Experimental technique is critical for assuring that the assumptions made at research level are neither too abstract nor too rigid to render the analytical or simulation results impractical aside from providing a platform for verification-of-concepts.

An SDR system is a radio communication system, where components that have typically been implemented in hardware (i.e. mixers, filters, amplifiers, modulators/demodulators, detectors. etc.) are implemented using software [127], which allows maximum reconfigurability. GNU radio is one of the most popular SDR platforms. Unlike most commodity 802.11 wireless cards, which often provides only few engineering details and limited controllability, GNU radios have the flexibility to operate the wireless networks under various configurations (frequency, tx power, data rate, and modulation type, etc.), and more detailed information such as RSSI, BER and PER can be obtained. Thanks to the efforts from both the communication and networking communities, many PHY implementations (e.g., MIMO system, OFDM and channel coding) [128, 129] are available, and basic MAC protocols especially CSMA/CA and the distributed coordination function (DCF) mode of IEEE 802.11 are also implemented, which can be used for experimental study of 802.11 protocols directly. SORA [130] is software radio platform with fully programmability on commodity PC architectures. One advantage of SORA is the adoption of PCIe bus for transferring high-fidelity digital waveform samples into PC memory, in contrast with USB2.0 and Gigabit Ethernet interfaces in USRP2. Another popular hardware platform for SDR is the WARP platform designed by a team at Rice University [131], which is a high-end system with custom hardware, support packages, design tools and application libraries.

SDR systems can thus provide full visibility and control of PHY parameters, which are crucial for cross-layer surveillance of wireless networks. There exist a few research projects targeted at building portable CR prototypes, e.g., the KU Agile Radio [132], Virginia Tech Chameleonic Radio [133], Microsoft Research KNOWS [134], just to name a few. Researchers at the University of Notre Dame have recently demonstrated

a battery-powered portable software radio prototype using primarily COTS components and open source software [135, 136]. USRP E1xx [137] is standalone embedded SDR platform featuring 512MB RAM and a USB On-the-GO interface that allows connections to external peripherals such as USB storage devices.

Existing testbeds with SDR components, however, primarily focus on the design and evaluations of protocols for spectrum agile medium access [138], interoperable communication [133], cooperative communications [129, 131, 136], and cognitive engine and waveform testing and performance [139, 140, 141]. In this work, we propose a SDR based research testbed for wireless monitoring and surveillance with superior visibility and controllability compared to WiFi-based solutions. In addition, the testbed is a programmable yet fully controlled setup for implementation and testing of many on-going research projects including wide-area spectrum sensing, attack modeling and countermeasure, distributed time synchronization, cross-layer resource management, tracking, and multimedia communications.

This chapter is organized as follows. Section 6.2 gives a background on the enabling technology for the testbed. The experimental testbed setup is given in Section 6.3. Section 6.4 explains the challenges encountered due to synchronization of the distributed USRPs. The potential applications of the testbed are discussed in Section 6.5. Section 6.6 concludes the chapter.

6.2 Background

Collection of Radio frequency (RF) signals over a wide range of spectrum requires receiver units that can be configured to scan a range of frequency bands within 50MHz-8GHz. The modular design of Universal Software Radio Peripheral (USRP) allows extension of the basic system using various daughter boards for RF transmitters and/or receivers at different frequency bands. The distributed RF trace collection setup shown in Figure 6.1 is an essential procedure for spectrum surveillance, testing different machine learning methods on real RF traces and Multiple Input Multiple output (MIMO) design.

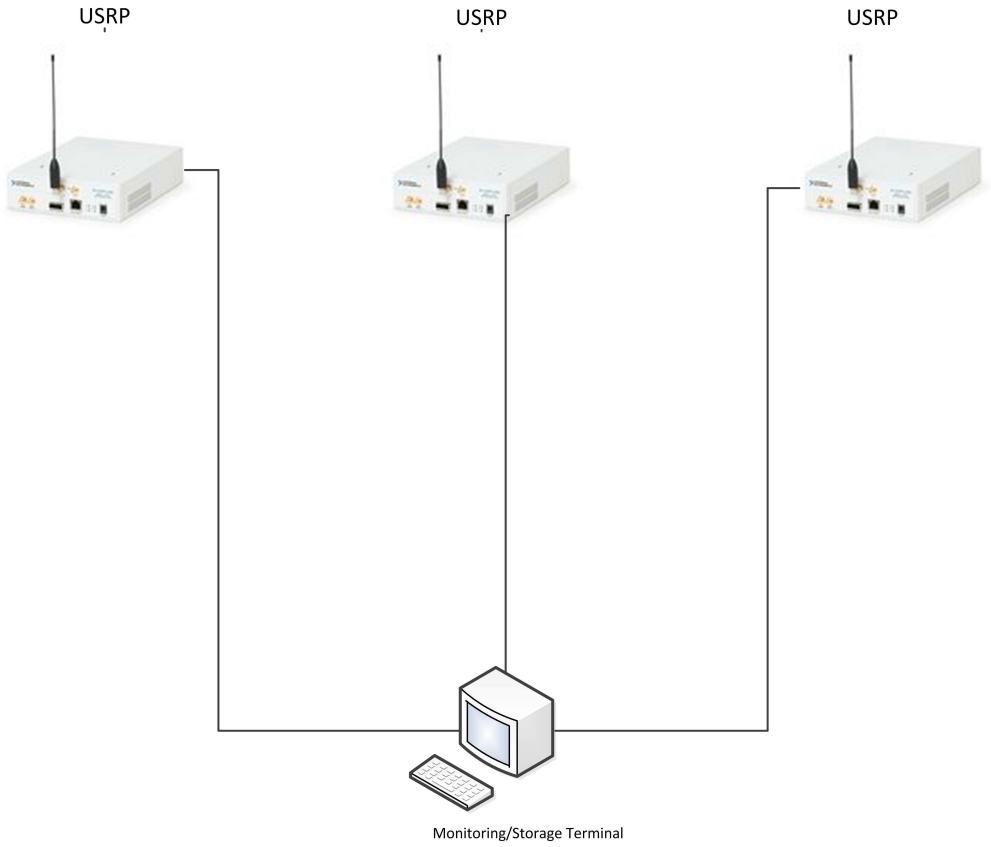

Figure 6.1 Distributed RF trace collection testbed.

The enablement offered by Software-Define Radio (SDR) ensures that components that have been implemented in hardware (e.g. mixers, filters, amplifiers, modulators/demodulators, etc.) can now be implemented by means of software on a personal computer or embedded system, this SDR can be achieved through combination of USRP (the hardware) and either GNU Radio [142] or LabVIEW [143] (the software).

This section reviews enabling technologies for RF trace collection testbed. The different types of USRPs used in trace collection are introduced, the USRP educational platform functions as a scalable system for communications experimentation, research and rapid prototyping [144, 145]. Different software platform such as LabView and GNURadio use to perform all the signal processing are introduced. The USRP combines with either GNU Radio or LabVIEW to form a Software Define Radio platform, which performs the required signal processing in software instead of using dedicated integrated circuits in hardware. The benefit is that since software can be easily replaced in the radio system, the same hardware can be used to create many kinds of radios for many different communications standards; thus, one software radio can be used for a variety of applications.

6.2.1 Hardware

There are variety of models of the USRP that use similar architecture. The USRP is made up of the motherboard which provides the following subsystems: FPGA, ADCs, DACs, clock generation and synchronization, host processor interface, and power regulation, all of these components are required for baseband processing of signals. The daughterboard, a modular front-end used for analog operations such as up/down-conversion, filtering, and other signal conditioning. This modularity permits the USRP to serve applications that operate between DC and 6 GHz. The FPGA performs several DSP operations, which ultimately provide translation from real signals in the analog domain to lower-rate, complex, baseband signals in the digital domain. In most use-cases, these complex samples are transferred to/from applications running on a host processor, which perform DSP operations. The code for the FPGA is open-source and can be modified to allow high-speed, low-latency operations to occur in the FPGA.

USRP

The NI USRP-29xx and USRP2 are tunable RF transceivers options covering 50 MHz - 6 GHz, stream up to 25MS/s baseband IQ for live host-based processing, they have ability to transmit and receive RF signals across a wide range of frequencies with up to 40 MHz of real-time bandwidth and plug-and-play MIMO support [146]. The NI USRP-293x has an integrated GPS-disciplined clock that provides improved frequency accuracy, synchronization capabilities, and GPS position information.

NI USRP RIO

The NI USRP RIO software defined radio platform its a 2x2 MIMO RF transceivers with independently tunable options from 50 MHz to 6 GHz which combines 2 full-duplex transmit and receive channels with 20 MHz/channel of real-time bandwidth and a large DSP oriented Xilinx Kintex 7 (410T) FPGA [147]. The Kintex-7 FPGA is a reconfigurable LabVIEW FPGA target that incorporates DSP48 coprocessing for high-rate, low-latency applications. The analog RF front end interfaces with the large Kintex 7 FPGA through dual ADCs and DACs clocked at 120MS/s. PCIe Express x4 connection back to the system controller allows up to 800 MB/s of streaming data transfer back to your desktop or PXI chassis, and 200 MB/s to your laptop. The 800 MB/s and 200 MB/s are not realizable in our distributed system now, this is due to the PCIe Express cable not long enough. The NI USRP-295x has an integrated GPS-disciplined clock that provides improved frequency accuracy, synchronization capabilities, and GPS position information.

6.2.2 Software

The USRP hardware driver (UHD) is the device driver provided by Ettus Research for use with the USRP product family. It supports Linux, MacOS, and Windows platforms. Several frameworks including LabVIEW, GNU Radio, MATLAB and Simulink use UHD. The functionality provided by UHD can also be accessed directly with the

UHD API, which provides native support for C++. Any other language that can import C++ functions can also use UHD. This is accomplished in Python through SWIG, for example. UHD provides portability across the USRP product family. Applications developed for a specific USRP model will support other USRP models if proper consideration is given to sample rates and other parameters [148].

GNURadio

GNU Radio is a free and open-source software development toolkit that provides signal processing blocks to implement software radios [149]. It can be used with readily-available low-cost external RF hardware to create software-defined radios, or without hardware in a simulation-like environment. It is widely used to support both wireless communications research and real-world radio systems. The software radio performs the required signal processing in software instead of using dedicated integrated circuits in hardware. GNU Radio applications are primarily written using the Python programming language, while the supplied, performance-critical signal processing path is implemented in C++ using processor floating point extensions.

LabVIEW

LabVIEW is a graphical programming language that uses icons instead of lines of text to create applications. In contrast to text-based programming languages, where instructions determine program execution, LabVIEW uses dataflow programming, where the flow of data determines execution. Graphical programming and dataflow execution are the two major ways LabVIEW is different from most other general-purpose programming languages. The LabVIEW development system provides an ideal way to interface with NI USRP hardware for the development and exploration of communications algorithms that process received signals and synthesize signals for transmission. The NI-USRP software driver provides functions (LabVIEW VIs) for the hardware / software configuration with tools for opening/closing sessions and performing read/ write operations.

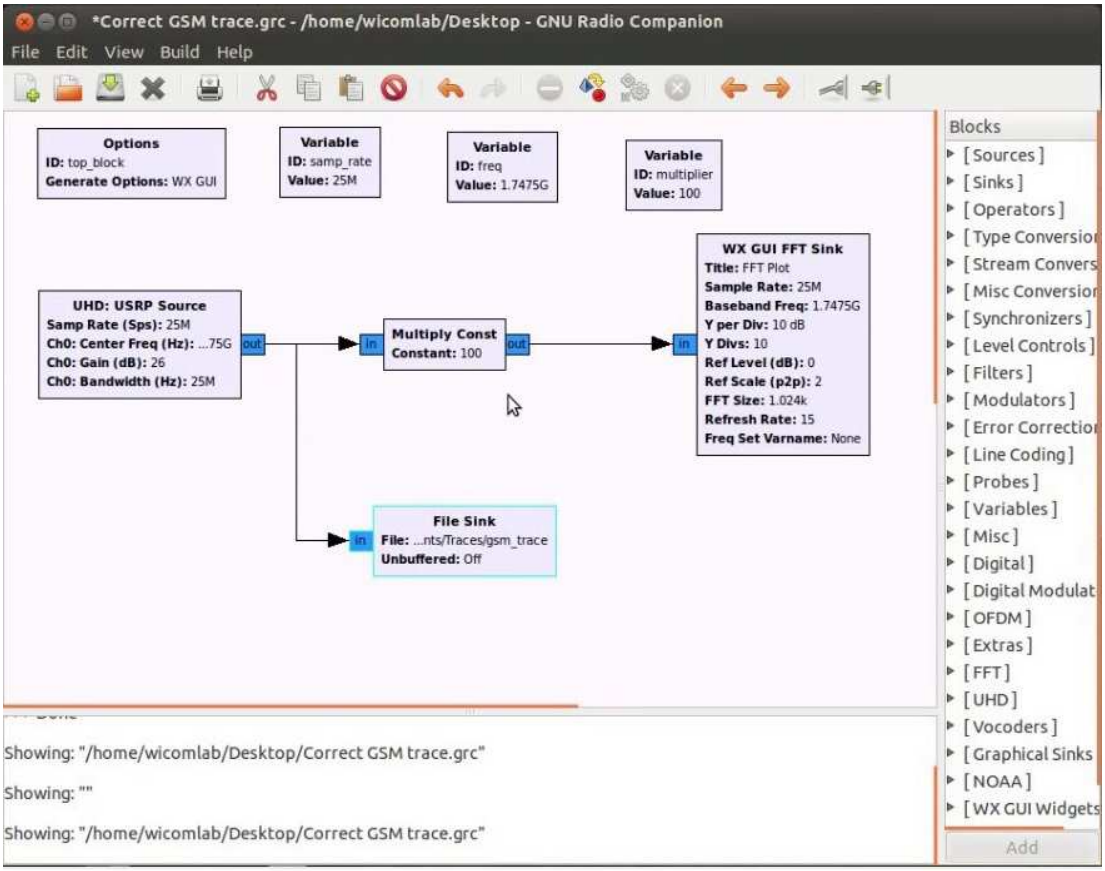

Figure 6.2 GNURadio Companion flow graph for RF trace collection in UMTS band 4.

6.3 Experimental Testbed Setup

Two experiments for the RF trace collection are considered, including a centralized trace collection setup and a distributed version. They are based on two different software framework, where the centralized case using GNURadio and USRP2 while the distributed case using LabVIEW and NI USRP-293x/295x.

6.3.1 Centralized Trace Collection

The centralized RF trace collection setup uses a single USRP2 node to collect the RF traces, we also created a replay setup for the RF trace. This case is mainly for benchmarking, such as estimating the noise floor and the change along time.

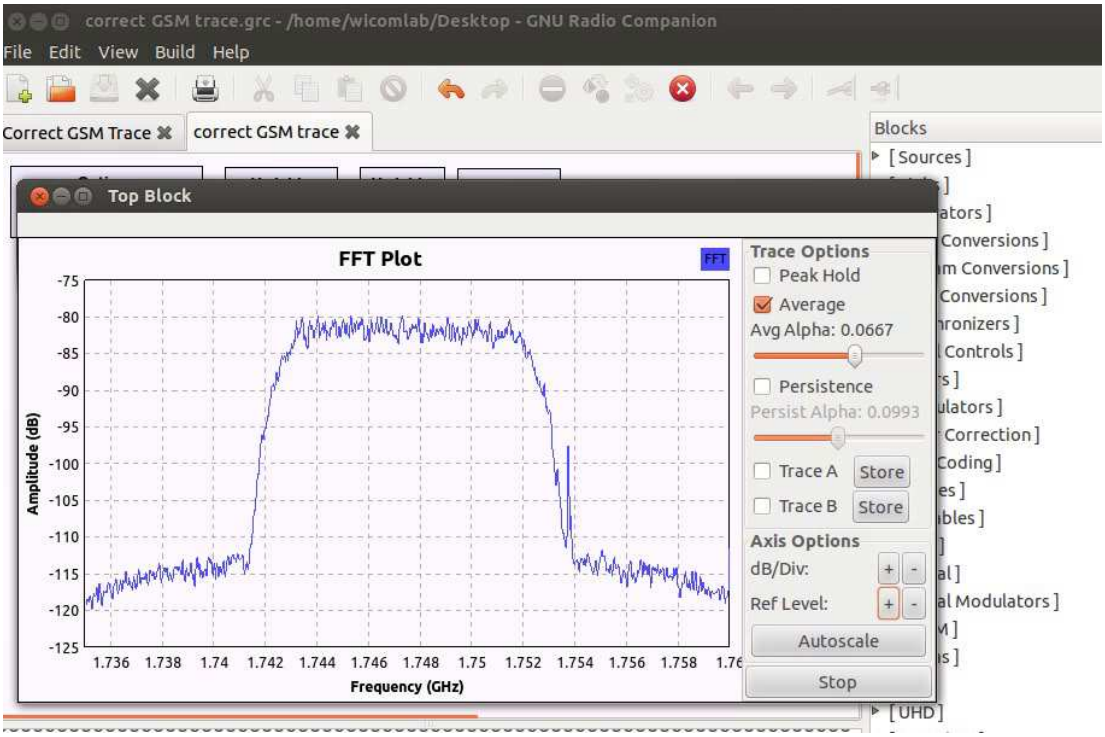

Figure 6.3 GNURadio Companion WX GUI FFT Sink display showing collected RF trace.

RF Trace Collection

Flowgraph for the collection of RF signal trace was set up. The blocks were connected as shown in Figure 6.2. A UHD: USRP Source block was configured at a centre frequency of 1.7475GHz to receive the RF signal from a transmitting mobile phone on the UMTS band 4. The RX daughterboard on the USRP 2 captures the RF signal and sends it through the analog to digital converter to the FPGA board on the USRP2. The signal is processed by the USRP FPGA and the streams of bits finally flows through the communication port to the USRP source. The sampling rate used is 25MHz. The 3G RF signal bandwidth is 5MHz and according to Nyquist sampling theorem, it is required that the sampling frequency be greater than or equal to twice the highest frequency component of the RF signal. The USRP Source block is connected to a Multiply Constant block to amplify the signal before being displayed on the WX GUI FFT Sink. A directory was created on the File Sink block to store the received RF signal from the UHD: USRP Source block. This will enable a replay of the received RF signal. The

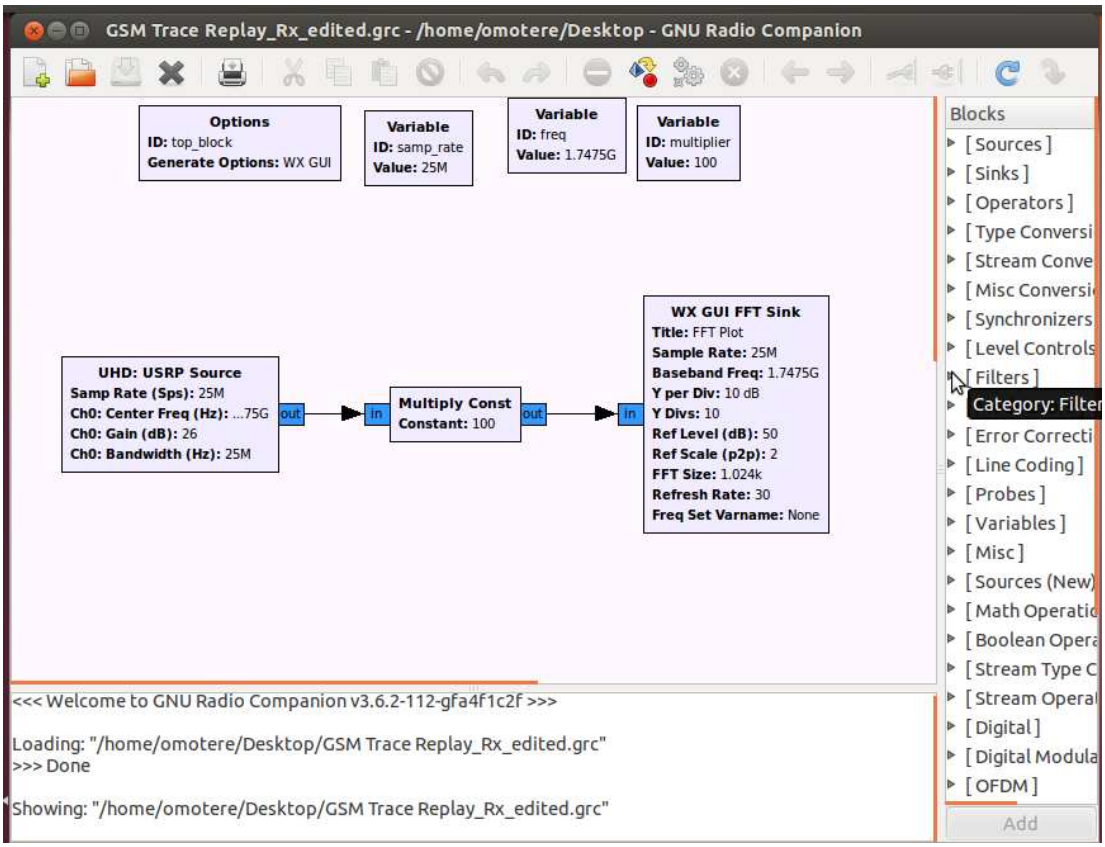

Figure 6.4 GNURadio Companion flowgraph for reception of the replayed trace.

FFT display is shown in Figure 6.3.

RF Replay Reception

A separate receiver system consisting of USRP2 and GNU Radio with the flowgraph shown in Figure 6.4 was setup to receive the replayed trace as the first validation step. The UHD: USRP Source is connected to WX GUI FFT Sink to display the received signal as shown in Figure 6.5.

6.3.2 Distributed Setup

The distributed RF trace collection setup uses three USRP nodes (NI USRP-295x/293x) shown in Figure 6.1 at different locations within the ECE building. Each of the USRPs are connected through a switch with an ethernet cable to a single PC in the WiComLab. Figure 6.7 shows the front panel representing the user interface containing

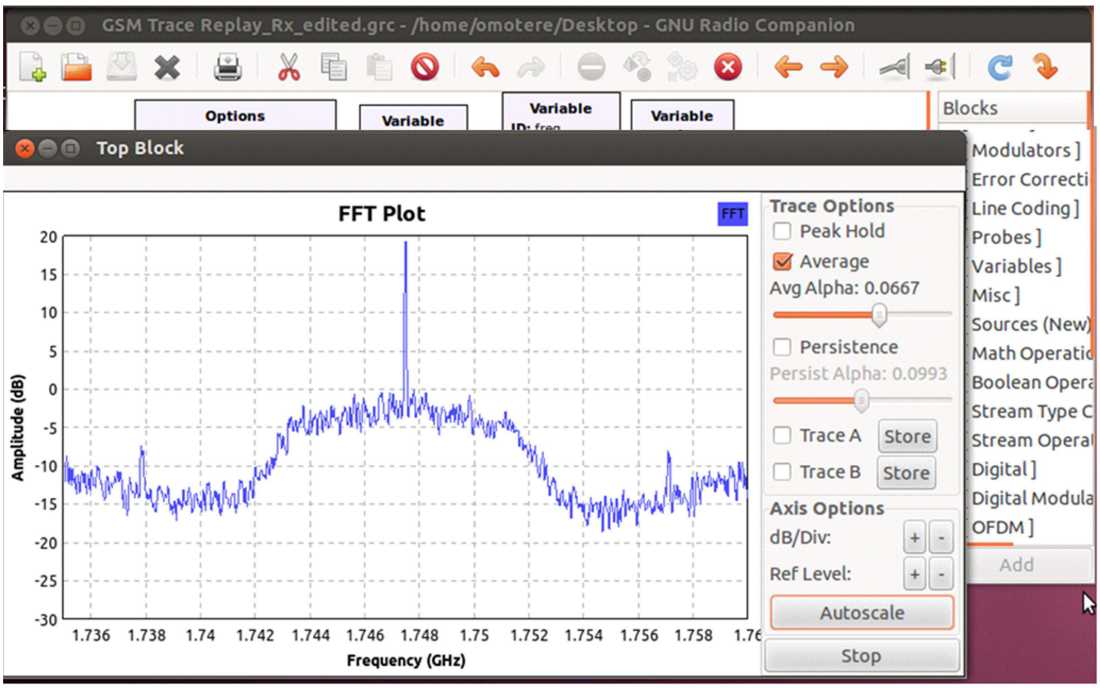

Figure 6.5 GNURadio Companion WX GUI FFT Sink display showing replayed traces received

the following parameters: the I/Q sampling rate, carrier frequency, sweep bandwidth and gain. If we increase the sampling rate we can effectively improve the accuracy of the sampling, which can accurately reconstruct the data from the transmitter. Reducing the sampling rate will increase the speed of data processing, which can improve the system performance in real time. LabVIEW as a software platform for SDR provides better programmability to configure the distributed RF trace collection testbed to scan different ranges of spectrum.

Figure 6.6 shows the measured average power for a certain period of time of the devices such as landmobile, mobile, aeronautical etc. operating in the 900 MHz band around the ECE building surroundings where the USRPs are located. The variation in power level taken by the USRPs is due to varying distances of the devices to the three USRPs and the transmitting power of the devices.

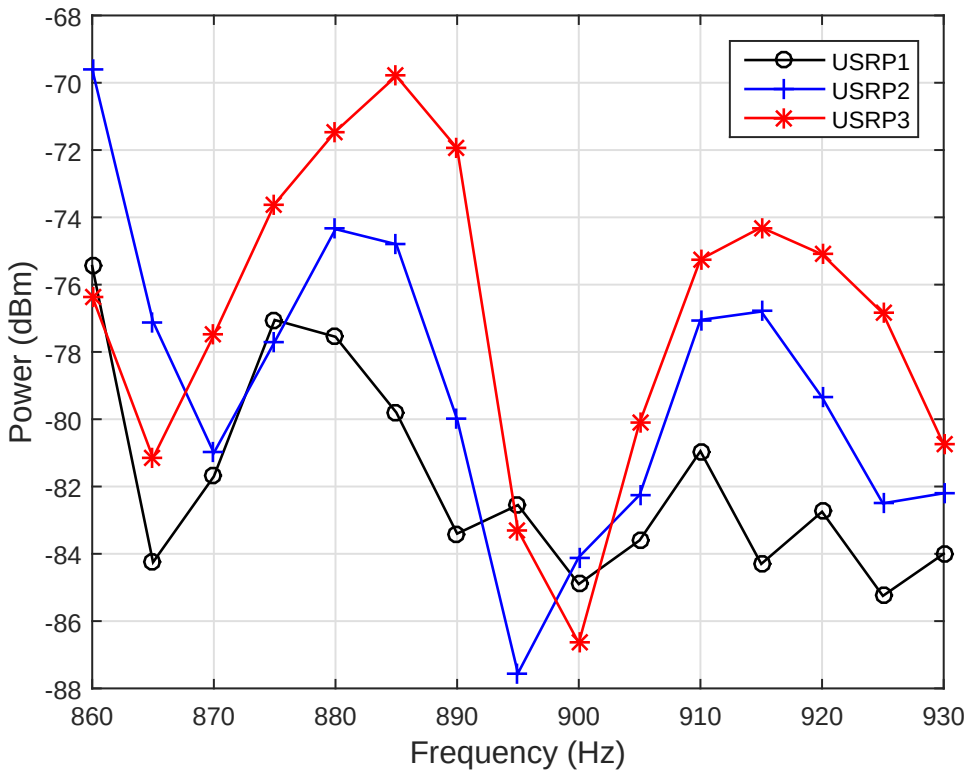

Figure 6.6 Average Power (dBm) in 900 MHz band

6.4 Synchronization of Radios in the Distributed Testbed

Synchronization is of great importance and one of the core techniques for any wireless distributed system, which is to maintain a unique global clock reference in the system. It ensures that the messages and events that took place in a system can be explained with a unique time reference. IEEE1588 standard [150] defines PTP(Precision Time Protocol) to synchronize different terminals in distributed measurement system. This is achieved either through transmitter-receiver a bidirectional pair-wise synchronization or receiver-receiver unidirectional broadcast synchronization. The transmitter-receiver case is a situation where one node, i.e. the receiver, exchanges messages with another node, i.e. the transmitter, to let the receiver synchronize to the transmitter's local time reference; and the receiver-receiver case is a situation where different receivers synchronize with each other, but not with the transmitter, comparing the message received from the transmitter for both time and frequency accuracy. In the former approach, the synchronization accuracy depends on the capability to assign a precise timestamp to both transmitted and received messages, while the latter only requires the timestamping of the received message. The receiver-receiver synchronization implies that all the nodes in the testbed must receive the RF trace in unison without time and frequency drift.

Different techniques have been developed to address the problem of synchronization. Typical algorithms for transmitter-receiver synchronization include Timing-Sync Protocol for Sensor Networks [151], Lightweight Time Synchronization [152], and Tiny-Sync and Mini-Sync [153]. This is performed by a handshake protocol between a pair of nodes, the mechanism involves the nodes exchanging their local time as a timestamp, subsequently calculating their clock offset and then synchronizing. The receiver-receiver synchronization can be implemented either by using Flooding Time Synchronization Protocol [154] or Reference Broadcast Synchronization [155]. The Reference Broadcast Synchronization is base on the idea that that a third party will broadcast a beacon to all the receivers. The beacon does not contain any timing information; instead the receivers will compare their clocks to one another to calculate their relative phase offsets.

The timing is based on when the node receives the reference beacon. For more than one receiver, it may require more than one broadcast to be sent. Increasing the broadcasts will increase the precision of the synchronization.

To implement the synchronization of the distributed nodes in our testbed, it is required that all Rx or Tx channels operate as a single receiver or transmitter with frequency and time synchronization and a phase coherent local oscillator (LO). The synchronization operation can be achieved by sharing a 10MHz reference clock and PPS time base among the distributed USRPs. Some version of the USRPs such as 293x and 295x has GPS disciplined clock while 292x and 294x do not have GPS disciplined clock, the GPS Disciplined Clock improves frequency accuracy, allows global synchronization and positioning, it also improves clock precision through disciplining. Using the disciplining technique, the GPS signals make minor corrections to the OCXO (Oven Controlled Oscillator), thus pushing the USRP frequency accuracy error towards zero (0.01 ppb). The distributed USRP systems can effectively act as time synchronized, phase coherent devices even though they might be separated over great distances. Those version without GPS disciplined clock can be equipped with external hardware such as OCXO based Thunderbolt® GPS Disciplined clock from Trimble which supplies a 10-MHz Ref Clock output and digital PPS output used to generate the clock. The OCXO provides a very accurate frequency source that operates without a GPS antenna installed. Adding a GPS antenna further improves synchronization through GPS disciplining and can provide a global concept of time [156]. The challenges with synchronizing our setup has to do with the distributed nature of the USRPs.

Challenges The cabling of the 10MHz Ref In and PPS Input of the USRPs to a single source of 10MHz and PPS signal is challenging due to the distributed nature of the USRPs (the USRPs are separated by more than 300ft) and the restrictions offer by available cable length. In addition, because our setup is indoors, little or no signal is received by the GPS receiver. It may be possible to connect GPS antenna from outdoor to the receiver indoor using a cable, however, the transmission time along different cables to each USRP will introduce synchronization errors. Therefore, it is not feasible to use GPS for synchronization in our setup. The precision clock in Personal

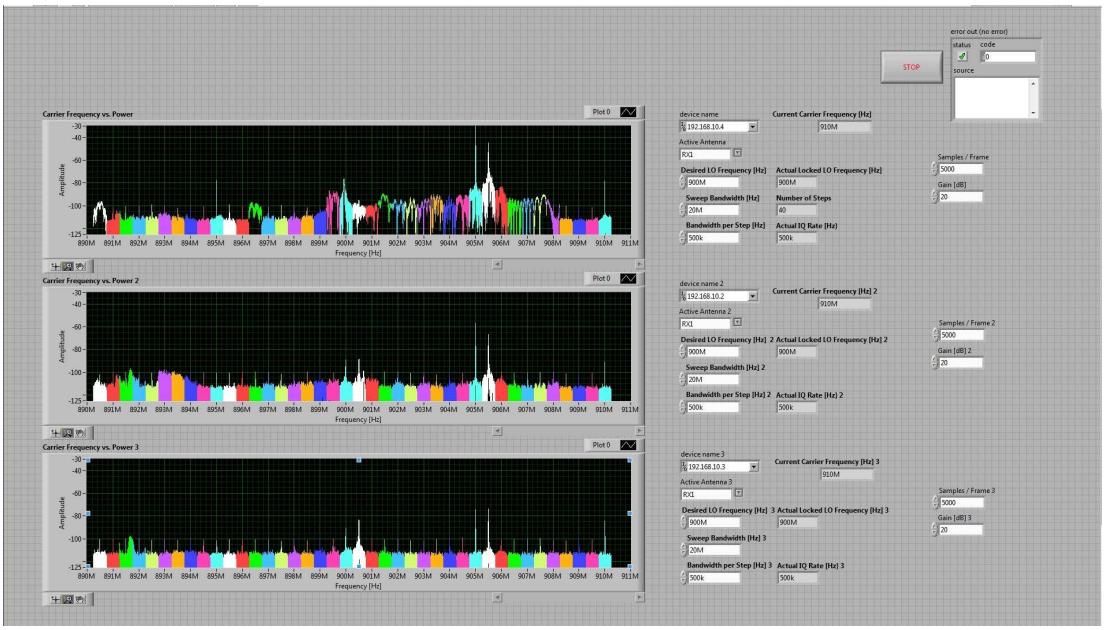

Figure 6.7 The LabVIEW front panel of the distributed USRPs for trace collection.

Computer (PC) is 1ms, this is not sufficient in wireless communication applications. In order to avoid error introduced by having to synchronize the host PCs of the USRPs, all the USRPs are connected to a single host PC through a switch where each USRP assign a unique IP address. Now the main synchronization error would come from the switch, which is small. We are exploring other possible approaches such as the Network Time Protocol [157] to further reduce this error.

6.5 Potential Applications

There has been an increase in the number of electronic devices and telecommunication systems, and it becomes very difficult to guarantee the correct operation of those devices and systems [158]. This has necessitated the need for RF spectrum monitoring through distributed RF trace collection. Spectrum monitoring can either be real time suitable for short term monitoring or it can be long-term [159]. Comparing to bulk commercial grade spectrum analyzer, real time monitoring of the spectrum can be achieved on the move by taking advantage of the portability of the USRP. Government regulatory agencies allocate different frequencies for various radio services, such

as broadcast television and radio, mobile phone systems, police and emergency communications, and a host of other applications. It is critical that each of these services operates at the assigned frequency and stays within the allocated channel. Transmitters and other intentional radiators often must operate at closely spaced adjacent frequencies. A key performance measure for the power amplifiers and other components used in these systems is the amount of signal energy that spills over into adjacent channels and causes interference.

Machine learning method is a viable technique for handling applications with large data sets with broad levels of high dimensionality, imbalance and datasets, which are particularly difficult to learn from make properly handling and analyzing such data almost impossible to do without the assistance of a computer [160, 161]. An important application of collected RF trace is in testing the efficacy of the different machine learning methods in predicting correctly the RF content of large data sets of the RF trace. Different machine learning technique with differing feature combinations can be compared [162, 163, 164]. This will allow us to quantify the contribution of each individual feature to determine the best combination of features and to find the appropriate machine learning approach.

The spatial correlation analysis of the distributed RF traces can help in the design of Multiple Input Multiple Output (MIMO) system. Spatial correlation is a measure of relationship between two antennas' signals [165, 166]. The ideal huge capacity anticipated by a MlMO system can be realized if there is no spatial correlation. However, in real propagation environments, MlMO channels are correlated due to low scattering and reduced spatial selectivity. Correlated channels of MIMO reduce the high-capacity potential considerably, suggesting that MIMO systems should be designed with low or no correlation. Design of systems with low correlation requires a full investigation of underlying parameters that strengthen spatial correlation.

6.6 Conclusions

Deploying USRPs for the distributed RF trace collection testbed instead of the NI PXI system offers flexibility, affordability and its easy programmability are key strengths of the NI USRP platform. As a PC-hosted peripheral that is programmable with NI LabVIEW, the NI USRP radio transceiver excels at these, this is due to the modular nature of the USRP compare to bulky nature of the PXI system. The PXI system is expensive to setup, if we consider the number of PXI required in spectrum surveillance application, the cost implication makes it unrealistic. In this chapter, we have described the centralized and distributed RF trace collection testbed, which has been built for spectrum monitoring and surveillance with superior visibility and controllability compared to WiFi-based solutions. In addition, the testbed is a programmable yet fully controlled setup for implementation and testing of design of MIMO system and to evaluate different machine learning techniques.

References

[1] R. North, N. Browne, and L. Schiavone, "Joint tactical radio system connecting the gig to the tactical edge," in *Proc. of IEEE MILCOM*, 2006.

[2] XG Working Group, *The XG Vision: RFC*. http://www.ir.bbn.com/ ramanath/pdf/rfc_vision.pdf.

[3] B. Frey, *Graphical Models for Machine Learning and Digital Communications.* MIT Press, Boston, MA, 1998.

[4] D. Koller and N. Friedman, *Probabilistic Graphical Models*, MIT Press, 2009.

[5] G. Ganesan and Y. Li, "Cooperative spectrum sensing in cognitive radio - Part I: Two user networks," *IEEE Trans. Wireless Commun.*, Vol.6, pp.2204–2213, June 2007.

[6] G. Ganesan and Y. Li, "Cooperative spectrum sensing in cognitive radio - Part II: Multiuser networks," *IEEE Trans. Wireless Commun.*, Vol.6, pp.2214–2233, June 2007.

[7] A. Ghasemi and E. S. Sousa, "Cooperative spectrum sensing for opportunistic access in fading environments," in *Proc. of IEEE New Frontiers in Dynamic Spectrum Access Networks (DySPAN)*, 2005.

[8] S. M. Mishra, A. Sahai and R. W. Brodersen, "Cooperative sensing among cognitive radios," in *Proc. of IEEE International Conference on Communications (ICC)*, June. 2006.

[9] J. Unnikrishnan and V. V. Veeravalli, "Cooperative sensing for primary detection in cognitive radio," *IEEE Journal on Selected Topics in Signal Processing*, vol.2, pp.18–27, 2008.

[10] J. S. Yedida, W. T. Freeman and Y. Weiss, "Understanding belief propagation and its generalizations," in *Exploring Artificial Intelligence in the New Millennium*, Chap.8, pp.2282–2312, Science and Technology Books, 2003.

[11] S. Zarrin and T. J. Lim, "Belief propagation on factor graphs for cooperative spectrum sensing in cognitive radio," in *Proc. of IEEE New Frontiers in Dynamic Spectrum Access Networks (DySPAN)*, 2008.

[12] H. Li, "Cooperative spectrum sensing via belief propagation in spectrum-heterogeneous cognitive radio systems, in *Proc. of IEEE WCNC*, pp. 1–6, 2010.

[13] H. Li, "Reconstructing spectrum occupancies for wideband cognitive radio networks: A matrix completion via belief propagation," in *Proc. of IEEE International Conference on Communications (ICC)*, Cape Town, South Africa, May 2010.

[14] H. Li and L. Qian, "Cross-network spectrum sensing for mission-critical cognitive radio networks: Collaboration through gateways", in Military Communications Conference (MILCOM), pp. 1041–1046, 2011.

[15] H. V. Poor and Olympia Hadjiliadis, *Quickest detection*, Cambridge University Press, 2009

[16] H. Li, C. Li, and H. Dai, "Quickest spectrum sensing in cognitive radio", in *Proc. 42nd Annu. Conf. Inf. Sci. Syst. (CISS08)*, pp. 203208, 2008.

[17] G. Lorden, "Procedures for Reacting to a Change in Distribution," *Ann. Math. statist.* , Vol. 42, pp. 1897–1908, 1971

[18] T. Oskiper and H. V. Poor, "Quickest detection of a random signal in background noise using a sensor array," *EURASIP Journal on Applied Signal Processing,*, pp. 13–24, Jan. 2005.

[19] Y. Zeng, Y.-C. Liang, A. T. Hoang, and R. Zhang, "A review on spectrum sensing for cognitive radio: Challenges and solutions," *EURASIP Journal on Advances in Signal Processing*, 2010.

[20] T. Yucek and H. Arslan, "A survey of spectrum sensing algorithms for cognitive radio applications," *IEEE Communications Surveys and Tutorials*, vol. 11, no. 1, pp. 116–130, quarter 2009.

[21] E. R. LLC, "USRP2 – the next generation of software radio systems [online]," http://www.ettus.com/downloads/ettus_ds_usrp2_v2.pdf.

[22] Y.-C. Liang, Y. Zeng, E. Peh, and A. T. Hoang, "Sensing-throughput tradeoff for cognitive radio networks," *IEEE Transactions on Wireless Communications*, vol. 7, no. 4, pp. 1326 –1337, 2008.

[23] R. Chiang, G. Rowe, and K. Sowerby, "A quantitative analysis of spectral occupancy measurements for cognitive radio," in *IEEE Vehicular Technology Conference (VTC) 2007-Spring*, april 2007, pp. 3016 – 3020.

[24] E. Candes and B. Recht, "Exact matrix completion via convex optimization," *Foundations of Computational Mathematics*, vol. 9, pp. 717–772, 2009.

[25] R. Keshavan, S. Oh, and A. Montanari, "Matrix completion from a few entries," in *ISIT*, 2009.

[26] B. Recht, M. Fazel, and P. Parrilo, "Guaranteed minimum rank solutions of matrix equations via nuclear norm minimization," *SIAM Review*.

[27] H. Li, "Reconstructing spectrum occupancies for wideband cognitive radio networks: A matrix completion via belief propagation," in *IEEE International Conference on Communications (ICC)*, may 2010, pp. 1 –6.

[28] T. Chan and J. Shen, "Mathematical models for local non-texture inpaintings," *SIAM Journal of Applied Mathematics*, vol. 62, no. 3, pp. 1019–1043, 2001.

[29] A. V. Oppenheim and R. W. Schafer, *Discrete-Time Signal Processing*. Upper Saddle River, NJ: Prentice-Hall, 1989.

[30] Y.-L. You and M. Kaveh, "A regularization approach to joint blur identification and image restoration," *IEEE Transactions on Image Processing*, vol. 5, no. 3, pp. 416 –428, mar 1996.

[31] T. Goldstein and S. Osher, "The split bregman method for l1-regularized problems," *SIAM J. Img. Sci.*, vol. 2, pp. 323–343, April 2009. [Online]. Available: http://portal.acm.org/citation.cfm?id=1658384.1658386

[32] P. Getreuer, "tvreg: Variational imaging methods for denoising, deconvolution, inpainting, and segmentation," Nov. 2009, downloadable with MATLAB source code at: `http://www.mathworks.com/matlabcentral/fileexchange/25997-tvreg-variational-imaging-methods`.

[33] J. Coughlan, "A tutorial introduction to belief propagation," Aug. 2009, slides.

[34] R. Szeliski, R. Zabih, D. Scharstein, O. Veksler, V. Kolmogorov, A. Agarwala, M. Tappen, and C. Rother, "A comparative study of energy minimization methods for markov random fields with smoothness-based priors," *IEEE Transactions on Pattern Analysis and Machine Intelligence*, vol. 30, no. 6, pp. 1068 –1080, Jun. 2008.

[35] R. H. Keshavan and S. Oh, "A gradient descent algorithm on the grassman manifold for matrix completion," *CoRR*, vol. abs/0910.5260, 2009.

[36] J. Perez-Romero, O. Sallent, and R. Agusti, "On the applicability of image processing techniques in the radio environment characterisation," in *IEEE Vehicular Technology Conference (VTC) 2009-Spring*, S2009, pp. 1 –5.

[37] L. Bolea, J. Pérez-Romero, R. Agustí, and O. Sallent, "Primary transmitter discovery based on image processing in cognitive radio," in *Proceedings of the 15th Open European Summer School and IFIP TC6.6 Workshop on The Internet of the Future*, ser. EUNICE '09. Berlin, Heidelberg: Springer-Verlag, 2009, pp. 178–187.

[38] G. Ganesan, Y. Li, B. Bing, and S. Li, "Spatiotemporal sensing in cognitive radio networks," *IEEE Journal on Selected Areas in Communications*, vol. 26, no. 1, pp. 5 –12, 2008.

[39] D. Donoho, "Compressed sensing," *IEEE Transactions on Information Theory*, vol. 52, no. 4, pp. 1289 –1306, april 2006.

[40] R. Baraniuk, E. Candes, R. Nowak, and M. Vetterli, "Compressive sampling [from the guest editors]," *IEEE Signal Processing Magazine*, vol. 25, no. 2, pp. 12 –13, march 2008.

[41] E. Candes and J. Romberg, "Sparsity and incoherence in compressive sampling," *Inverse Problems*, vol. 23, no. 3, p. 969, 2007.

[42] A. Ghasemi and E. Sousa, "Collaborative spectrum sensing for opportunistic access in fading environments," in *First IEEE International Symposium on New Frontiers in Dynamic Spectrum Access Networks*, nov. 2005, pp. 131 –136.

[43] P. Potier and L. Qian, "Network Management of Cognitive Radio Ad Hoc Networks," in *CogART'11*, 2011, pp. 33–38.

[44] Federal Communications Commission. Spectrum policy task force report. *ET Docket no. 02-135* Nov 2002; .

[45] Mitola III J, Maguire Jr G. Cognitive radio: making software radios more personal. *IEEE Personal Communications* Aug 1999; **6**(4):13 –18, 10.1109/98.788210.

[46] Haykin S. Cognitive radio: brain-empowered wireless communications. *IEEE Journal on Selected Areas in Communications* Feb 2005; **23**(2):201 – 220, 10.1109/JSAC.2004.839380.

[47] Akyildiz IF, Lee WY, Chowdhury KR. Crahns: Cognitive radio ad hoc networks. *Ad Hoc Networks* 2009; **7**(5):810 – 836, 10.1016/j.adhoc.2009.01.001. http://www.sciencedirect.com/science/article/pii/S157087050900002X.

[48] Potier P, Qian L. Network management of cognitive radio ad hoc networks. *CogART'11*, 2011; 33–38.

[49] Lu Y, Wang W, Zhong Y, Bhargava B. Study of distance vector routing protocols for mobile ad hoc networks. *Pervasive Computing and Communications, 2003. (PerCom 2003). Proceedings of the First IEEE International Conference on*, 2003; 187 – 194, 10.1109/PERCOM.2003.1192741.

[50] Chen W, Jain N, Singh S. ANMP: ad hoc network management protocol. *IEEE Journal on Selected Areas in Communications* Aug 1999; **17**(8):1506–1531, 10.1109/49.780355.

[51] IEEE Draft Standard for Information Technology -Telecommunications and information exchange between systems - Wireless Regional Area Networks (WRAN) - Specific requirements - Part 22: Cognitive Wireless RAN Medium Access Control (MAC) and Physical Layer (PHY) specifications: Policies and procedures for operation in the TV Bands. *IEEE P802.22/D1.0, December 2010* 20 2010; :1 –598.

[52] Akyildiz I, Lee WY, Chowdhury K. Spectrum management in cognitive radio ad hoc networks. *IEEE Network* 2009; **23**(4):6 –12, 10.1109/MNET.2009.5191140.

[53] Yucek T, Arslan H. A survey of spectrum sensing algorithms for cognitive radio applications. *Communications Surveys Tutorials, IEEE* quarter 2009; **11**(1):116–130, 10.1109/SURV.2009.090109.

[54] Arianandа D, Lakshmanan M, Nikoo H. A survey on spectrum sensing techniques for cognitive radio. *Cognitive Radio and Advanced Spectrum Management, 2009. CogART 2009. Second International Workshop on*, 2009; 74–79, 10.1109/COGART.2009.5167237.

[55] Leinwand A, Fang K. *Network Management - A Practical Perspective*. Addison-Wesley, 1993.

[56] Bellcore. Generic requirements for operations based on the telecommunications management network architecture October 1996.

[57] ITU-T. Tmn management functions February 2000.

[58] Kim H, Shin K. Efficient discovery of spectrum opportunities with mac-layer sensing in cognitive radio networks. *Mobile Computing, IEEE Transactions on* may 2008; **7**(5):533 –545, 10.1109/TMC.2007.70751.

[59] Wang H. *Telecommunications Network Management: Standards, Applications, and Future Trends*. McGraw-Hill, 1999.

[60] Sorrells C, Potier P, Qian L, Li X. Anomalous spectrum usage attack detection in cognitive radio wireless networks. *2011 IEEE International Conference on Technologies for Homeland Security (HST)*, 2011; 384 –389, 10.1109/THS.2011.6107900.

[61] Xu H, Jin J, Li B. A secondary market for spectrum. *INFOCOM, 2010 Proceedings IEEE*, 2010; 1 –5, 10.1109/INFCOM.2010.5462277.

[62] Akyildiz I, Lee WY, Vuran M, Mohanty S. A survey on spectrum management in cognitive radio networks. *IEEE Communications Magazine* 2008; **46**(4):40 –48, 10.1109/MCOM.2008.4481339.

[63] Wang CX, Chen HH, Hong X, Guizani M. Cognitive radio network management. *Vehicular Technology Magazine, IEEE* 2008; **3**(1):28 –35, 10.1109/MVT.2008.919405.

[64] Tsagkaris K, Akezidou M, Galani A, Demestichas P. Evaluation of signalling loads in a cognitive network management architecture. *International Journal of Network Management* 2012; **22**(3):235–260, 10.1002/nem.803. http://dx.doi.org/10.1002/nem.803.

[65] Zhao Y, Mao S, Neel J, Reed J. Performance evaluation of cognitive radios: Metrics, utility functions, and methodology. *Proceedings of the IEEE* april 2009; **97**(4):642 –659, 10.1109/JPROC.2009.2013017.

[66] Clancy T, Walker B. Predictive dynamic spectrum access. *Proc. SDR Forum Technical Conference*, Orlando, Florida, USA, 2006.

[67] Yarkan S, Arslan H. Binary time series approach to spectrum prediction for cognitive radio. *Vehicular Technology Conference, 2007. VTC-2007 Fall. 2007 IEEE 66th*, 2007; 1563 –1567, 10.1109/VETECF.2007.332.

[68] Geirhofer S, Tong L, Sadler B. Cognitive radios for dynamic spectrum access - dynamic spectrum access in the time domain: Modeling and exploiting white space. *IEEE Communications Magazine* may 2007; **45**(5):66 –72, 10.1109/MCOM.2007.358851.

[69] Geirhofer S, Tong L, Sadler B. A measurement-based model for dynamic spectrum access in wlan channels. *IEEE Military Communications Conference*, 2006; 1 –7, 10.1109/MILCOM.2006.302405.

[70] Cormio C, Chowdhury KR. A survey on mac protocols for cognitive radio networks. *Ad Hoc Networks* 2009; **7**(7):1315 – 1329, 10.1016/j.adhoc.2009.01.002. http://www.sciencedirect.com/science/article/pii/S1570870509000043.

[71] Shiang HP, van der Schaar M. Distributed resource management in multihop cognitive radio networks for delay-sensitive transmission. *Vehicular Technology, IEEE Transactions on* 2009; **58**(2):941 –953, 10.1109/TVT.2008.925308.

[72] Firoiu V, Borden M. A study of active queue management for congestion control. *INFOCOM 2000. Nineteenth Annual Joint Conference of the IEEE Computer and Communications Societies. Proceedings. IEEE*, vol. 3, 2000; 1435 –1444 vol.3, 10.1109/INFCOM.2000.832541.

[73] Mahmoud H, Yucek T, Arslan H. Ofdm for cognitive radio: merits and challenges. *IEEE Wireless Communications* april 2009; **16**(2):6 –15, 10.1109/MWC.2009.4907554.

[74] Lo BF. A survey of common control channel design in cognitive radio networks. *Physical Communication* 2011; **4**(1):26 – 39, 10.1016/j.phycom.2010.12.004. http://www.sciencedirect.com/science/article/pii/S1874490710000406.

[75] Cormio C, Chowdhury KR. Common control channel design for cognitive radio wireless ad hoc networks using adaptive frequency hopping. *Ad Hoc Networks* 2010; **8**(4):430 – 438, 10.1016/j.adhoc.2009.10.004. http://www.sciencedirect.com/science/article/pii/S1570870509001127.

[76] Potier P, Sorrells C, Wang Y, Qian L, Li H. Network-wide spectrum situation reconstruction using total variation inpainting in cognitive radio ad hoc networks. *Global Telecommunications Conference (GLOBECOM 2011), 2011 IEEE*, 2011; 1 –5, 10.1109/GLOCOM.2011.6133635.

[77] Tran D, Raghavendra H. Congestion adaptive routing in mobile ad hoc networks. *Parallel and Distributed Systems, IEEE Transactions on* nov 2006; **17**(11):1294 –1305, 10.1109/TPDS.2006.151.

[78] Kumaran TS, Sankaranarayanan V. Early congestion detection and adaptive routing in manet. *Egyptian Informatics Journal* 2011; **12**(3):165 – 175, 10.1016/j.eij.2011.09.001. http://www.sciencedirect.com/science/article/pii/S1110866511000387.

[79] Proakis J. *Digital Communications*. 4 edn., McGraw-Hill Science/Engineering/Math, 2000.

[80] *New Architectures and Disruptive Technologies for the Future Internet: The Wireless, Mobile and Sensor Network Perspective*. NSF Wireless Mobile Planning Group, 2005. http://www.winlab.rutgers.edu/docs/faculty/documents/WMPG_draft_report_v2_9.23.pdf.

[81] B. Frey, *Graphical Models for Machine Learning and Digital Communications*. MIT Press, Boston, MA, 1998.

[82] G. Ganesan and Y. Li, "Cooperative spectrum sensing in cognitive radio - Part I: Two user networks," *IEEE Trans. Wireless Commun.*, Vol.6, pp.2204–2213, June 2007.

[83] G. Ganesan and Y. Li, "Cooperative spectrum sensing in cognitive radio - Part II: Multiuser networks," *IEEE Trans. Wireless Commun.*, Vol.6, pp.2214–2233, June 2007.

[84] A. Ghasemi and E. S. Sousa, "Cooperative spectrum sensing for opportunistic access in fading environments," in *Proc. of IEEE New Frontiers in Dynamic Spectrum Access Networks (DySPAN)*, 2005.

[85] D. Koller and N. Friedman, *Probabilistic Graphical Models*, MIT Press, 2009.

[86] H. Li, "Reconstructing spectrum occupancies for wideband cognitive radio networks: A matrix completion via belief propagation," in *Proc. of IEEE International Conference on Communications (ICC)*, Cape Town, South Africa, May 2010.

[87] S. M. Mishra, A. Sahai and R. W. Brodersen, "Cooperative sensing among cognitive radios," in *Proc. of IEEE International Conference on Communications (ICC)*, June. 2006.

[88] J. Mitola, "Cognitive radio for flexible mobile multimedia communications," in *Proc. of IEEE Int. Workshop Mobile Multimedia Communications*, pp. 3–10, 1999.

[89] E. Peh and Y. C. Liang, "Optimization for cooperative sensing in cognitive radio networks," in *Proc. of IEEE Global Communications Conference (Globecom)*, 2007.

[90] E. Peh, Y. C. Liang, Y. L. Guan and Y. H. Zeng, "Optimization for cooperative sensing in cognitive radio networks: A sensing-throughput tradeoff view," *IEEE Trans. on Vehicular Technology*, vol.58, pp.5294–5299, 2009.

[91] J. Pearl, *Probabilistic Reasoning in Intelligent Systems: Network of Plausible Systems*, Morgan Kaufmann Publishers, 1988.

[92] F. Penna, R. Garello and M. A. Spirito, "Distributed inference of channel occupation probabilities in cognitive networks via message passing," in *Proc. of IEEE New Frontiers in Dynamic Spectrum Access Networks (DySPAN)*, 2010.

[93] Z. Quan, S. Cui and A. H. Sayed, "Optimal linear cooperation for spectrum sensing in cognitive radio networks," *IEEE Journal on Selected Topics in Signal Processing*, vol.2, pp.28–40, 2008.

[94] C. Sun, W. Zhang and K. B. Letaief, "Cluster-based cooperative spectrum sensing in cognitive radio systems," in *Proc. of the 18th International Symposium on Personal, Indoor and Mobile Radio Communications (PIMRC)* 2007.

[95] J. Unnikrishnan and V. V. Veeravalli, "Cooperative sensing for primary detection in cognitive radio," *IEEE Journal on Selected Topics in Signal Processing*, vol.2, pp.18–27, 2008.

[96] M. Wellens,J. Riihijarvi, P. Mähönen, "Spatial statistics and models of spectrum use," *Elsevier Computer Communications*, Aug. 2009.

[97] J. S. Yedida, W. T. Freeman and Y. Weiss, "Understanding belief propagation and its generalizations," in *Exploring Artificial Intelligence in the New Millennium*, Chap.8, pp.2282–2312, Science and Technology Books, 2003.

[98] S. Zarrin and T. J. Lim, "Belief propagation on factor graphs for cooperative spectrum sensing in cognitive radio," in *Proc. of IEEE New Frontiers in Dynamic Spectrum Access Networks (DySPAN)*, 2008.

[99] Y. Zeng, Y. C. Liang, A. T. Hoang and R. Zhang, "A review on spectrum sensing for cognitive radio: Challenges and solutions," *EURASIP Journal on Advances in Signal Processing*, pp.1–15, 2010. 2008.

[100] K. Barty, P. Carpentier and P. Girardeau, "Decomposition of large-scale stochastic optimal control problems," preprint, 2009.

[101] M. Chiang, S. H. Low, A. R. Calderbank and J. C. Doyle, "Layering as optimization decomposition: A mathematical theory of network architectures," *Proceedings of the IEEE*, vol.95, pp.255–312, 2007.

[102] K.R. Chowdhury, M.D. Felice and I.F. Akyildiz, "TP-CRAHN: A transport protocol for cognitive radio ad-hoc networks," in *Proc. of IEEE Conference on Computer Communications (Infocom)*, April. 2009.

[103] J. Jia, Q. Zhang and X. Shen, "HC-MAC: A hardware-constrained cognitive MAC for efficient spectrum management," *IEEE Journal on Selected Areas in Communications*, vol. 26, pp. 106–117, Jan. 2008.

[104] F. Kelly, "Charging and rate control for elastic traffic," *European Transactions on Telecommunications*, vol.8, pp.33–37, 1997.

[105] F. Kelly, A. Maullo and D. Tan, "Rate control in communication networks: Shadow prices, proportional fairness and stability," *Journal of the Operational Research Society*, vol.49, pp.237–252, 1998.

[106] H. Ma, L. Zheng and X. Ma, "Spectrum-aware routing for multi-hop cognitive radio networks with a single transceiver," in *Proc. of the Cognitive Radio Oriented Wireless Networks and Communications (CrownCom)*, May. 2008.

[107] A. Ruszczyński and Shapiro (edt.), *Stochastic Programming*, Handbooks in Operations Research and Management Science, vol.10, Elsevier, 2003.

[108] A. Sampath, L. Yang, L. Cao, H. Zheng and B.Y. Zhao, "High throughput spectrum-aware routing for cognitive radio based ad hoc networks," in *Proc. of the International Conference on Cognitive Radio Oriented Wireless Networks and Communications (CrownCom)*, May. 2008.

[109] Y. Shi and Y. T. Hou, "A distributed optimization algorithm for multi-Hop cognitive radio networks," in *Proc. of IEEE Conference on Computer Communications (Infocom)*, April. 2008.

[110] H. Su and X. Zhang, "Cross-Layer based opportunistic MAC protocols for QoS provisionings over cognitive radio wireless networks," *IEEE Journal on Selected Areas in Communication*, vol. 26, pp. 118–129, Jan. 2008.

[111] R. Urgaonkar and M. J. Neely, "Opportunistic scheduling with reliability guarantees in cognitive radio networks," *IEEE Trans. Mobile Computing*, vol. 8, pp. 766–777, June. 2009.

[112] J. Wang, L. Li, S. H. Low and J. C. Doyle, "Cross-layer optimization in TCP/IP networks," *IEEE/ACM Trans. Netw.*, vol.13, no.3, pp.582–586, June 2005.

[113] Q. Wang and H. Zheng, "Route and spectrum selection in dynamic spectrum networks," in *Proc. of IEEE Consumer Communications Communications and Networking Conference (CNCC)*, Jan. 2006.

[114] S. Shin, H. Park, and W. Kwon, "Mutual Interference Analysis of IEEE 802.15.4 and IEEE 802.11b," *Computer Networks*, vol. 51, no. 12, pp. 3338–3353, August 2007.

[115] J. Huang, G. Xing, G. Zhou, and R. Zhou, "Beyond Co-Existence: Exploiting WiFi White Space for Zigbee Performance Assurance," in *Proceedings of the 18th IEEE International Conference on Network Protocols*, Kyoto, Japan, October 2010, pp. 305–314.

[116] X. Zhang and K. G. Shin, "Enabling Coexistence of Heterogeneous Wireless Systems: Case for ZigBee and WiFi," in *Proceedings of the 12th ACM International Symposium on Mobile Ad Hoc Networking and Computing*, Paris, France, May 2011, pp. 1–11.

[117] H. Kim, J. Choi, and K. Shin, "Wi-Fi 2.0: Price and Quality Competitions of Duopoly Cognitive Radio Wireless Service Providers with Time-Varying Spectrum Availability," in *Proceedings of the 30th Annual IEEE International Conference on Computer Communications*, Shanghai, China, April 2011, pp. 2453–2461.

[118] L. Luo and S. Roy, "Analysis of Dynamic Spectrum Access with Heterogeneous Networks: Benefits of Channel Packing Scheme," in *Proceedings of the IEEE Global Telecommunications Conference*, Honolulu, HI, USA, December 2009, pp. 1–7.

[119] P. Zhu, J. Li, and X. Wang, "Scheduling Model for Cognitive Radio," in *Proceedings of the 3rd International Conference on Cognitive Radio Oriented Wireless Networks and Communications*, Singapore, Singapore, May 2008, pp. 1–6.

[120] J. Xie, I. Howitt, and A. Raja, "Cognitive Radio Resource Management Using Multi-Agent Systems," in *Proceedings of the 4th IEEE Consumer Communications and Networking Conference*, Las Vegas, NV, USA, January 2007, pp. 1123–1127.

[121] J. Salo, L. Vuokko, H. M. El-Sallabi, and P. Vainikainen, "An Additive Model as a Physical Basis for Shadow Fading," *IEEE Transactions on Vehicular Technology*, vol. 56, no. 1, pp. 13–26, January 2007.

[122] IEEE Std 802.22.1-2010, "IEEE Standard for Information Technology - Telecommunications and Information Exchange between Systems - Local and Metropolitan Area Networks - Specific Requirements - Part 22.1: Standard to Enhance Harmful Interference Protection for Low-Power Licensed Devices Operating in TV Broadcast Bands," November 2010.

[123] J. Venkataraman, M. Haenggi, and O. Collins, "Shot Noise Models for Outage and Throughput Analyses in Wireless Ad Hoc Networks," in *Proceedings of the IEEE Military Communications Conference*, Washington, D.C., USA, October 2006, pp. 1–7.

[124] J. Venkataraman and M. Haenggi, "Maximizing the Throughput in Random Wireless Ad Hoc Networks," in *Proceedings of the 42st Annual Allerton Conference on Communication, Control, and Computing*, Monticello, IL, USA, October 2004, pp. 1–9.

[125] E. R. LLC, "USRP2 – the next generation of software radio systems [online]," http://www.ettus.com/product.

[126] "GNU radio project [online]," http://gnuradio.org/redmine/projects/gnuradio/wiki.

[127] J. Mitola, "Software radios–survey, critical evaluation and future directions," in *Proc. National Telesystems Conference (NTC)*, 1992, pp. 13/15–13/23.

[128] "Adroit gnu radio development project [online]," https://acert.ir.bbn.com/projects/adroitgrdevel/.

[129] "Hydra project [online]," http://hydra.ece.utexas.edu/testbed/.

[130] Microsoft Research Software Radio (Sora). [Online]. Available: http://research.microsoft.com/en-us/projects/sora/

[131] "Wireless open-access research platform (WARP) [online]," http://warp.rice.edu/.

[132] "KU agile radio [online]," http://agileradio.ittc.ku.edu.

[133] "Virginia tech chameleonic radio [online]," http://www.ece.vt.edu/swe/chamrad.

[134] "Microsoft research knows project. [online]," http://research.microsoft.com/netres/projects/KNOWS.

[135] M. Dickens, B. Dunn, and J. N. Laneman, "Design and implementation of a portable software radio," *IEEE Communications Magazine*, vol. 46, no. 8, pp. 58–66, August 2008.

[136] G. J. Bradford and J. N. Laneman, "An experimental framework for evaluating cooperative diversity," in *Proc. Conf. Inform. Sci. and Syst. (CISS)*, Mar. 2009.

[137] "EttusE110 – e100 series embedded sdr [online]," http://www.ettus.com/downloads/ USRP_E100_Series_temporary_datasheet.pdf.

[138] A. Crohas, "Practical implementation of a cognitive radio system for dynamic spectrum access," Master's thesis, University of Notre Dame, Aug. 2008.

[139] "CORNET: Cognitive radio network testbed (cornet) at virginia tech [online]," http://wireless.vt.edu/coreareas/.

[140] O. Omotere, L. Qian, and R. Jantti, "Performance bounds of prioritized access in coexisting cognitive radio networks," in *Cognitive Radio Oriented Wireless Networks and Communications (CROWNCOM), 2014 9th International Conference on*, June 2014, pp. 197–202.

[141] O. Omotere, L. Qian, and X. Du, "Performance bound of ad hoc device-to-device communications using cognitive radio," in *Globecom Workshops (GC Wkshps), 2013 IEEE*, Dec 2013, pp. 654–659.

[142] M. Bruno, M. Murdy, P. Perreault, A. M. Wyglinski, and J. McNeill, "Widely tunable rf transceiver front end for software-defined radio," in *Military Communications Conference, 2009. MILCOM 2009. IEEE*, Oct 2009, pp. 1–6.

[143] H. C. Bui and L. Franck, "Cost effective emulation of geostationary satellite channels by means of software-defined radio," in *Metrology for Aerospace (MetroAeroSpace), 2014 IEEE*, May 2014, pp. 538–542.

[144] Spectrum Monitoring with NI USRP. [Online]. Available: http://www.ni.com/white-paper/13882/en/

[145] M. Wellens and P. Mähönen, "EnglishLessons learned from an extensive spectrum occupancy measurement campaign and a stochastic duty cycle model," *English-Mobile Networks and Applications*, vol. 15, no. 3, pp. 461–474, 2010. [Online]. Available: http://dx.doi.org/10.1007/s11036-009-0199-9

[146] NI USRP-292x/293x Datasheet. [Online]. Available: http://www.ni.com/datasheet/pdf/en/ds-355

[147] Overview of the NI USRP RIO Software Defined Radio. [Online]. Available: http://www.ni.com/white-paper/52119/en/

[148] UHD Start. [Online]. Available: http://code.ettus.com/redmine/ettus/projects/uhd/wiki

[149] GNU Radio. [Online]. Available: http://gnuradio.org/redmine/projects/gnuradio/wiki

[150] "Ieee 1588 standard for a precision clock synchronization protocol for networked measurement and control systems," p. 8 November 2002 (Version 1).

[151] S. Ganeriwal, R. Kumar, and M. B. Srivastava, "Timing-sync protocol for sensor networks," in *Proceedings of the 1st International Conference on Embedded Networked Sensor Systems*, ser. SenSys '03. New York, NY, USA: ACM, 2003, pp. 138–149. [Online]. Available: http://doi.acm.org/10.1145/958491.958508

[152] J. van Greunen and J. Rabaey, "Lightweight time synchronization for sensor networks," in *Proceedings of the 2Nd ACM International Conference on Wireless Sensor Networks and Applications*, ser. WSNA '03. New York, NY, USA: ACM, 2003, pp. 11–19. [Online]. Available: http://doi.acm.org/10.1145/941350.941353

[153] M. Sichitiu and C. Veerarittiphan, "Simple, accurate time synchronization for wireless sensor networks," in *Wireless Communications and Networking, 2003. WCNC 2003. 2003 IEEE*, vol. 2, March 2003, pp. 1266–1273 vol.2.

[154] M. Maróti, B. Kusy, G. Simon, and A. Lédeczi, "The flooding time synchronization protocol," in *Proceedings of the 2Nd International Conference on Embedded Networked Sensor Systems*, ser. SenSys '04. New York, NY, USA: ACM, 2004, pp. 39–49. [Online]. Available: http://doi.acm.org/10.1145/1031495.1031501

[155] J. Elson, L. Girod, and D. Estrin, "Fine-grained network time synchronization using reference broadcasts," *SIGOPS Oper. Syst. Rev.*, vol. 36, no. SI, pp. 147–163, December 2002. [Online]. Available: http://doi.acm.org/10.1145/844128.844143

[156] Building an Affordable 8x8 MIMO Testbed with NI USRP. [Online]. Available: http://www.ni.com/white-paper/14311/en/

[157] L. Wang, J. Fernandez, J. Burgett, R. Conners, and Y. Liu, "An evaluation of network time protocol for clock synchronization in wide area measurements," in *Power and Energy Society General Meeting - Conversion and Delivery of Electrical Energy in the 21st Century, 2008 IEEE*, July 2008, pp. 1–5.

[158] O. Postolache, P. Girao, S. Antunes, and F. Tavares, "Rf spectrum monitoring and management system based on an rf receiver multi-server architecture," in *Intelligent Data Acquisition and Advanced Computing Systems (IDAACS), 2011 IEEE 6th International Conference on*, vol. 1, Sept 2011, pp. 176–179.

[159] LabVIEW-Based Spectrum Occupancy Measurements. [Online]. Available: http://www.arsr-swicom.org.uk/papersandposters/2012/arsr-papers/ENajafzaden-Spectrum-Occupancy.pdf

[160] M. Ghanavati, R. Wong, F. Chen, Y. Wang, and C.-S. Perng, "An effective integrated method for learning big imbalanced data," in *Big Data (BigData Congress), 2014 IEEE International Congress on*, June 2014, pp. 691–698.

[161] D. Dittman, T. Khoshgoftaar, R. Wald, and A. Napolitano, "Simplifying the utilization of machine learning techniques for bioinformatics," in *Machine Learning and Applications (ICMLA), 2013 12th International Conference on*, vol. 2, Dec 2013, pp. 396–403.

[162] U. Dogan, J. Edelbrunner, and I. Iossifidis, "Autonomous driving: A comparison of machine learning techniques by means of the prediction of lane change behavior," in *Robotics and Biomimetics (ROBIO), 2011 IEEE International Conference on*, Dec 2011, pp. 1837–1843.

[163] P. Panigrahi, "A comparative study of supervised machine learning techniques for spam e-mail filtering," in *Computational Intelligence and Communication Networks (CICN), 2012 Fourth International Conference on*, Nov 2012, pp. 506–512.

[164] E. Lowe, M. Butkiewicz, M. Spellings, A. Omlor, and J. Meiler, "Comparative analysis of machine learning techniques for the prediction of logp," in *Computational Intelligence in Bioinformatics and Computational Biology (CIBCB), 2011 IEEE Symposium on*, April 2011, pp. 1–6.

[165] M. Ozdemir, E. Arvas, and H. Arslan, "Dynamics of spatial correlation and implications on mimo systems," *Communications Magazine, IEEE*, vol. 42, no. 6, pp. S14–S19, June 2004.

[166] D. McNamara, M. Beach, and P. Fletcher, "Spatial correlation in indoor mimo channels," in *Personal, Indoor and Mobile Radio Communications, 2002. The 13th IEEE International Symposium on*, vol. 1, Sept 2002, pp. 290–294 vol.1.